Faculty of Engineering and Science

Department of Applied Geology

A Study on the Earthquake Generating Faults in Ranau region, Sabah using Satellite Images and Field Investigation

Navakanesh M Batmanathan

This thesis is presented for the Degree of
Master of Philosophy (Geology)
of
Curtin University

July 2018

Declaration

To the best of my knowledge and belief this thesis contains no material previously published by any other person except where due acknowledgment has been made.

This thesis contains no material which has been accepted for the award of any other degree or diploma in any university.

(Include where applicable)

Human Ethics (For projects involving human participants/tissue, etc) The research presented and reported in this thesis was conducted in accordance with the National Health and Medical Research Council National Statement on Ethical Conduct in Human Research (2007) – updated March 2014. The proposed research study received human research ethics approval from the Curtin University Human Research Ethics Committee (EC00262), Approval Number #.....

or

Animal Ethics (For projects involving animal use) The research presented and reported in this thesis was conducted in compliance with the National Health and Medical Research Council Australian code for the care and use of animals for scientific purposes 8th edition (2013). The proposed research study received animal ethics approval from the Curtin University Animal Ethics Committee, Approval

Number #.....

Signature: ……..

Date: 19 July 2018……..

Abstract

This thesis investigates the evidence of active tectonics in Sabah, Malaysia, which is part of the Borneo Island. The motivation to work on active tectonics of the region directly comes from the disaster associated with the medium magnitude earthquake that occurred on 5th June 2015 and devastated a large portion of Ranau region, and caused an unfortunate loss of 18 precious lives. The first step is geomorphic analysis of landforms that is carried out throughout the region to produce a base map. The standard mapping procedures are adapted, which are followed by detailed geomorphic, and morphometric analysis where all the major and minor active landforms are mapped. The geomorphic mapping includes the identification of topographic breaks, triangular facets, wine-glass canyon, changes in river channels, past fault scarps, linear valleys, and uplifted / tilted Quaternary to Recent landforms. The data obtained from geomorphic analysis exercise is digitally processed using ArcGIS software, specifically the hydrography data plots. Our geomorphic data result reveals a number of active normal faults, which have also influenced the courses of streams and formed a number of knickpoints, which are indicators of active movements. This is evident in some of the upstream regions of rivers namely Sg. Mesilou A, Mesilou B and Mesilou C. These knickpoints are not related to bedding and are consistent with faulting events. The field visits also reveal a number of normal faults with NW or SE dipping plane, particularly in Ranau and Kundasang region. All the mapped faults in field are old faults, and have not disrupted any younger stratigraphic marker, which clearly indicates that the faults are much older. However, the strike and dip direction of the old faults is consistent with the normal fault that hosted the June-2015 event, and therefore, it is possible that the instrumental and historical seismicity in Sabah is related to these faults, which are formed in response to stresses that are mainly tectonic in origin. The use of Ground Penetrating Radar (GPR) also suggested a number of normal faults that are mapped in Sabah. However, the lack of field evidence of fault rupture associated with June 2015 earthquake suggests that this particular event occurred on a blind fault, which could mean that perhaps younger events occur on blind faults. And this explains the scarcity of field evidence of Quaternary to Recent rupturing. The fact that geomorphic analysis shows some of the major active faults in the region could also mean that such faults are covered with thick sediments, and have undergone intense erosion because of the dominant weathering effects in tropical conditions that the region witnesses throughout the year.

Table of Content

List of Figures

List of Tables

List of Abbreviation

Af ----------Asymmetric Factor

Bs ---------- Basin Shape Index

EM ---------- Electromagnetic

Er ----------Basin Elongation Ratio

GDEM ---------- Global Digital Elevation Model

GPR ---------- Ground Penetrating Radar

GPS ---------- Global Positioning System

HI ---------- Basin Hypsometry

M_L ---------- Local Magnitude

Mw ----------Moment Magnitude

PGA ----------Peak Ground Acceleration

RTA ---------- Rough Terrain Antenna

RTC ---------- Rough Terrain Cart

SL----------Stream Length Gradient Index

Smf ----------Mountain Front Sinuosity

SRTM---------- Shuttle Radar Topography Mission

TRI ----------Terrain Ruggedness Index

USGS ----------United States Geological Society

Vf ----------Valley Floor Width to Valley Floor Height

Acknowledgement

A special note of appreciation to my supervisors, Dr. Afroz Ahmad Shah, Dr. M. V. Prasanna, Dr. Nagarajan Ramasamy and Ms. Illiya Amalina for their assistance, guidance and advice for making this project possible.

My special appreciation to my fellow friends, Mr. Hong Hui Tan and Rajesh Babu Chuncula, with whom I spent many hours on discussion and exchanging of ideas.

And not forgetting the Malaysian Meteorological Department (MET) for providing me information related to earthquake and disasters.

I would also like to give my endless gratitude to Faculty of Engineering and Science and Graduate School for providing full tuition few waiver and National Geographic Society for providing me the Young Explorer Grant to conduct my research in Ranau, Sabah.

Lastly, this project would not have been possible without the support and understanding of my family. Both my parents deserve my gratitude, as their understanding have given me the inspiration to complete this project on a positive note. And not forgetting my grandmother Madame Tanapakiam for giving me the morale support throughout the whole course and the project paper.

Chapter 1
Introduction

1.1. Background

Sabah is located in the northwest of Borneo, and the present tectonic setting shows (Fig. 1) that it is caged by the active plate margins of Indo-Australian plate, the Sunda plate and the Philippine Sea plate. The historical and instrumental earthquake data (Mooney et al., 2012) demonstrate that this region is mostly free from earthquakes that could be related to the active tectonic processes operating at the surrounding plate margins, and it seems possible that this portion of Sunda plate is tectonically stable (Shah, 2016; Tongkul, 2017; Wang et al., 2017; Shah et al., 2018). The Mw 6.0 Ranau earthquake which occurred on the 5th June 2015 led to intense ground shaking, which triggered landslides and rock falls along Mt. Kinabalu that killed 18 people. The main shock was felt at least 300 km away and even affected the residents in Kota Kinabalu (Wang et al., 2017). However, the occurrence of medium magnitude earthquakes in this region have revised the need to understand what really causes such events, and a number of recent studies have shown that plate tectonics could be a key to the ongoing deformation within the Sunda plate. If this is true, then, we are seeing intraplate earthquakes (Talwani, 2014; 2016) in this region because certainly the seismicity is not related to the ongoing subduction that encircles this region (Fig. 1). Although a number of past studies have tried to explain these complexities (Balaguru et al., 2003; Cullen, 2010; Hall, 2002; 2013; Hesse et al., 2009; Hinz et al., 1985; Hutchison, 2005; King et al., 2010a; 2010b; 2010c; Lambiase et al., 2002; Morley, 2009; Sapin et al., 2009; 2011; 2013;) but bulk of these studies have not produced data on the detailed structural field investigations, and also lack extensive geomorphic work, which are fundamental to understand the ongoing deformation in the region, and whether the deformation is in-sequence or out of sequence (Mukherjee et al., 2010a; 2010b; 2013; 2015), and the pattern of deformation is intra or inter-plate related processes

Therefore, this study aims to build the structural and geomorphic framework of Ranau region with the motivation to map, and understand the active deformation and what causes it; the questions that are still vigorously debated (Mathew et al., 2015; 2016a; 2016b; Menier et al., 2017; Wang et al., 2017; Shah et al., 2018).

1.2. Research Gap

Since the current understanding on active tectonics and earthquakes in Sabah is at a very initial stage and research involving tectono-geomorphology is slowly accumulating to get a better picture of the geological and tectonic architecture of the Ranau region (Sandal, 1996; Simons et al., 2007; Hesse et al., 2009; King et al., 2010a; 2010b; 2010c; Sapin et al., 2013; Hall, 2013; Wang et al., 2016; Wang et al., 2017; Shah et al., 2018), however, such works are still limited in extent, and lack field details (Mathew et al., 2015; Shah, 2016; Shah et al., 2018). This is mainly because the cause of earthquakes in Northwest Borneo is yet to be fully explored, primarily since all of the seismogenic faults have not been mapped (Shah, 2016; Shah et al., 2018), and the mechanism of their occurrence remains largely unknown. One of the major reasons for the lack of extensive studies on the geological investigations is the occurrence of thick forest cover, and the lack of access to most of the Borneo Island, and importantly the consensus that this part of Sunda plate is tectonically stable (Tongkul, 2017; Wang et al., 2017). This has profoundly affected the scientific investigation in the region and the story is similar to what happened after 2001 Bhuj earthquake that killed more than 11000 people, and similarly the perception towards tsunamic research changed after the devastating under ocean earthquake and tsunami of 2004 that occurred in Indian Ocean

The story is exactly similar in Malaysia when an Mw 6 earthquake struck Sabah on 5th June 2015. This suggested that the faults are active and could bring more damage in the near future. A detailed investigation on the active faults could provide an answer for the earthquake recurrence in this region. The present study is the first attempt to carry out a Ground Penetrating Radar (GPR) survey, with detailed tectonic interpretation and mapping of seismogenic faults in this region.

The principal questions to be answered are:

1) Does the investigation on the active versus inactive faults provides answer for the earthquake recurrence in this region?

2) Is Ranau tectonically active region, and is it prone to earthquake of Mw = 6 or greater in the near future?

3) What was the main cause of 5th June 2015 earthquake that occurred in Ranau, Sabah?

1.3. Aim / Objective

Geological field investigation in Ranau, Sabah are aimed to map the active geomorphic features, and to measure the displacement on earthquake-generating faults with the following objective:

a) To map the fault zones across Ranau region with the help of satellite images
b) To identify sub-surface geometry of faults by GPR investigation

1.4. Study area

This research work primarily focuses on Ranau region, Sabah, Malaysia which is located at the Northwest of Borneo The historical and instrumental earthquake data shows that the Ranau region has been experiencing small to moderate magnitude earthquakes throughout the history, and the recorded data shows it (Figure 1.2). The medium magnitude earthquake seem to have a pattern, and such events occur every 25 years (Tongkul, 2015). What controls this pattern, and does it really have any scientific meaning is one of the major research questions that needs to be explored. The earthquake geology of the recent two medium magnitude earthquakes (Fig 1.2) shows that these are nucleated on normal faults (Tongkul, 2015; Shah, 2016; Wang et al., 2017; Shah et al., 2018), and were the reason for extensive landslides in the region, that includes a series of rock avalanche that hit the famous tourist attraction the Mount Kinabalu, and resulted in a loss of 18 people (Tongkul, 2015; Wang et al., 2017). As a result of the earthquake, more detailed studies begun with an idea of determining the cause of the earthquake generating faults (Shah, 2016; Shah et al., 2018).

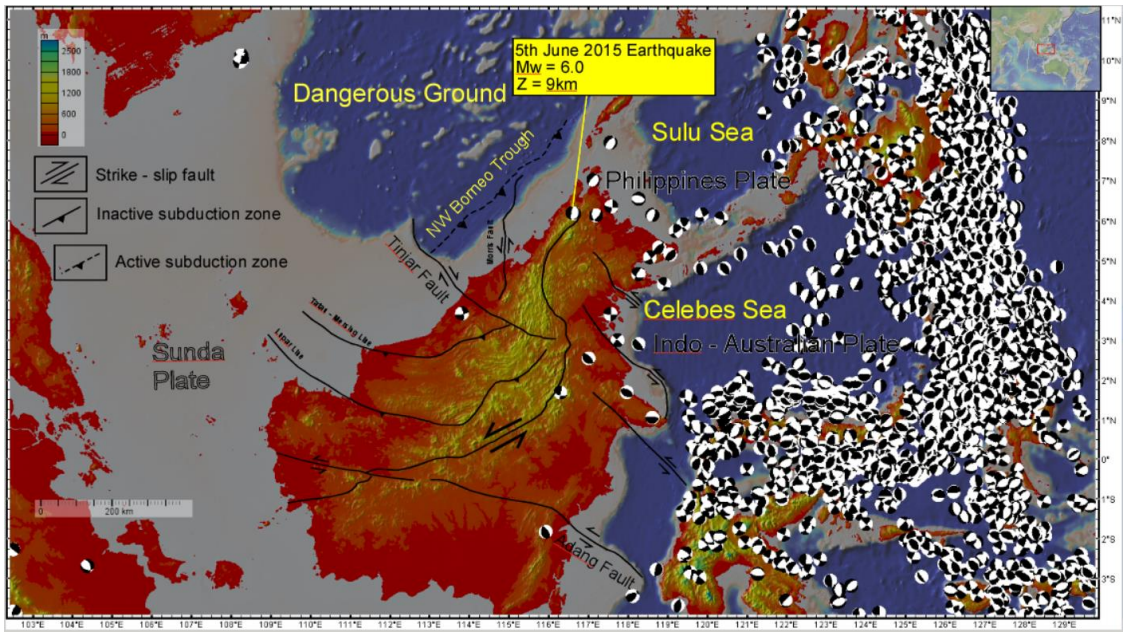

Figure 1.1 seismological data and major faults overlaid on the satellite images (Modified from Geomap app, 2018)

Based on Figure 1.1, the regional tectonic map of the region is surrounded by active plate boundaries of the Sunda, Indo – Australian and Philippines plates. However, the earthquake focal plane mechanism shows a significant number of earthquakes clustered in and around Sabah.

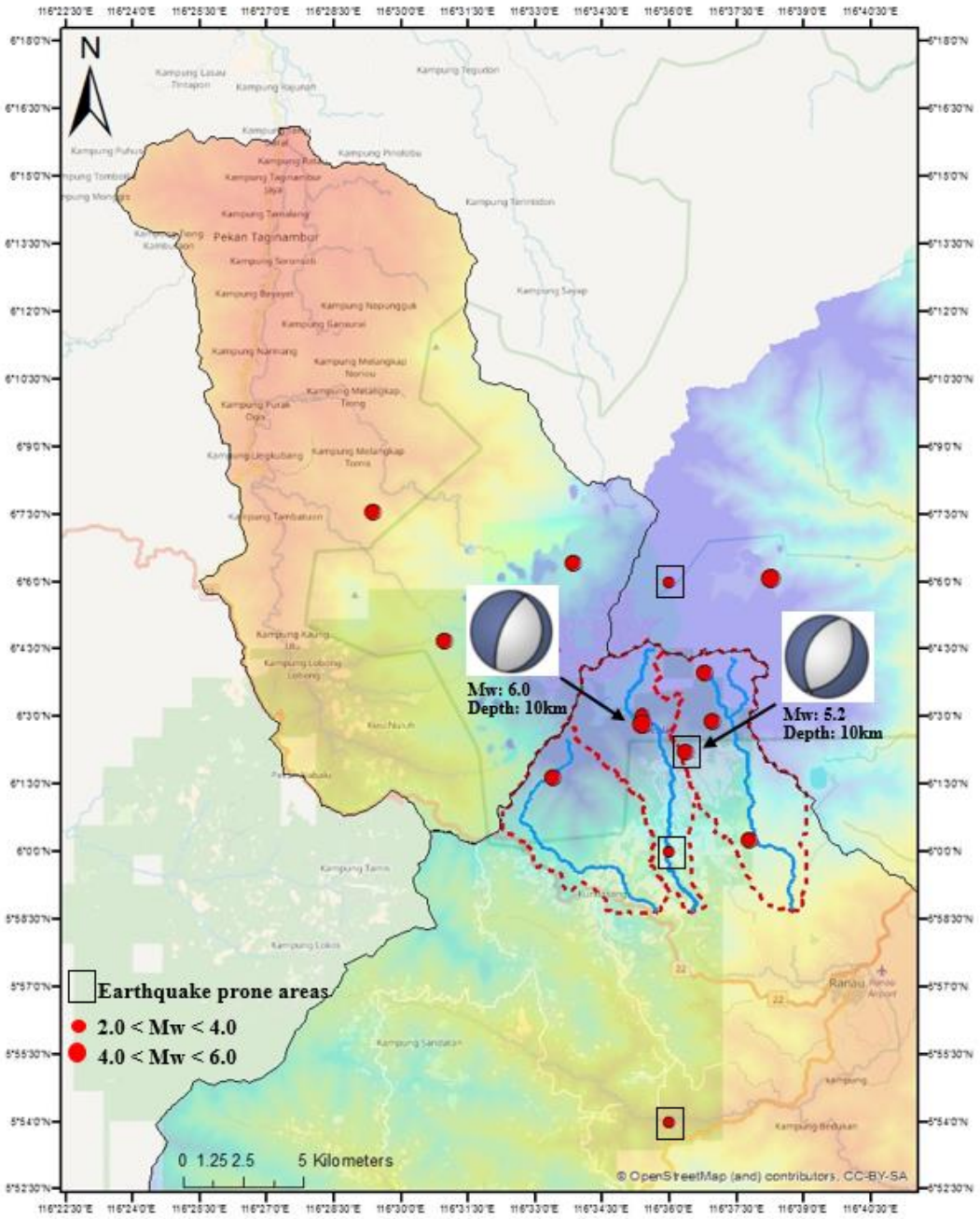

Figure 1.2 Earthquake distribution and fault plane solution of 5th June 2015 and 8th March 2018 earthquake.

1.5. Topography of the Ranau region

The Ranau area has a low terrain compared to the surrounding area (e.g. Kundasang) which shows prominent terrain throughout the region. These variations in terrain can be determined from google maps under terrain mode. The Ranau area is located within an intermontane basin. Nonetheless, a few intermontane basins are located nearby to the study area and are surrounded by normal faults such as Marakau fault, Outcrop A and Outcrop F. Besides that, land-use of the study area are mainly divided into state land and indigenous territory, causing probable effects on the topography. The thriving economy and constant demand of natural resources in Borneo has led to an increase in commercial logging, widening agriculture and plantation developments such as palm oil plantations, are consequently causing a degradation of the tropical rain forests (Ichikawa, 2007), and eventually rapid erosions of fragile soft rocks (Yamakura et al., 1995; Mathews et al., 2016a; 2016b).

Chapter 2
Literature Review

2.1. Regional Geology

Northwest Borneo is located at a triple junction point between the Sunda plate, the Indo – Australian plate and the Philippines Sea plate. However, the tectonics and structure of Northwest Borneo has been strongly debated for many years by various researchers (Haile, 1962; Hall, 2002; Hutchison, 2005; Morley, 2009; Hall, 2013; Shah, 2016; Tongkul, 2017; Shah et al., 2018). The main cause of active deformation in the Borneo Island is yet to be determined, primarily because it requires detailed field investigation, which are difficult in a terrain that is inaccessible, and covered in thick forests. However, past studies have taken the advantage of remote sensing data to explore the topography, geology, and geomorphology of the region (Shah, 2016; Mathew et al., 2016a; 2016b; Menier et al., 2017; Wang et al., 2017; Shah et al., 2018). These works have greatly improved the understanding of geology, tectonics, and gravity related deformation (Banda & Honza., 1996; Hall, 2002; Hutchison, 2005; Morley, 2009; Hall, 2013; Shah, 2016; Tongkul, 2017; Shah et al., 2018) but still a large portion of work is needed to map and understand the geologic scientific wisdom of this region that will make way for pinpointing the probable causes of faulting that is ongoing in the region. is required to map the entire fault zone, and to fully understand the past and the latest slip on the fault. Furthermore, previous research (Balaguru et al., 2003; Cullen, 2010; Hall, 2002; 2013; Hesse et al., 2009; Hinz et al., 1985; Hutchison, 2005; King et al., 2010a; 2010b; 2010c; Lambiase et al., 2002; Morley, 2009; Sapin et al., 2009; 2011; 2013; Simons et al., 2007) have contributed significant amount of works. However, new field-based studies is required, which includes dating and sediment provenance studies. The geology of major parts of Northwest Borneo and causes of magmatism remains largely unknown. Thus, information on crustal thickness and mantle structure is required to elucidate the geology around Northwest Borneo. Also, more vital evidences must be provided for the causes of extension, rotation and upliftment. The links between onshore and offshore studies must be improved for better understanding of the structural evolution of Northwest Borneo.

2.2. Northwest Borneo

Different deformation structures across this region is the product of subduction between proto South China Sea and Borneo (Hinz & Schluter, 1985; Wannier et al., 2011). Thus, the tectonism is highly associated with strong folding, basement upliftment and wrench faulting (Darman & Sidi, 2000; Cullen, 2010; Menier et al., 2014). Previous studies have clearly shown that broad NW-SE trending synclines are observed in the coastal regions while narrow anticlines are from further inland (Balaguru et al., 2003). Ostensibly, multiple-stage folding and thrusting sequence is observed (Wang et al., 2016). The active crustal shortening affecting this region could have reactivated the older extensional fault as younger reverse fault are observed in the surface as uplifted fluvial terraces (Mathew et al., 2016b). However, the main structure of Sabah is a well-developed NE-SW trending fold and thrust belt, which indicates NW-SE compression, attributed to large crustal-scale gravity driven mechanism and the orogenic collapse of the NW Borneo since 1.9 Ma (Sandal, 1996; Balaguru et al., 2003; Hesse et al., 2009; Morley, 2009; Cullen, 2010; King et al., 2010a, 2010b; Sapin et al., 2013). However, Hall (2013) has stated that there is no plate convergence in NW Borneo region and most deformation along this region is a result of extension. The extension occurred due to rapid trench rollback, which is marked by the deep regional unconformity (DRU) and gravity gliding in onshore region (Hall, 2013). On the contrary, the evidence from GPS suggests that shear deformation is concentrated along Northwest Borneo and does not illustrate any extensional deformation that supports the idea of gravity driven collapse of the Crocker Range (Mustafar et al., 2017). Previous research have stated three possible reasons for the present motion of Northwest Borneo as crustal shortening (Simons et al., 2007; Hesse et al., 2009), gravity sliding (Sandal, 1996; King et al., 2010; Sapin et al., 2013; Hall, 2013) and localized stress model (Wang et al., 2017).

2.3. Geological Field Locations in Sabah

A number of earthquake generating faults have been mapped in Ranau Sabah region, and this includes the Mensaban and Lobou-Lobou faults (Mohamed, 2012; Yusoff et al., 2016). However, previous researches have clearly stated that the NW Borneo margin was inactive due to low seismicity (Sapin et al., 2009). The recent (5^{th} June 2015) earthquake proves that the Northwest Borneo is seismically active with an average of above Mw 4 on the seismic scale, despite demonstrating no substantial motion between Central Borneo and Sunda Plate (Menier et al., 2017; Wang et al., 2017; Shah et al., 2018). These are mostly shallow focused with a combination of normal, thrust and strike slip fault and suggests the whole region is a destructive prone region as a result of shallow earthquakes. Other faults includes Perancangan fault, Lahad Datu faults, Keningau fault, Danum fault, Binuang fault, Tabin fault and Beluran fault (Yan, 2010). In addition, Menier et al. (2017) have provided causes of recent tectonic events in the study area, which includes subduction of NW Borneo Trough to the present day, regional compression, extensional settings, convergence of blocks, and far-field stress that can be directly linked to the recent seismic events.

On the other hand, previous study has postulated that the direction and rate of motion for East Malaysia (Sabah and Sarawak states) and South Peninsular Malaysia had a major change after the 2004 Sumatra – Andaman earthquake (Gill et al., 2015). Such an interpretation implies that a long term post seismic deformation occurred due to the 2004 earthquake. Based on focal mechanism solution provided by USGS, a normal fault with a near vertical dipping direction is obvious, which suggests a sudden crustal collapse as normal fault subsidence.

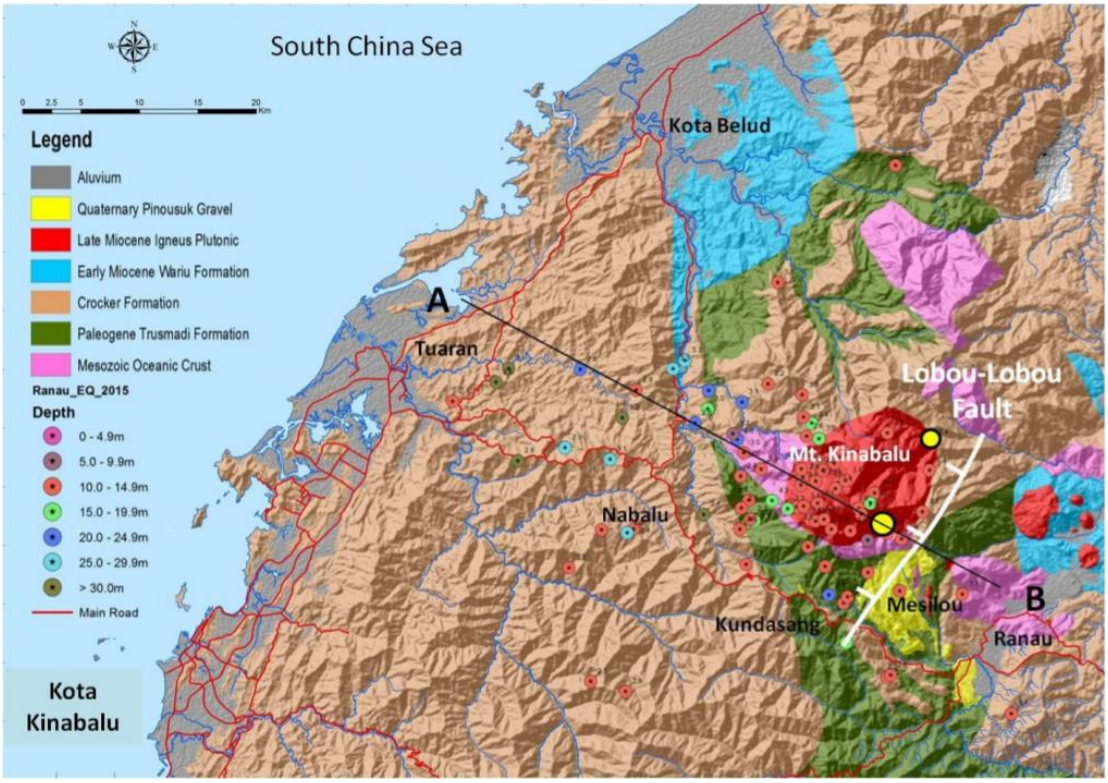

Figure 2.1 Earthquake generating fault in Ranau area (Modified after Tongkul, 2015)

Based on Figure 2.1, the Lobou – Lobou fault seems to be oriented NE – SW, with a 70° dipping towards NW (Tongkul, 2015). Also, the length of the fault is approximately 10 km and displacement is around 0.5 m. However, Wang et al. (2017) stated that the 5th June 2015 earthquake did not rupture the surface, and the surface deformation on Mt. Kinabalu is less than 3 cm. This indicates that it is an unknown blind fault, it is seismically active and it may rupture again in the near future.

2.4. Common methods used in earthquake study

The most efficient methods are morphometric analysis, geomorphic mapping and field investigation. These methods serve as an important aspect of earthquake studies across the globe (Malik & Mohanty, 2007; El Hamdouni et al., 2008; John & Rajendran, 2008; Pedrera et al., 2009; Dehbozorgi et al., 2010; Font et al., 2010; Toudeshki & Arian, 2011; Dar et al., 2014; Mathew et al., 2016a; 2016b). And, the use of Ground Penetrating Radar (GPR) in such studies is essential as the geometry of active and inactive faults can be determined (Malik et al., 2007; Burdette et al., 2012; Mohapatra et al., 2014; Bubeck et al., 2015).

2.4.1. Ground Penetrating Radar (GPR) Survey

GPR is widely used by many geoscientists to identify the geometry of fault scarp (Figure 2.2), which can be used to study seismic slip (Malik et al., 2007; Burdette et al., 2012; Mohapatra et al., 2014; Bubeck et al., 2015). And, vital information on colluvial wedges, disrupted and displaced strata can be observed from GPR (Dentith et al., 2010). It is capable of identifying topographic features of seismic origin. In addition, the statement above can be further supported with evidence from Burdette et al. (2012), who carried out a GPR survey to determine the geometry and displacement of siliciclastic sediments in Apalachicola, Florida. However, data processing is the most crucial part in order to obtain filtered results for the better interpretation. Several works have demonstrated that the orientation of the antenna plays a major role in minimizing the reflection and diffraction caused by the discontinuities (Malik et al., 2007; Mohapatra et al., 2014). According to Malik et al. (2007), processing methods such as time – zero correction, band pass filters, finite impulse response filters, auto gain control and topographic correction must be applied to remove any discontinuities as result of reflection and diffraction. On the other hand, types of lithological and topographical variations must be considered as an important factor during the GPR survey. For example, conductive material must be avoided because it will rapidly reduce the penetration depth of the electromagnetic wave (EM). Thus, GPR survey has to be conducted through shallow penetration using dry resistive materials and ideally be free from conductive deposits such as clay (Bubeck et al., 2015). Malik et al (2007) also stated that the auto gain control is applied for high elevated regions to improve resolution and topographic correction for normalizing the surface.

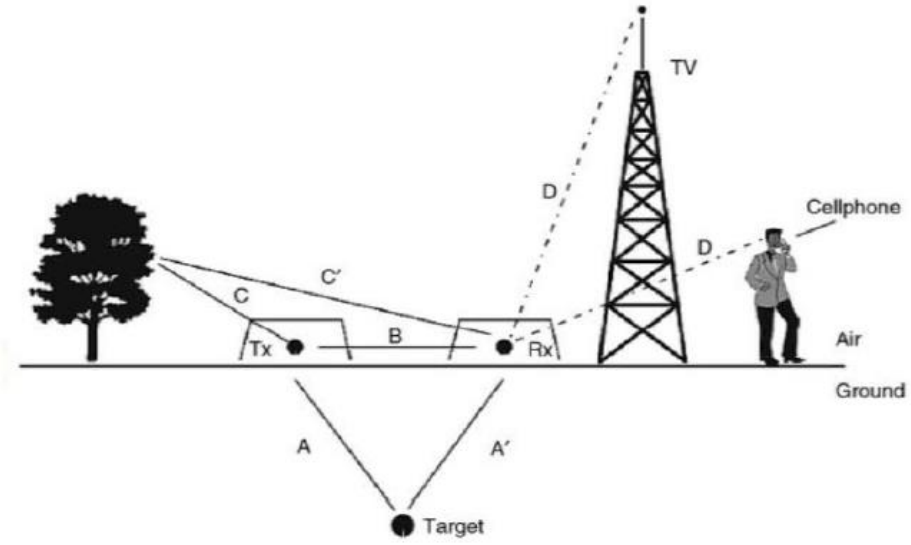

Figure 2.2 GPR system detects reflected signal and diffraction discontinuities (MALA, 2015)

2.4.2. Morphometric Indices

The use of morphometric analysis in earthquake study is common, especially among geoscientists. However, previous works have demonstrated that the following indices are widely used; concavity index (θ), mountain front sinuosity (Smf), stream length gradient index (SL), valley floor width to valley floor height (Vf), asymmetric factor (Af), basin hypsometry (HI), basin shape index (Bs), basin elongation ratio (Er) and terrain ruggedness index (TRI) (Hack, 1973; Bull & Mcfadden, 1977; Rockwell et al., 1984; Keller & Pinter, 2002; Silva et al., 2003; Peters & Van Balen, 2007; Viveen et al., 2012; Hurtgen et al., 2013; Kale et al., 2014; Fountoulis et al., 2015; Zygouri et al., 2015). Shyu et al. (2005) stated that the geometry and slip characteristics of the faults can be determined by observing the deformation patterns of fluvial terraces via morphometric analysis with 40m resolution satellite imageries. Most of the indices have been extensively used in faulted regions with high deformation rates (Pedrera et al., 2009). In addition, these methods were mainly focused on fluvial system and valley morphology, which seems to prove that the anomalies are produced by tectonic uplift and erosional processes (Malik & Mohanty, 2007; El Hamdouni et al., 2008; John & Rajendran, 2008; Pedrera et al., 2009; Dehbozorgi et al., 2010; Font et al., 2010; Toudeshki & Arian, 2011; Dar et al., 2014; Mathew et al., 2016a; 2016b). The anomaly changes along the rivers' longitudinal profile of NW Borneo was determined using these methods (Sapin et al., 2011; Mathew et al., 2015; 2016b)

Recent studies show the use of geodetic absolute rates with morphometric indices to evaluate active tectonics in tectonically unstable regions (Gao et al., 2016). With the advancement of technology, a great variety of satellite images and digital topographic data (such as Digital Elevation Models : DEMs) together with Geographic Information System (GIS) software enables the geomorphic characteristics of drainages, stream networks and temporal stages of landscape development to be effectively interpreted (Slaymaker, 2001; Hajam et al., 2013; Waikar & Nilawar, 2014). In addition, these ideal methods provide an accurate and more comprehensive understanding of the natural landforms (Tarboton et al., 1991; Dietrich et al., 1993; Montgomery & Foufoula – Georgiou, 1993; Moglen & Bras, 1995; Tucker, 1996; Sklar & Dietrich, 1998; Weissel and Seidl, 1998; Synder et al., 2000). Also, these methods have been applied successfully in locations which have thick vegetation covers such as Borneo Island (Mathew et al., 2016a; 2016b; Menier et al., 2017).

Chapter 3
Methodology

3.1. Research Methodology

In this chapter, the detailed methodology of the different analyses is presented and summarised as follows.

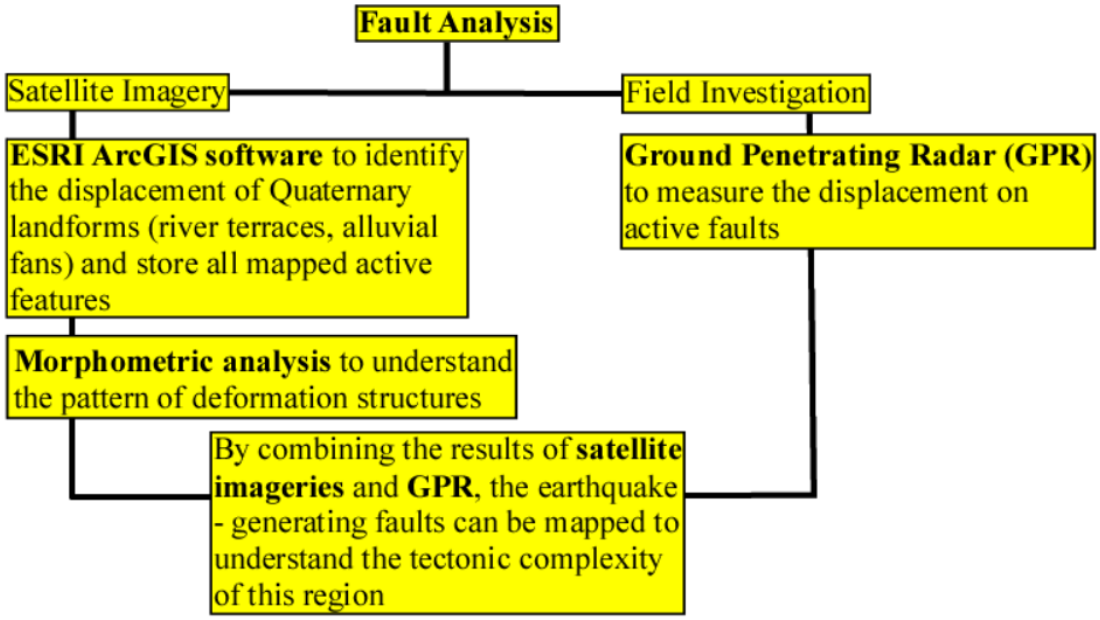

Figure 3.1 The flow chart of the methodology adopted for this study.

3.1.1. Morphometric Analysis

High resolution satellite images (e.g. SRTM and ASTER GDEM) is analysed under Geographic Information System (GIS) for the computation of various tectono-morphometric indices to further understand the patterns of deformation structures in Ranau, Sabah. The four common geomorphic parameters such as elongation ratio (Schumn, 1956), stream length index (Hack, 1973), hypsometric integral (Strahler, 1957) and longitudinal profile were used to elucidate the level of tectonic complexity in the region and also to characterize the rupture ages and cumulative displacement on faults. The equations used for calculating geomorphic indices are presented below:

Elongation Ratio: $R_e = 1.128 \times \sqrt{A} / L_b$

Where, R_e is basin elongation ratio; A is the area of the basin; L_b is the length of the basin.

Stream Length Gradient Index: $\mathbf{SL = (\Delta H / \Delta L) / L}$

Where, SL is stream length; ΔH is change in elevation of the reach; ΔL is the length of the reach; L is the total length from midpoint to the highest point along the stream.

Hypsometric Integral: $HI = (H_{mean} – H_{min}) / (H_{max} – H_{min})$

Where, HI is hypsometric integral; H_{mean} is mean elevation; H_{min} is minimum elevation; H_{max} is maximum elevation.

Longitudinal Profile: Elevation – Distance Plot

3.1.2. Pre – Fieldwork investigation

Pre-fieldwork investigation involves examination of satellite images that includes SRTM, where mapping of geomorphic features such as triangular facets, wineglass canyon, topographic breaks and fault scarps was achieved (Shah, 2016; Wang et al., 2017; Shah et al., 2018). Based on the geomorphological mapping, the active features were identified by investigating the displacement of Quaternary to Recent landforms such as river terraces and alluvial fans. In addition, the Peak Ground Acceleration (PGA) together with records of low to moderate earthquakes in Sabah from 2015 to May 2017 (Mw $\geq$ 4.0) were obtained from Malaysian Meteorological Department. With the help of Canvas X software, the PGA and earthquake recurrence dataset was compared with geomorphological features to produce a map and database of faults that have tectono-geomorphological expression.

The geological field investigation was carried out in February and April of 2017. The locations visited are shown in (Figure 4.28). A total of 50 outcrops are visited and most of these expose Miocene rocks that are dominantly sandstone interbedded with shale (Figure 4.29). Prior to the fieldwork, detailed mapping and tectonic interpretation of Ranau region was conducted to select the best suitable location for fieldwork. The second phase of this study potentially concentrates on measuring the displacement on active or inactive faults via GPR (Figure 4.38) and to identify subsurface deformation across the selected region. The locations for GPR survey were selected based on the map and database of earthquake generating faults, which were mapped according to the geomorphological parameters and past records of earthquake recurrence in this region.

3.2. Ground Penetrating Radar (GPR)

Ground Penetrating Radar (GPR) was an important aspect in this research. The equipment consists of five important components. Firstly, the Rough Terrain Cart (RTC) functions as an encoder, which measures the distance covered by the GPR. Also, it carries the rest of the components after assembly. The next feature is commonly known as an A/D converter, which is an Electronic Unit. The purpose of this unit is to act as an interface that converts signals from analog to digital and vice versa. It also connects to the RTC components, which triggers the transmitter to transmit a pulse. The main component of the GPR is the control unit, as it serves as a link to every component through a connection of wires.

Two antennas were used in this research primarily, a 50 MHz unshielded antenna (Rough Terrain Antenna), and a 500 MHz shielded antenna (Rough Terrain Cart). The 50 MHz was more consistently used, and it consisted of a single transmitter and receiver. The recorded data was observed through the monitor, which was used to visualize the sub – surface data while the survey was ongoing. The components mentioned above are displayed in Figure 3.2. The processing of the data used in several methods required all the necessary software to be installed. Further details on data processing are elaborated in the next section.

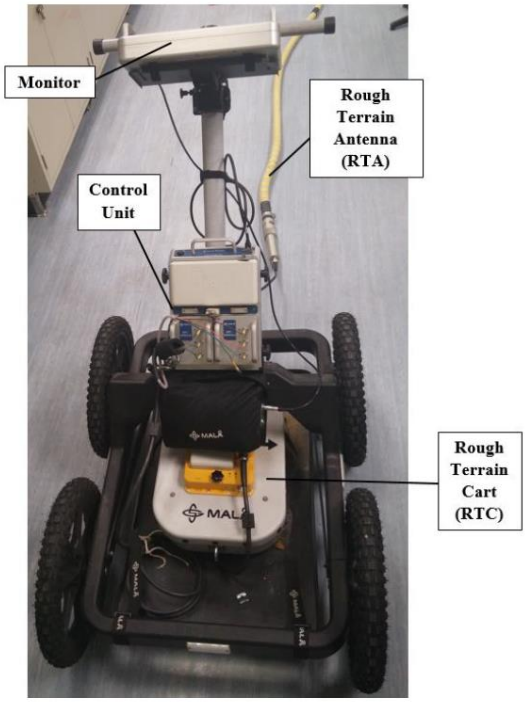

Figure 3.2 the labelled components of the GPR equipment.

3.2.1. Survey

Both 2 – Dimensional (2D) and 3 – Dimensional (3D) surveys were carried out to study the subsurface environment of the study area. Firstly, proper planning and risk assessment was done beforehand to ensure the effectiveness and safety of the GPR data collection.

2D survey

2D survey was done along Marakau road, near Paragliding Park and in areas with normal faults. In order to mitigate the risk, the person who was handling GPR had to wear a safety vest and push the GPR on the shoulder of the road. Also, it requires two person to handle a GPR to ensure that the 50 MHz unshielded RTA antenna, which has a ± 2 m flexible tube attached behind the cart, was always aligned with the GPR's movement. This is because the antenna might curve to the side when the GPR is going up or down a slope which may cause inaccurate dataset. Other than that, it was also to prevent the antenna from drifting to the driving lane. The person at the back was also in charge of recording the GPS location in the beginning and ending of the survey line. However, the most important aspect is that the GPR locations must be recorded at the last antenna of the RTA, as it was the receiver antenna. This was to ensure the accuracy of the locations of the survey line shown on a map.

3D Survey

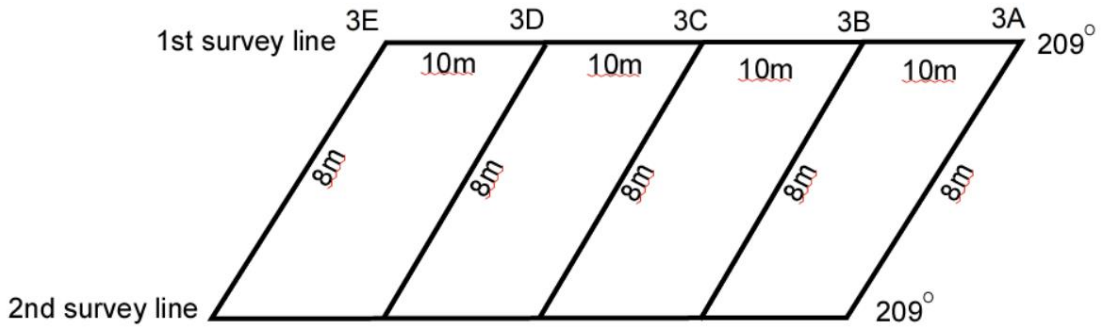

Figure 3.3 illustrates the sketch of a GPR 3D survey line.

The 3 – Dimensional survey was conducted on many waypoints, which are located in Marakau road. However, this particular survey required pushing the GPR on the side of the road as well as across it. Similar safety procedures as the 2D survey were needed, therefore extra planning was required for the process. The most suitable survey line for the 3D data acquisition was to have them parallel to the strike of the fault plane as well as perpendicular to it. In this case, the strike of the fault was 209, thus five lines were made across the road with a measured azimuth of 209 with one of the line being behind the fault plane as a reference point. These lines have an interval of 10 meters between one another. The layout of the survey line is displayed in Figure 3.3. In addition, to make the survey more effective in the field, all the lines were planned before carrying out the GPR survey and each of the lines were marked clearly on the field. One of the main challenges in this survey was that the side of the road was not wide enough to lay out the 50 MHz antenna. Therefore, the 3D survey was conducted with 500 MHz antenna only, which is limited to only 5m penetration depth.

3.2.2. Ground Penetrating Radar (GPR) Data Processing

The Mala Radexplorer software was used to process GPR dataset. This is a commercial software which requires a USB dongle to start the software, which was provided along with the program.

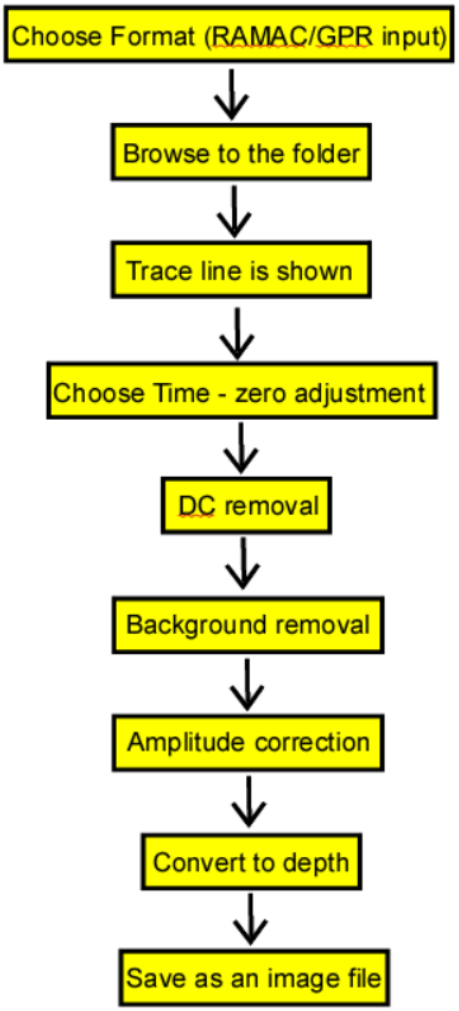

Figure 3.4 explains the GPR processing steps.

3.3. Stream network and Watershed boundaries

Stream network and watershed boundaries were generated using hydrology tools under the spatial analyst function. The most important step before initiating is Georeferencing the satellite image to WGS 1984. The following step involves the use of Fill tool, which will help to remove any voids and filling sinks. From here, the Flow Direction is applied to show the steepest direction from the grid cells, followed by the Flow Accumulation tool. This tool helps to accumulate grid cells that are draining to any specific cells in the Digital Elevation Model (DEM). However, if the attribute table for flow accumulation is not available, it must be built. This process is essential as the recorded data on stream network will be stored here. To build an attribute table, Data Management tools is selected and followed by raster properties. After creating the attribute table, stream can be generated with the aid of the Stream Link tool, which assigns a unique number to each stream segment in the raster format. After this step, the Stream Order tool is selected to organize the stream network in order. The following step is using the Stream to Feature tool. This step is vital because it converts from raster format to polyline feature class. Therefore, by converting to a different class, the Flow Length tool can be used to measure the flow distance from each grid cell to downstream segment of Digital Elevation Model (DEM). By completing the previous step, the drainage basin can be created with the Basin tool. This particular tool connects the grid cells with the same features to form a drainage basin. The final step of stream generation is creating the watershed boundary. This feature converts from raster format to polygon.

Chapter 4
Results and Interpretation

4.1. Geomorphic Mapping and SL index

The formation of knickpoints is one of the key geomorphic indices that are used to map the active geomorphic features related to tectonic or gravitational forces (Malik & Mohanty, 2007; El Hamdouni et al., 2008; John & Rajendran, 2008; Pedrera et al., 2009; Dehbozorgi et al., 2010; Font et al., 2010; Toudeshki & Arian, 2011; Dar et al., 2014; Mathew et al., 2016a; 2016b). The work presented below shows that a number of knickpoints locations are mapped in the study area (Figure 4.3). For example, multiple knickpoints along Sg. Mesilou are related to SE dipping normal fault (Kinabalu Park Fault) that we have mapped and such a configuration coincides with the knickpoints along the upstream region of Mesilou B (Figure 4.3). The evidence from geomorphic mapping suggest most of the normal faults in Ranau and Kundasang region display E – SE dipping with N – S or NE – SW trend (Figure 4.1). A number of channels are offset along the faults, which varies from few centimetres to kilometres. For example, the Mesilou B shows deflected stream along the Kinabalu Park Fault. However, the deflection of Sg. Mesilou is not consistent across the faulting region, and this implies that a number of reactivation events may occur. Also, we have mapped a few triangular facets, which represents the remnant of old faults. The intermontane basins in Ranau region shows the evidence of NW - SE extension which led to normal fault subsidence (e.g. Marakau Fault) (Fig 4.1). Ostensibly, most of the basins are concentrated along the eastern part of Mt. Kinabalu and, this proves that most extension occurred mainly along this region.

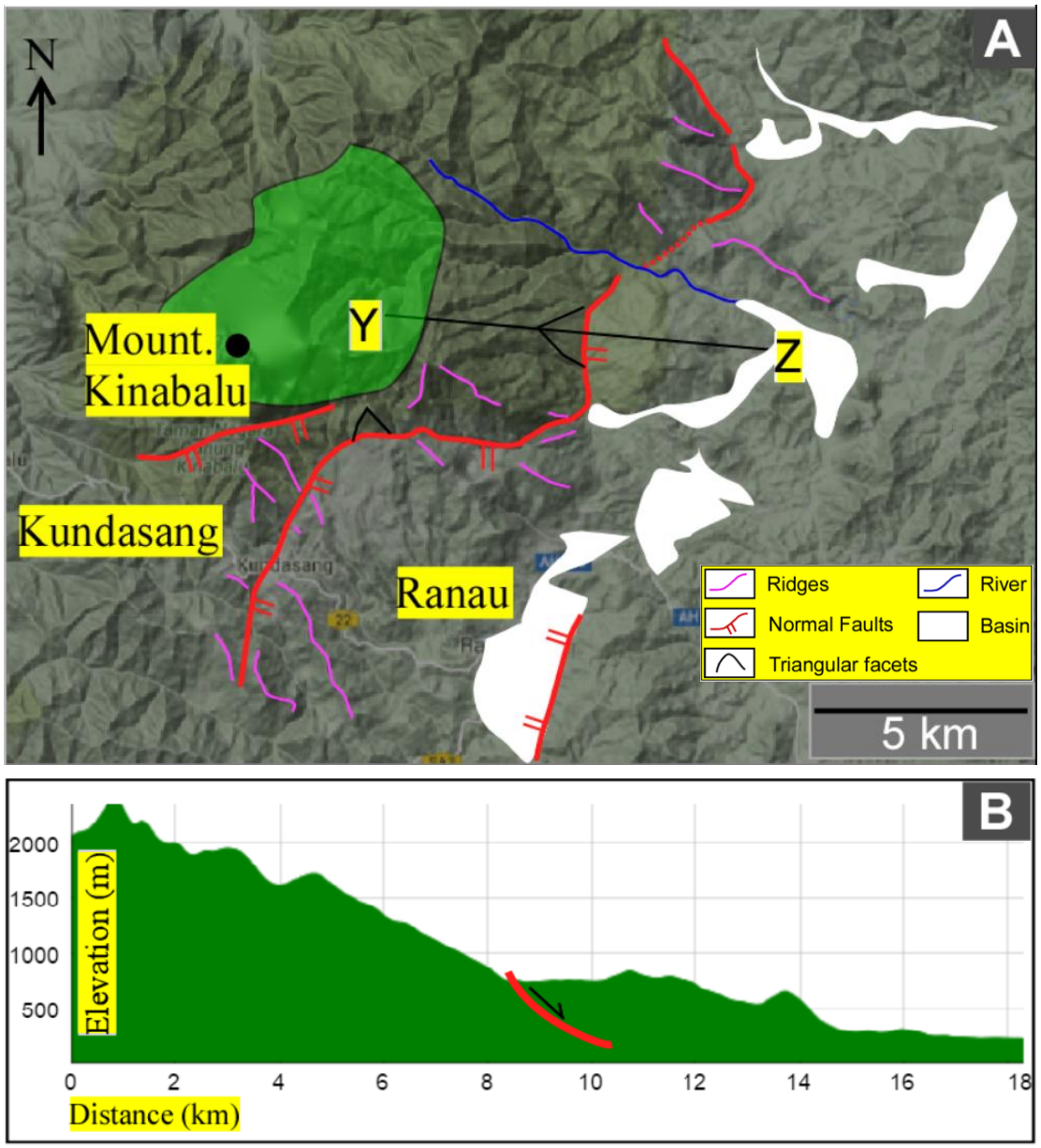

Figure 4.1 depicts the Mt. Kinabalu and its surrounding regions, specifically on Kundasang and Ranau region. (A) Interpreted Google Image (B) Topographic Profile.

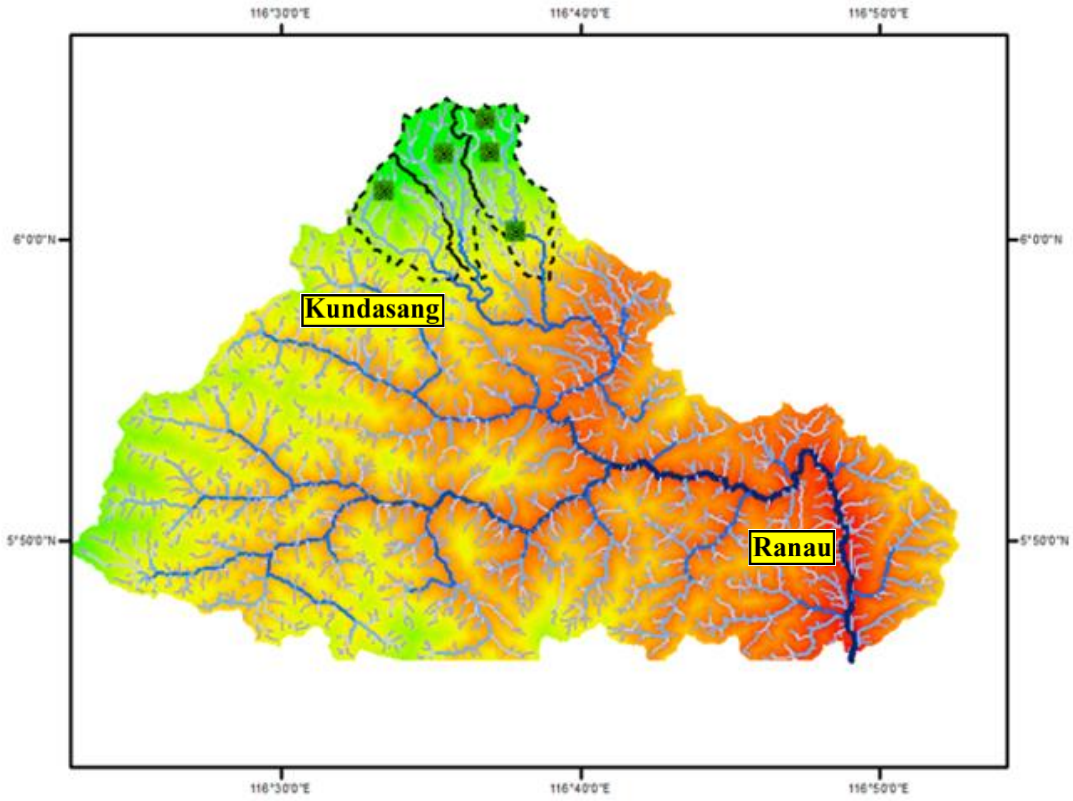

No	Date	Time (UTC)	ml ≥4.0	Depth(km)
1	2015-06-04	23:15:45	6.0	9.0
2	2015-06-05	13:12:16	4.2	10.0
3	2015-06-17	21:58:22	4.0	10.0
4	2015-06-23	09:32:30	4.3	13.4
5	2015-07-26	16:10:10	4.4	10.0

Figure 4.2 the sub – basin of Mt. Kinabalu and its surroundings. The study area and drainages across the region is illustrated above.

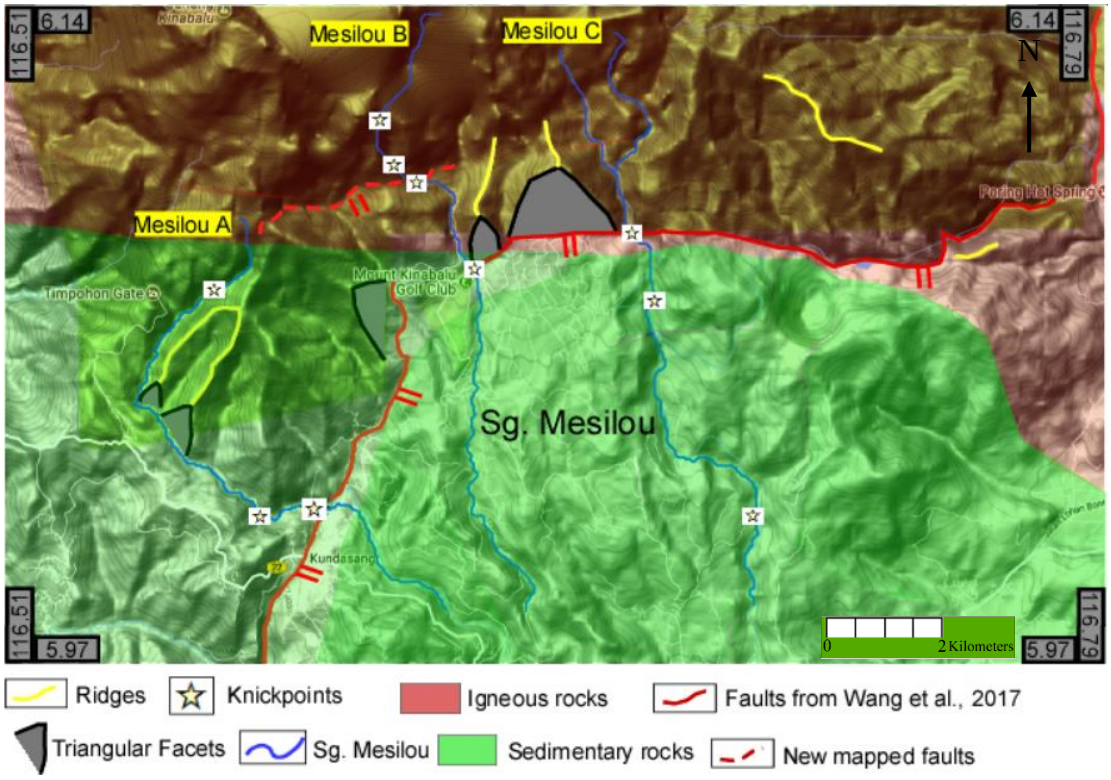

Figure 4.3 rock types and knickpoints overlaid on the topographic map.

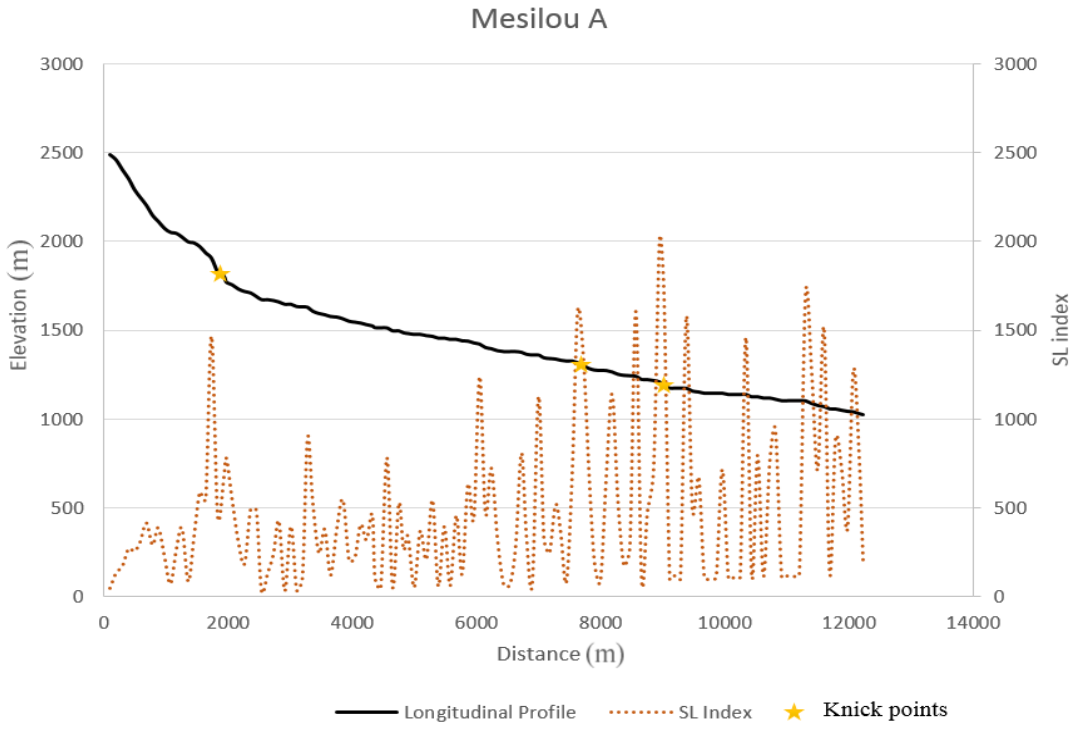
Mesilou A
Elevation (m)
SL index
Distance (m)
0
500
1000
1500
2000
2500
3000
0
2000
4000
6000
8000
10000
12000
14000
Longitudinal Profile
SL Index
Knick points

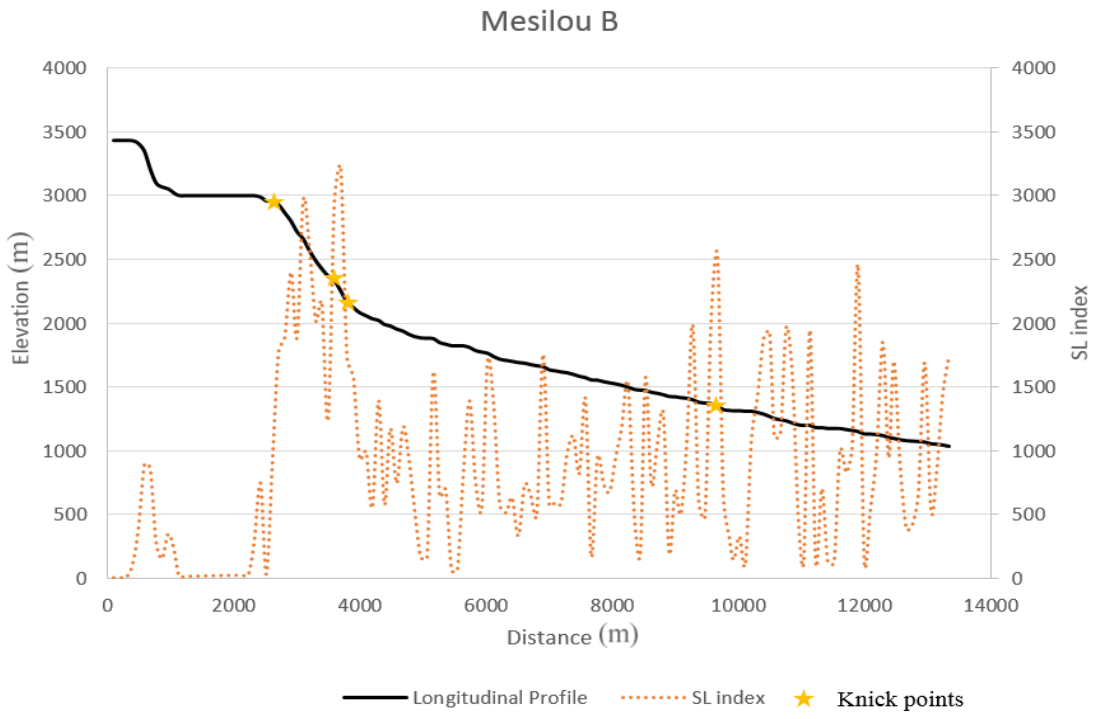
Mesilou B
Elevation (m)
SL index
Distance (m)
0
500
1000
1500
2000
2500
3000
3500
4000
0
2000
4000
6000
8000
10000
12000
14000
Longitudinal Profile
SL index
Knick points

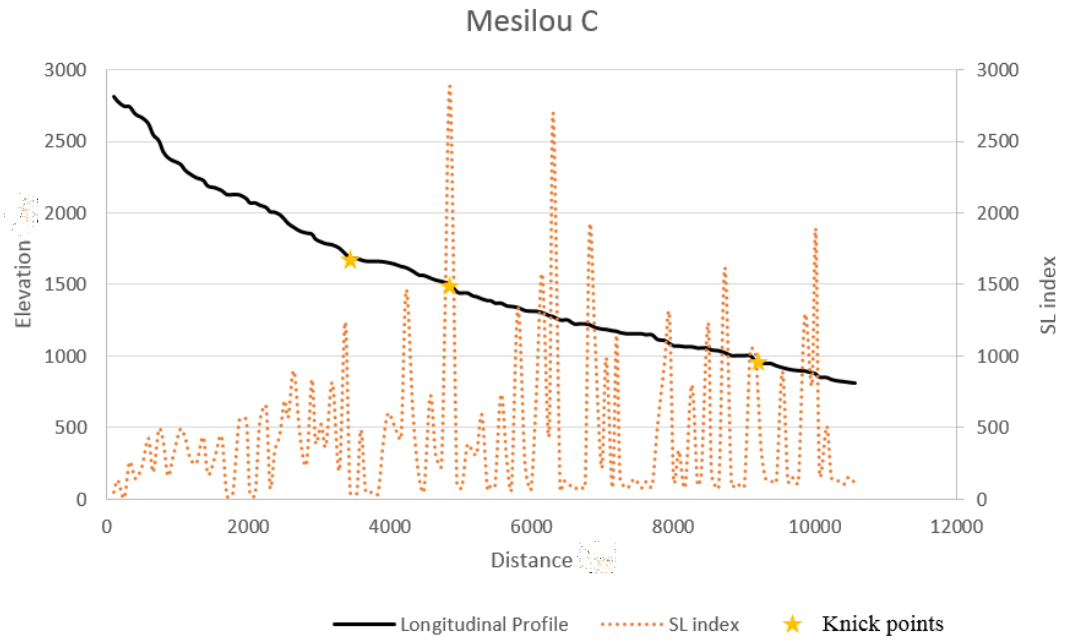

Figure 4.4 the longitudinal profile and SL index of Sg. Mesilou A, B and C.

Based on Figure 4.4, the knickpoints along River A and C seems to occur at an elevation of between 1000 and 2000 m while River B is between 2000 and 3000 m. However, the evidence of normal faulting along the upstream region of River B is remarkable as such landform displays a huge displacement on SE direction, which accommodates almost 600 m movement on the hanging wall (red box on River B profile). This particular normal fault appears to be steeply dipping and coincides with the geomorphic mapping. Therefore, our findings provide some insights into the evidence of normal faulting across Mt. Kinabalu and its surroundings. Based on Figure 4.2, the mainshock and aftershock of 5th June 2015 earthquake occurred in similar areas, possibly related to the mapped faults.

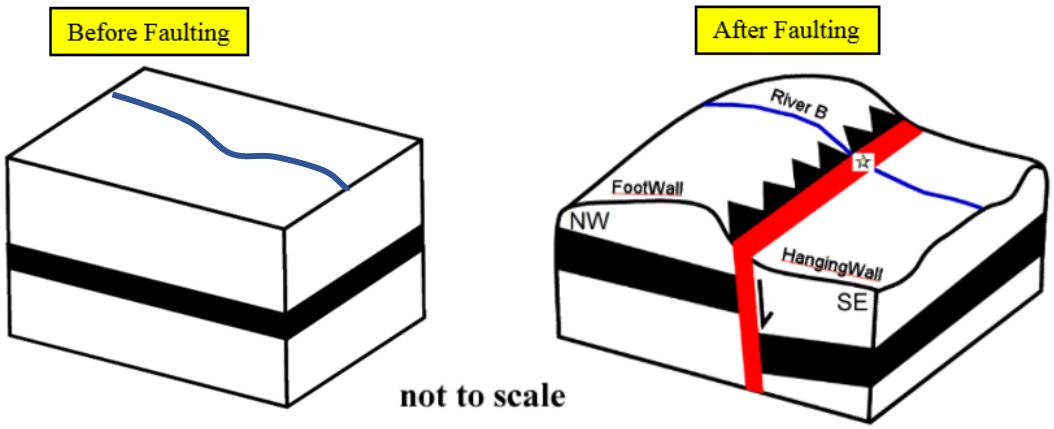

Figure 4.5 depicts two models with before and after faulting features. The model seems to accommodate the NW – SE extension, which led to S – SE dipping normal faults.

To further validate our findings, a descriptive model with S – SE dipping normal faults are shown in Figure 4.5. Such model presents NW – SE extension along River B, with clear faulting expression, triangular facets and knickpoint. Also, the regional evidence shows similar faulting style across the eastern section of Mt. Kinabalu areas as illustrated in Figure 4.1.

4.2. Elongation Ratio

The level of tectonic complexity across north central zone was determined using the area and length of the basin. Morphometric analysis was carried out in the respective locations, which are tectonically unstable and experience frequent recurrence of earthquakes. The elongation ratio calculation shows that sub – watersheds that are less than 0.7 are subjected to tectonic activity.

Elongation ratio of watershed boundary:

a) (< 0.7) – Highly elongated

b) (0.7 to 0.8) – Slightly elongated

c) (0.8 to 0.9) – Oval

d) (0.9 to 1.0) – Circular

However, Ranau and Kundasang are located in a slightly elongated region, which implies that these regions experience lesser tectonic activity compared to highly elongated regions. On the contrary, such an interpretation seems inadequate and obscured because Ranau and Kundasang

region frequently experience intraplate earthquakes around Mt. Kinabalu (Tongkul et al., 2017; Wang et al., 2017).

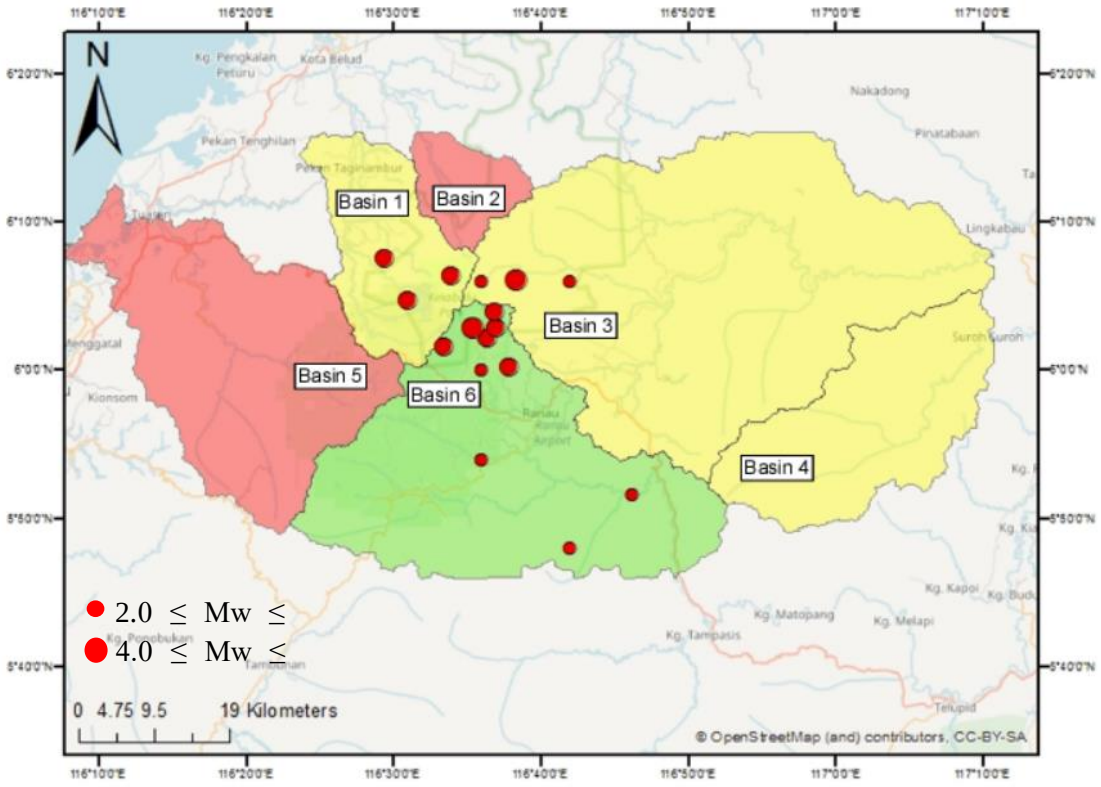

Figure 4.6 the elongation ratio for the study area

Based on Figure 4.6, 6 watershed boundaries were studied using the elongation ratio method. This however shows that most intraplate earthquakes are clustered in and around NW Borneo, specifically in Basin 6. This particular basin is surrounded by a range of earthquakes, which includes the 5th June 2015 and 8th March 2018 events.

Table 4.1
The elongation ratio for 6 watersheds boundary across north central zone.

Watershed No.	Elongation Ratio	Indication	Intensity of tectonic activity
1	0.693	Highly elongated	Very High
2	0.869	Oval	Low
3	0.697	Highly elongated	Very High
4	0.667	Highly elongated	Very High
5	0.814	Oval	Low
6	0.772	Slightly elongated	High

The intensity of deformation seems very peculiar across this region as it demonstrates lesser tectonic activity in an area where earthquake occurs frequently. However, other basins such as 1, 3 and 4 illustrates very high intensity and these basins are surrounding the Mt. Kinabalu region as portrayed in Figure 4.6

4.3. Hypsometry Integral

From the hypsometric curves of upstream region, it can be observed that the selected regions reflect both concave and convex curves. In certain parts of the location, it exhibits an S – shaped curve. Within this localized tectonic framework, we are able to demarcate the elevation and area of the sub – basins to elucidate the level of erosion across this region. The hypsometry curve below reflects the age and level of tectonic complexity, which might provide a solid evidence for the prevalence of intensive deformation and frequent recurrence of intraplate earthquakes. Thus, the analysis was carried out in areas which are considered tectonically unstable and frequently experiencing low to moderate earthquakes.

HI for selected regions:

a) Values close to 0 indicates the region is old and highly eroded

b) Values close to 1 indicates the region is young and slightly eroded

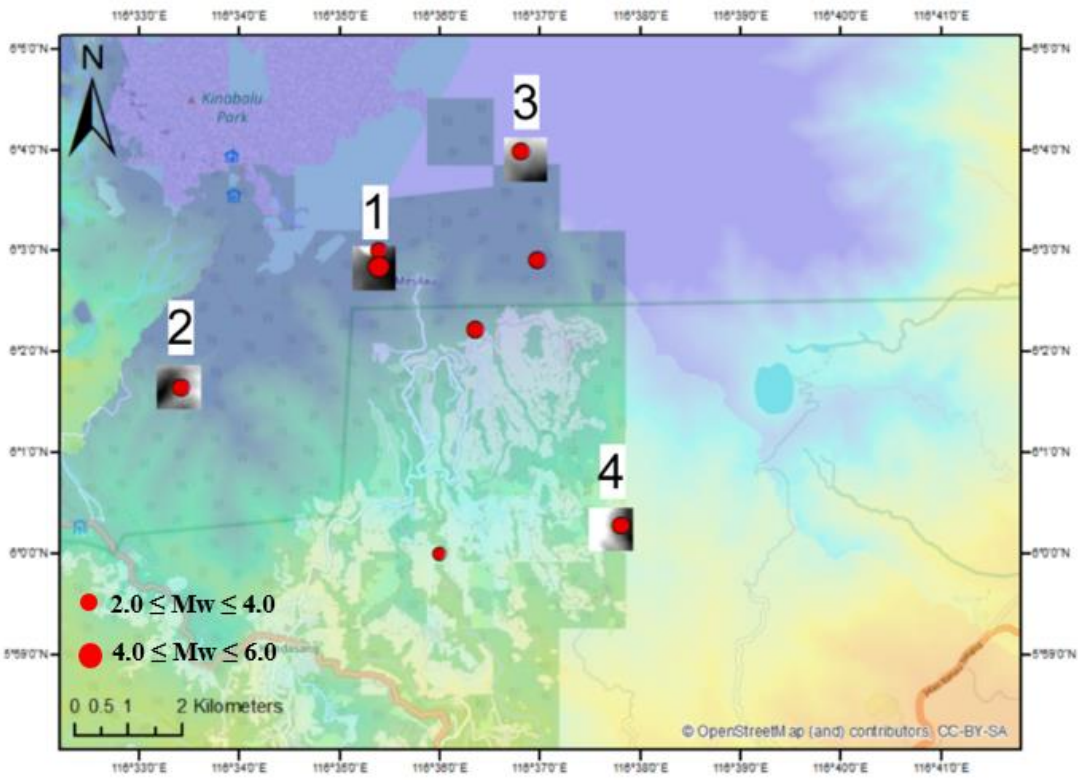

Figure 4.7 Map of tectonically unstable areas in Ranau and Kundasang

Hypsometric analysis was selected in areas where the majority of earthquake recurrence occurs. The four major areas can be further sub – divided into 12 basins to elucidate the complexity of the region. Most of these hypsometry curves were correlated with faulted regions to conclude our evidence on geomorphic mapping across this region. However, there is a clear variation in the shapes of the curve, which implies the changes in boundary conditions shows a mixed of deformation that have shaped the current topography of the study area.

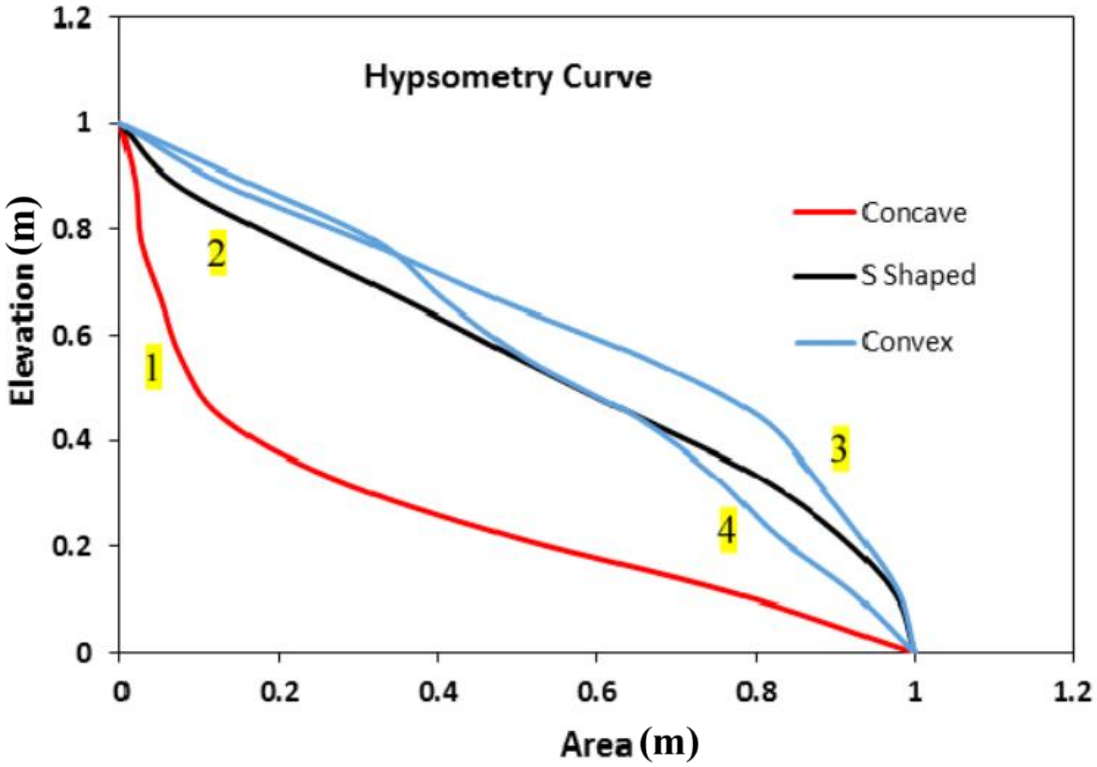

Figure 4.7 the hypsometry curve of Area 1, 2, 3 and 4.

Based on Figure 4.7, it can be observed that Area 1 reflects concave curves, which clearly indicates old and highly eroded regions. On the contrary, Area 3 and 4 attains a convex and complex hypsometric curve. This can be attributed to young and slightly eroded region. The data clearly demonstrates an upliftment trend across the eastern part of the study area. But it does not provide any constraint on the location of active faulting. Moreover, Area 2 seems to have acquired an S – shaped curve, which signals to a moderately eroded region. The upstream region of the area seems to be concave and progressively changed to convex as it moves downstream.

Table 4.2
The hypsometric integral of Area 1, 2, 3 and 4 in Ranau and Kundasang region.

No.	Hypsometric Integral	Curve	Indication
1	0.365	Concave	Old, highly eroded region
2	0.460	S - shape	Moderately eroded
3	0.538	Convex	Young, slightly eroded region
4	0.487	Convex	Young, slightly eroded region

According to Table 4.2, the rate of erosion across the region is identified. It clearly demonstrates the stages of geomorphic development (youthful, mature, subdued peneplain stage, variation in denudational processes) (Strahler, 1957). In the study area, three stages of erosion cycle development were determined. Mainly, youthful stages are identified across Area 3 and 4, while mature and subdued peneplain stage were concentrated in Area 1 and 2. The comparison between different hypsometry curves provides the changes in the initial stage of slope prior to its watershed development.

Area 1

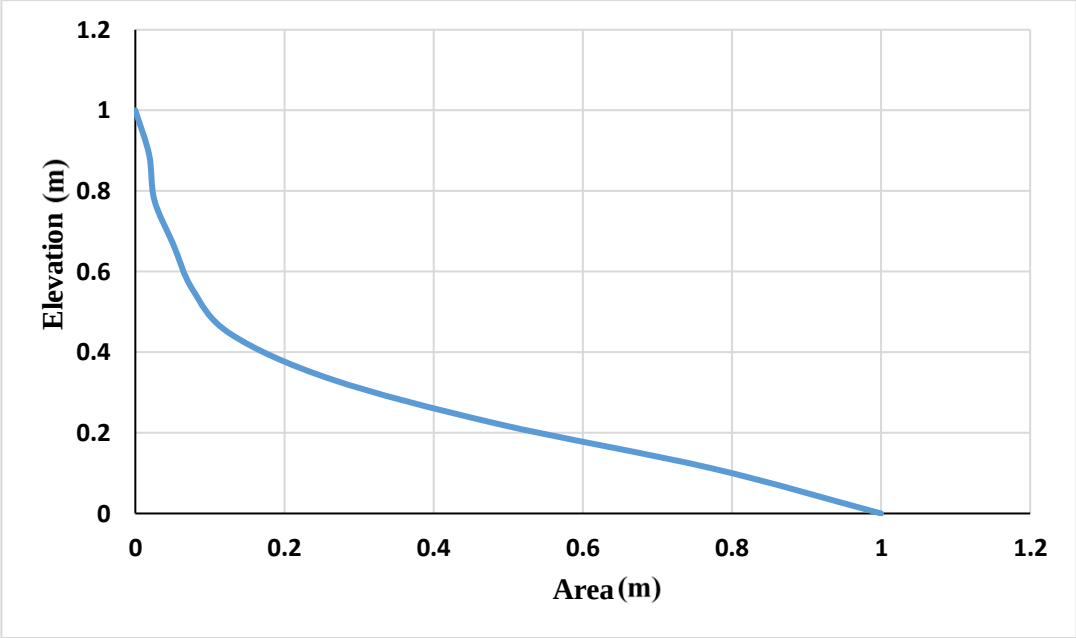

Figure 4.8 the subdued peneplain stage of a basin

Area 2

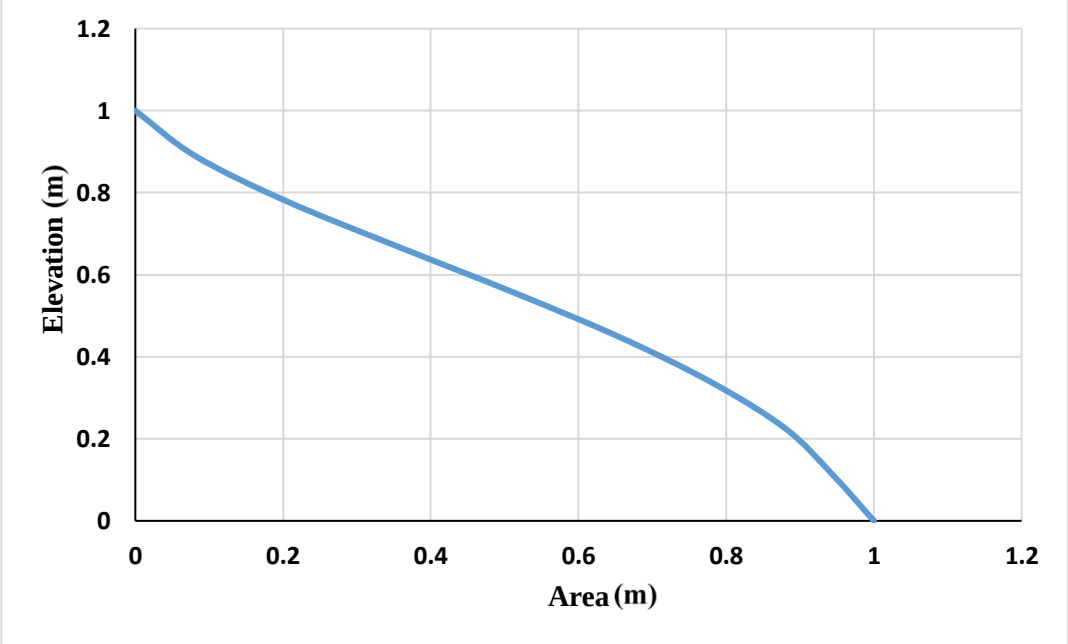

Figure 4.9 the mature stage of a basin

Area 3

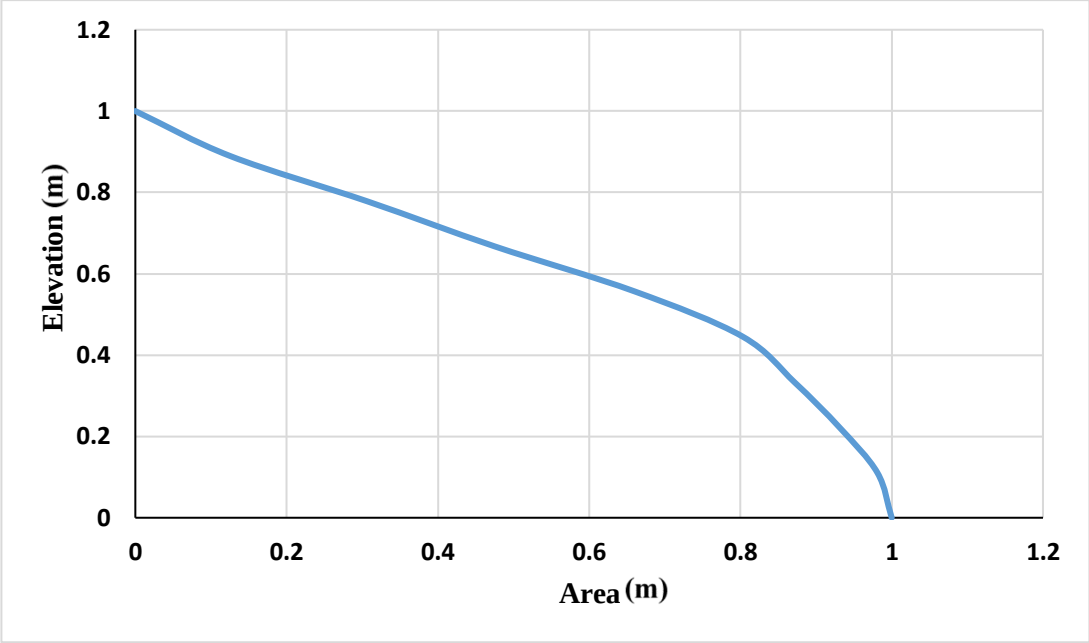

Figure 4.10 the youthful stage of a basin.

Area 4

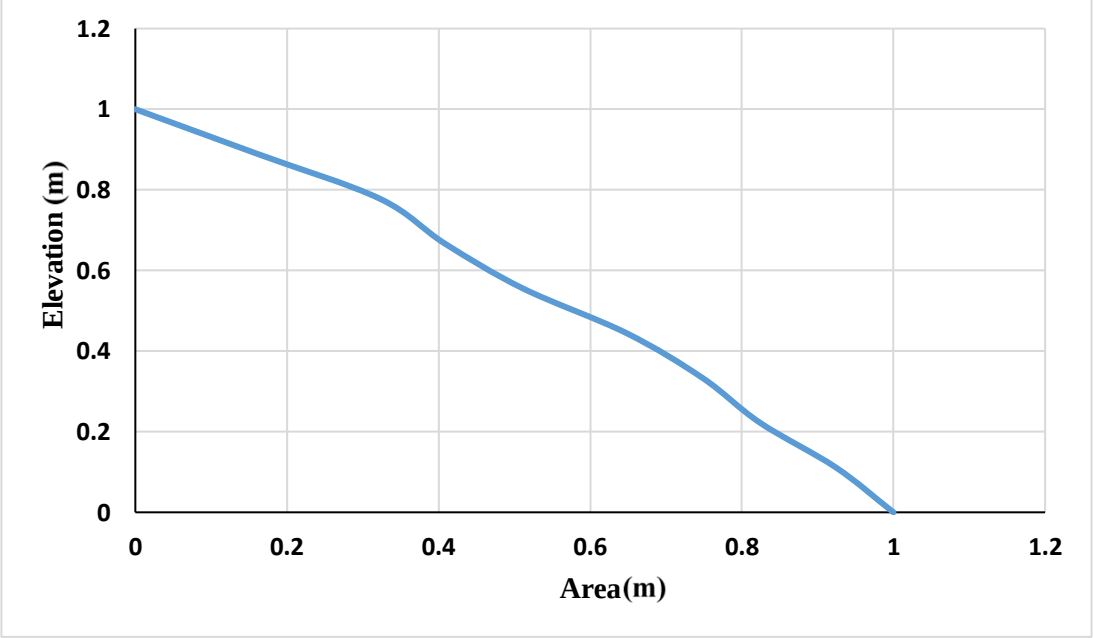

Figure 4.11 the youthful stage of a basin.

4.3.1. Sub – Basin 1

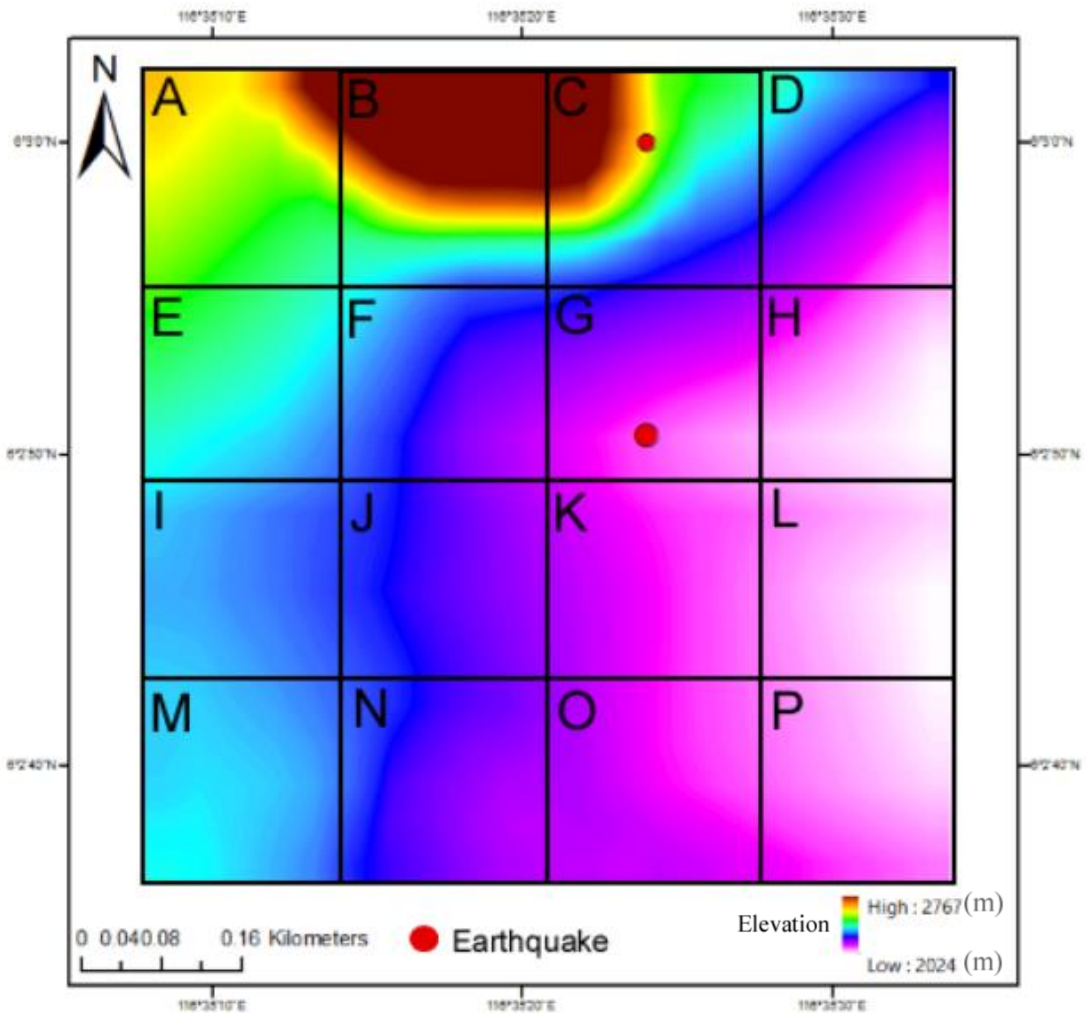

Figure 4.12 the sub – basin 1.

Area 1 was sub – divided into 16 equal grids to explain the variation in denudational processes within the basin. The 200 m x 200 m subdivision provides various geomorphic stages across the region, mainly dominated by concave and complex curves which shows the subdued peneplain stage of the basin.

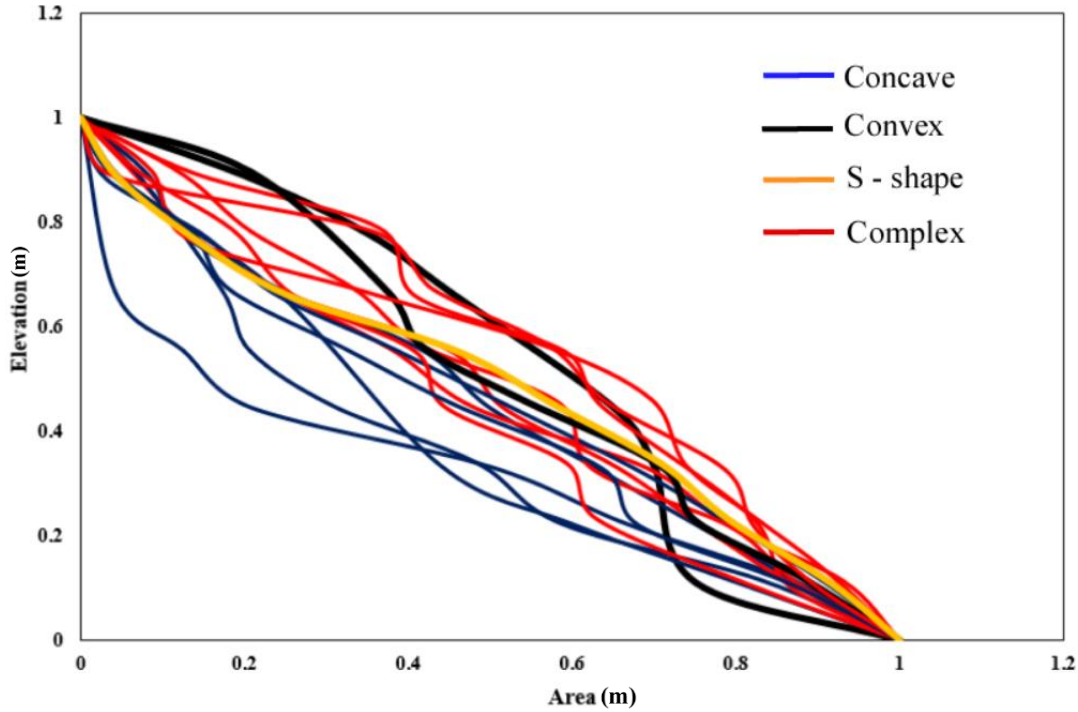

Figure 4.13 depicts the geomorphic stage of sub basin 1

Our tectono - geomorphic assessment provides robust evidence of a wide variety of geomorphic stages within the sub - basins. However, there are clear variations in the shape of the basin as portrayed in Figure 4.13 (sub – basin graph). Accordingly, complex features seem to be experiencing variation in denudational processes as well as topography. Rapid change of elevation in relatively short distance might illustrate its irregular form. This interpretation implies that it could be tectonically controlled. On the contrary, two convex curves were identified and it appears to form youthful at initial stage and subdues progressively as it moves downstream.

Table 4.3
The hypsometric integral, curve and its indication on sub - basin 1

No.	Hypsometric Integral	Curve	Indication
A	0.246	Concave	Old, highly eroded region
B	0.519	Convex	Young, slightly eroded region
C	0.359	Concave	Old, highly eroded region
D	0.380	Concave	Old, highly eroded region
E	0.403	Complex	Variation in denudational process
F	0.374	Complex	Variation in denudational process
G	0.390	Concave	Old, highly eroded region
H	0.272	Concave	Old, highly eroded region
I	0.506	Complex	Variation in denudational process
J	0.421	Complex	Variation in denudational process
K	0.401	Complex	Variation in denudational process
L	0.438	Convex	Young, slightly eroded region
M	0.489	Complex	Variation in denudational process
N	0.388	Concave	Old, highly eroded region
O	0.493	Complex	Variation in denudational process
P	0.417	S – Shape	Moderately eroded

Based on Table 4.3, the sub – basins of Area 1 exhibits various topographic landforms, which could be a direct evidence of complex deformation across this region. It appears to form variations in denudational process, which might provide an insight into tectonic processes of north central zone. However, S – shape curve was identified towards the downstream area, which suggests mature basin that are moderately eroded.

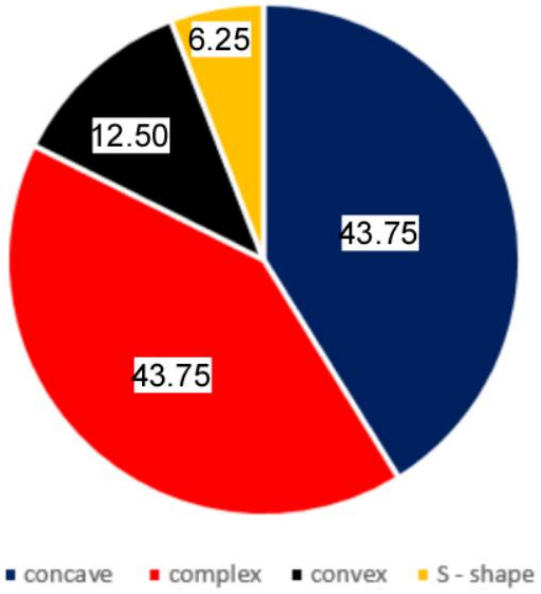

Figure 4.14 the four main curves in sub - basin 1.

Figure 4.14 shows concave and complex curve contributes to 87.5 % of the area, such interpretation implies variations in boundaries conditions that lead to different geomorphic stages across the region. In addition, convex and S – shape curves covers about 12.5 % and 6.25 % of the area, which is minimal in comparison with concave and complex curves.

4.3.2. Sub – basin 2

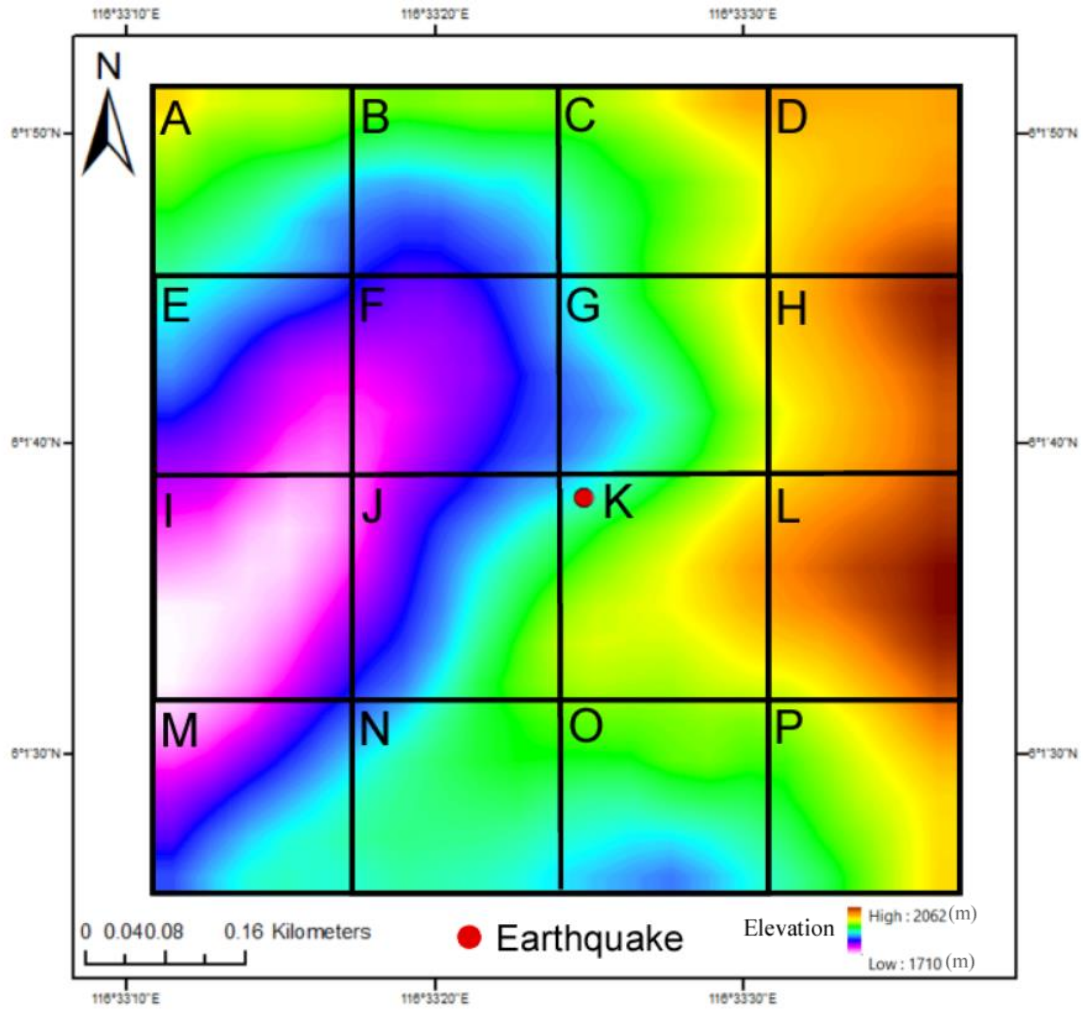

Figure 4.15 the sub – basin of Area 2.

Based on Figure 4.15, the areas are equally sub – divided into 16 grids (200m x 200m). The highest elevation across this area is 2062 m, which is located nearby the Kundasang region. However, the hypocentres seem to have occurred at an elevation of between 1800 – 1900 m.

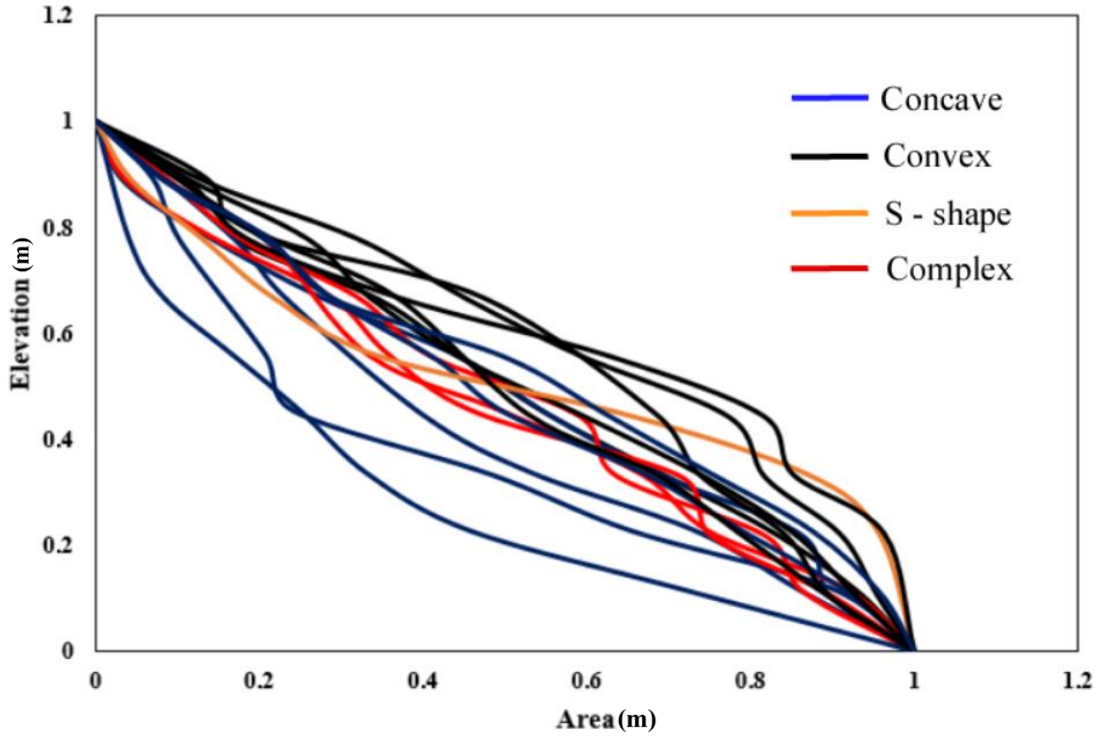

Figure 4.16 demonstrates the hypsometric curves across sub – basin 2.

Mainly controlled by convex and concave curves. Within the localized tectonic framework, erosion is occurring rapidly which led to a high percentage of concavity and complex features across this region.

Table 4.4
Hypsometric integral, curve and its indication across Area 2.

No.	Hypsometric Integral	Curve	Indication
A	0.429	Convex	Young, slightly eroded region
B	0.411	Concave	Old, highly eroded region
C	0.401	Concave	Old, highly eroded region
D	0.273	Concave	Old, highly eroded region
E	0.374	Complex	Variation in denudational process
F	0.391	Complex	Variation in denudational process
G	0.442	Complex	Variation in denudational process
H	0.403	Concave	Old, highly eroded region
I	0.218	Concave	Old, highly eroded region
J	0.472	Convex	Young, Slightly eroded region
K	0.461	S – shape	Moderately eroded
L	0.542	Convex	Young, slightly eroded region
M	0.571	Convex	Young, slightly eroded region
N	0.539	Convex	Young, slightly eroded region
O	0.527	Convex	Young, slightly eroded region
P	0.430	Concave	Old, highly eroded region

Based on Table 4.4, the area appears to be topographically young and slight erosion can be seen towards the downstream region. In contrast, higher elevation areas are dominated by both concave and complex curves, which indicates a variation in denudational process. Such a variation occurs specifically in centre of the area. However, our findings suggest that earthquake hypocentres in Area 2 occurred on a mature basin and possibly explains the complex nature of inactive and active faulting across the area.

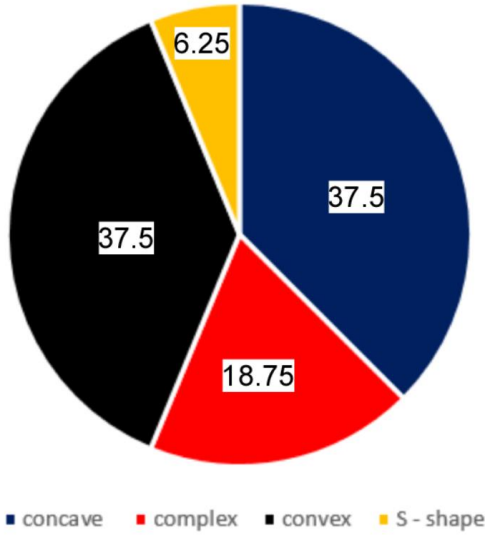

Figure 4.17 the four main curves in Area 2

According to Figure 4.17, the majority of the area is mainly controlled by concave and convex curve, which is about 75% of the area. Such interpretation implies that variations in erosional processes can form different features within the region. Ostensibly, the complex structures seem to be dominating 18.75% of the area, which is relatively high for such curves. From observation, the complex features tend to form lesser in areas with high percentage of young topographic terrain.

4.3.3. Sub basin 3

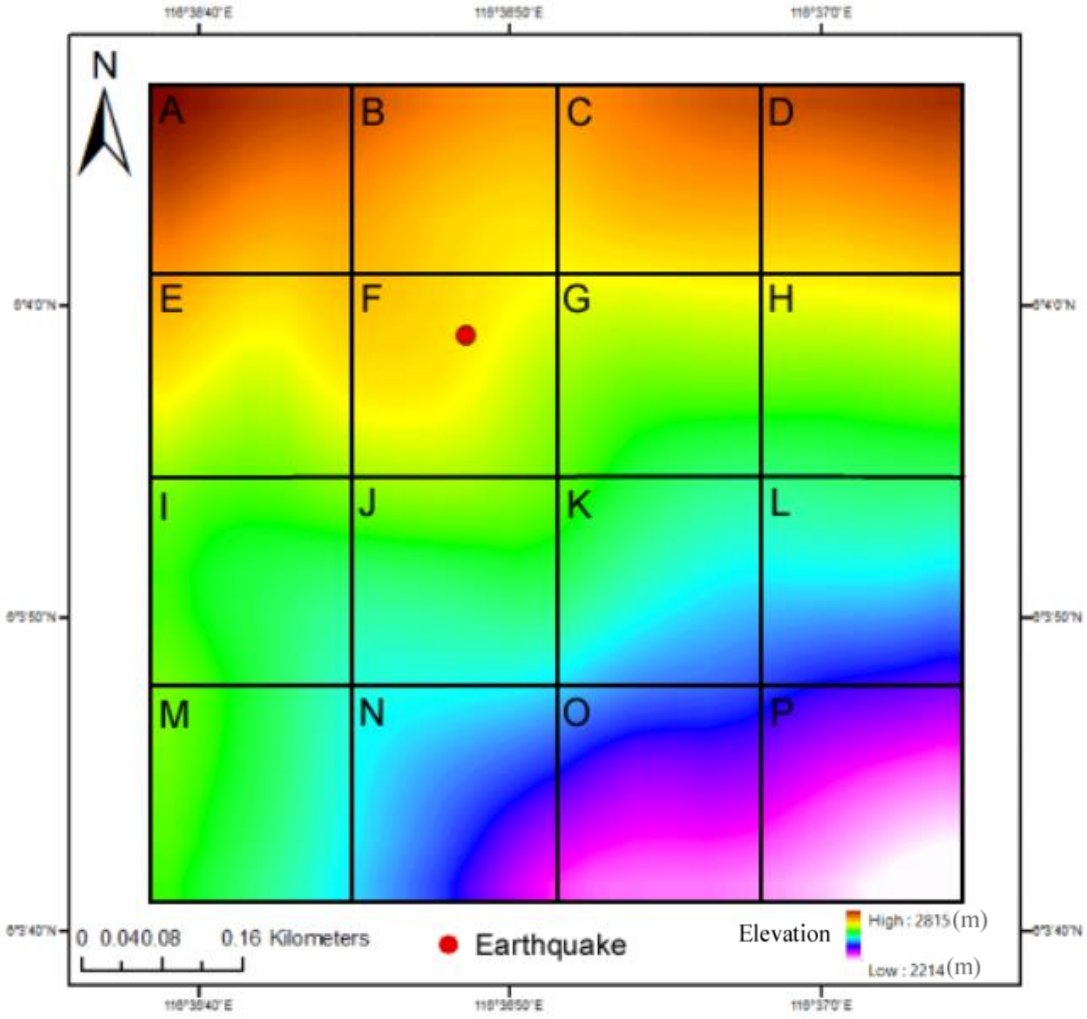

Figure 4.18 the sub – basin 3.

Based on Figure 4.18, the areas are equally sub – divided into 16 grids (200 m x 200 m). The highest elevation across this area is 2815 m, which is located away from Kundasang and Ranau region. However, the hypocentres seem to be located at an elevation of between 2600 and 2800 m.

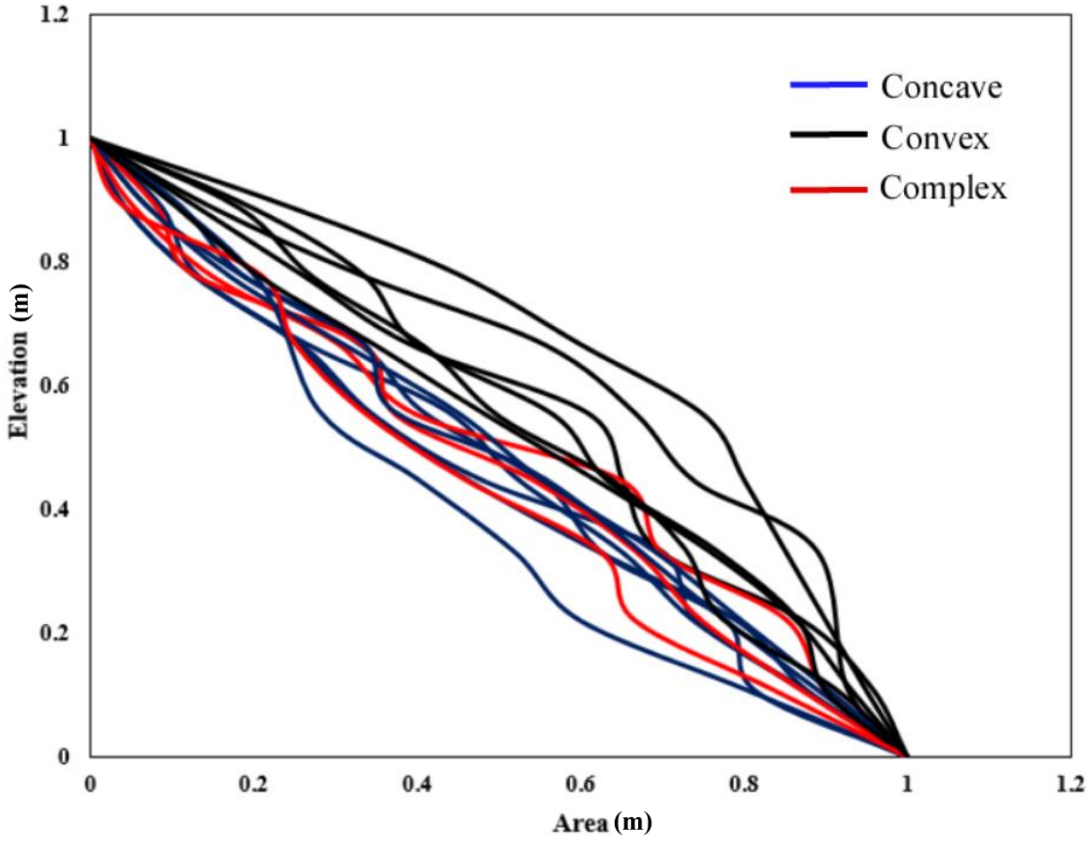

Figure 4.19 the hypsometric curves across the sub – basin 3.

Based on Figure 4.19, Area 3 is controlled by young topography with slight erosion. This seems peculiar as previous studies have postulated that the entire region is experiencing rapid erosion rate (Mathew et al., 2016a; 2016b; Menier et al., 2017). However, it proves that within a localized framework we can expect various complex features in response to regional scale structures.

Table 4.5
Hypsometric integral, curve and its indication across sub – basin 3.

No.	Hypsometric Integral	Curve	Indication
A	0.397	Concave	Old, highly eroded region
B	0.357	Concave	Old, highly eroded region
C	0.395	Concave	Old, highly eroded region
D	0.414	Concave	Old, highly eroded region
E	0.390	Complex	Variation in denudational process
F	0.483	Convex	Young, slightly eroded region
G	0.512	Complex	Variation in denudational process
H	0.413	Concave	Old, highly eroded region
I	0.568	Convex	Young, slightly eroded region
J	0.406	Concave	Old, highly eroded region
K	0.412	Concave	Old, highly eroded region
L	0.538	Convex	Young, slightly eroded region
M	0.491	Convex	Young, slightly eroded region
N	0.640	Convex	Young, slightly eroded region
O	0.343	Complex	Variation in denudational process
P	0.445	Convex	Young, slightly eroded region

Table 4.5 illustrates the erosional stages in response to various tectonic movements. It appears to be topographically young, which suggest slight erosion across this region. However, the upstream area is old and highly eroded owing to climate perturbations. With such variation in denudational process, we are able to demarcate the earthquake distribution and erosional features within this tectonic framework. However, the earthquake distribution across Area 3 suggest differently, as it shows topographically young features with slight erosion. Therefore, the results seem consistent with regional hypsometry curves.

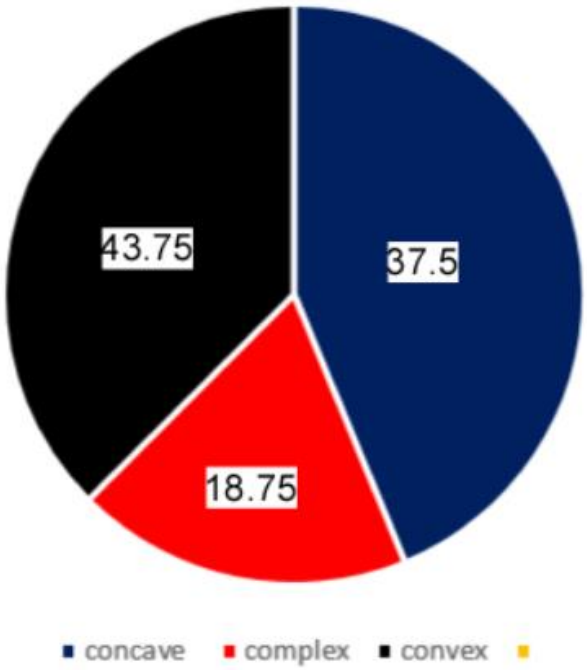

Figure 4.20 the main curves of sub – basin 3.

Figure 4.20 clearly demonstrated that the sub – basin of Area 3 is consistent with regional hypsometric curves. The entire region is mainly controlled by convex curves (topographically young), which is about 43.75% of the total area. However, the complex features are unusually high in areas which are dominantly controlled by young terrains. Owing to climatic perturbations, we can expect relatively high percentages of concavity across this region.

4.3.4. Sub – basin 4

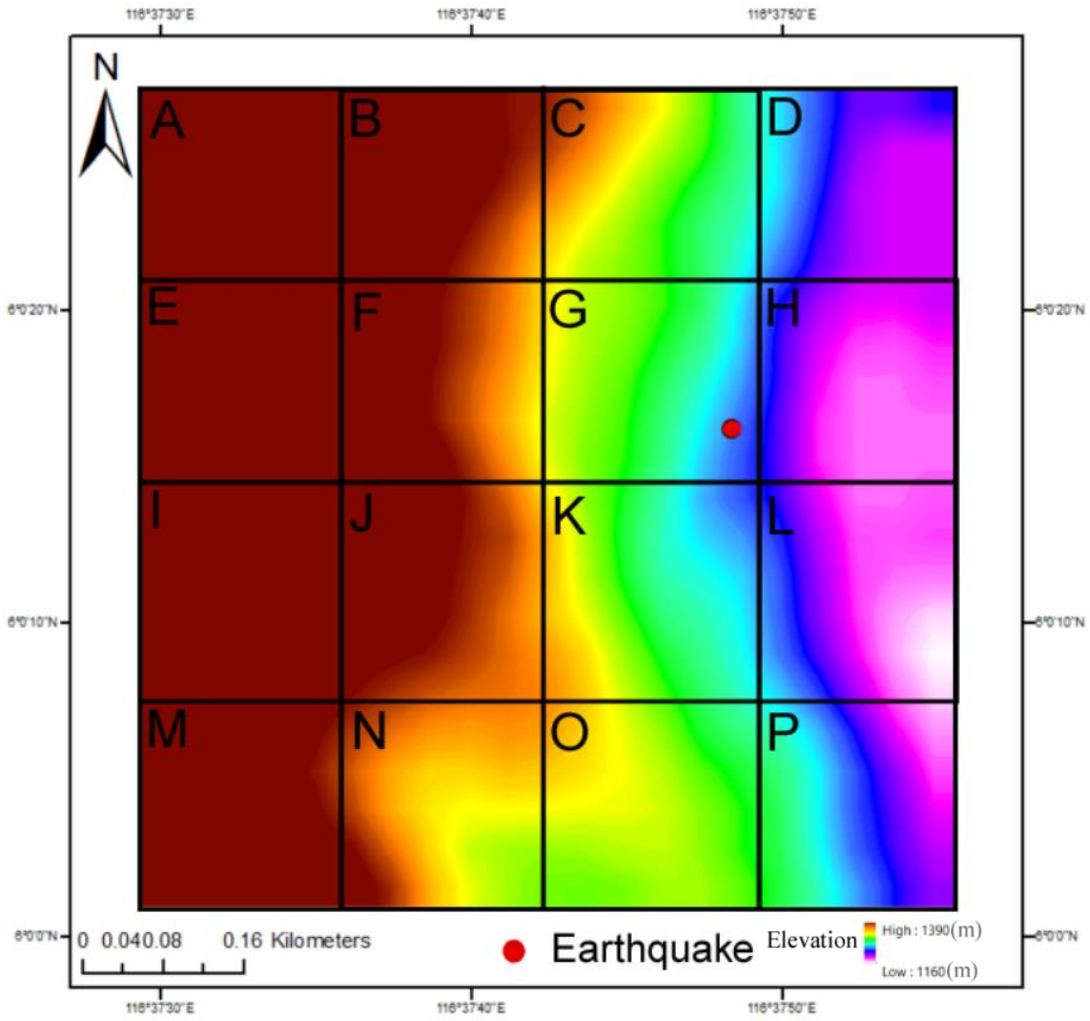

Figure 4.21 the sub – basin 4.

Based on Figure 4.21, the areas are equally sub – divided into 16 sections (200m x 200m). The highest elevation across this area is 1392m, which is located nearby to the Kundasang and Ranau region. However, the earthquake hypocentres seem to have occurred at an elevation of between 1200 and 1300m.

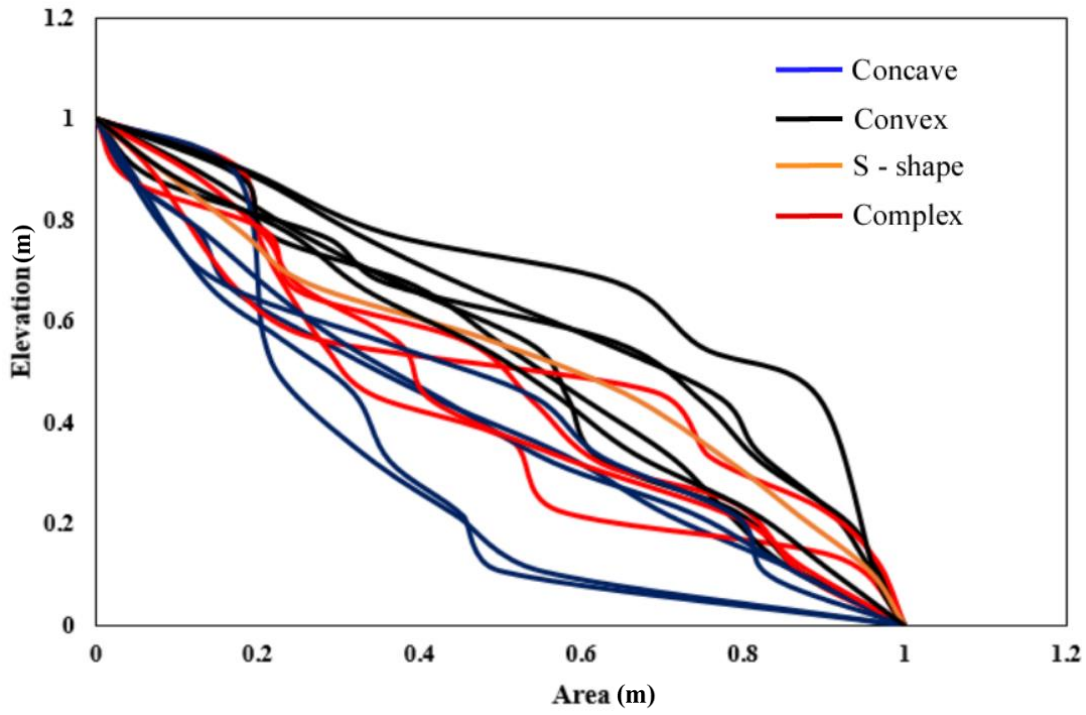

Figure 4.22 demonstrates the hypsometric curves across the sub – basin 4.

The area mainly consists of young and slight erosion regions, which is about 37.5% of the area. However, the complex features are relatively high, especially in a topographically young area, which covers about 25%. In contrary, there is no clear pattern of geomorphic stages across this region and it appears to be scattered. Owing to high rate of concavity curves, the sub – basin seems to have formed in old and highly eroded regions as well.

Table 4.6
Hypsometric integral, curve and its indication across sub – basin 4.

No.	Hypsometric Integral	Curve	Indication
A	0.513	Convex	Young, slightly eroded region
B	0.573	Convex	Young, slightly eroded region
C	0.328	Concave	Old, highly eroded region
D	0.276	Concave	Old, highly eroded region
E	0.350	Complex	Variation in denudational process
F	0.458	Convex	Young, slightly eroded region
G	0.522	Convex	Young, slightly eroded region
H	0.226	Concave	Old, highly eroded region
I	0.415	Complex	Variation in denudational process
J	0.399	Complex	Variation in denudational process
K	0.363	Concave	Old, highly eroded region
L	0.368	complex	Variation in denudational process
M	0.608	Convex	Young, slightly eroded region
N	0.362	Concave	Old, highly eroded region
O	0.469	S – shape	Moderately eroded
P	0.492	Convex	Young, slightly eroded region

The sub - basin 4 has undergone various geomorphic stage, owing to variations in denudational processes. It appears to be highly controlled by young topography, which are consistent with regional hypsometry curves. The pattern of earthquake distribution across this region seems to be correlated with regional features. However, our findings in Kundasang and Ranau area provides robust evidence of old faulting, possibly reactivated as normal fault in response to Mt. Kinabalu upliftment (Wang et al., 2017). This interpretation seems sound as the geomorphic mapping suggests likewise, therefore it may provide a better understanding on the tectonic landforms in and around the central north zone of Sabah.

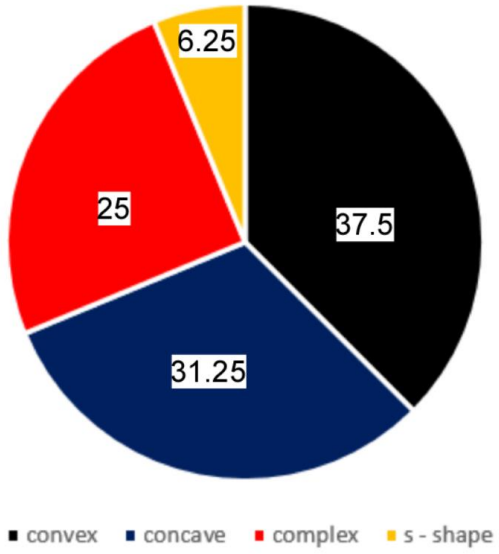

Figure 4.23 the main curves of Area 4

Figure 4.23 provides conclusive assumption on geomorphic stages across sub – basin of Area 4. It is mainly dominated by concave and convex curves, which is about 68.75% of the total area. On the other hand, the complex features forms are unusually high in this area, which is peculiar as such features tend to form lesser in areas with high percentage of young topographic terrains.

4.4. Earthquake statistics records

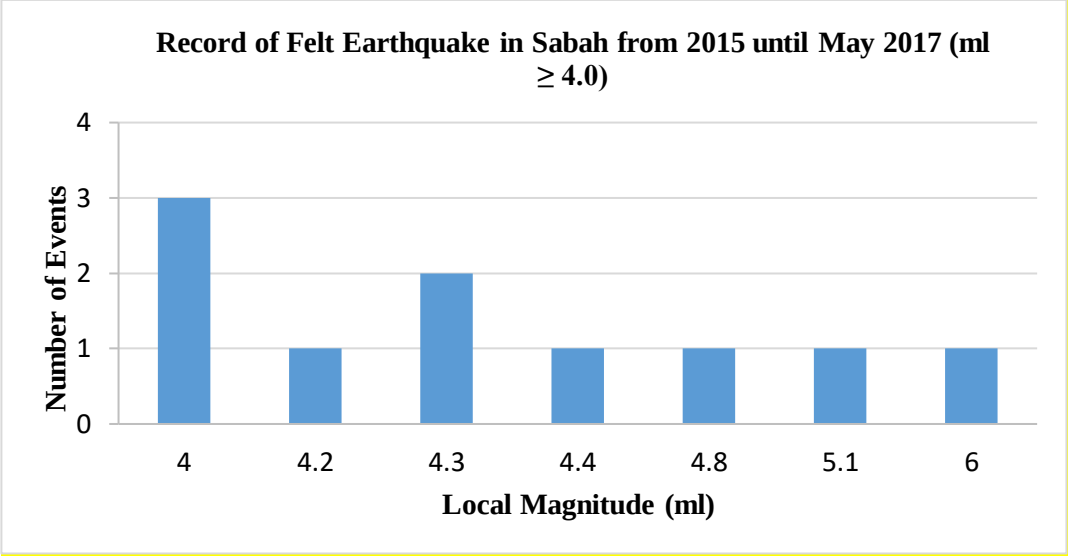

Figure 4.24 record of felt earthquake observed in Sabah from 2015 to May 2017.

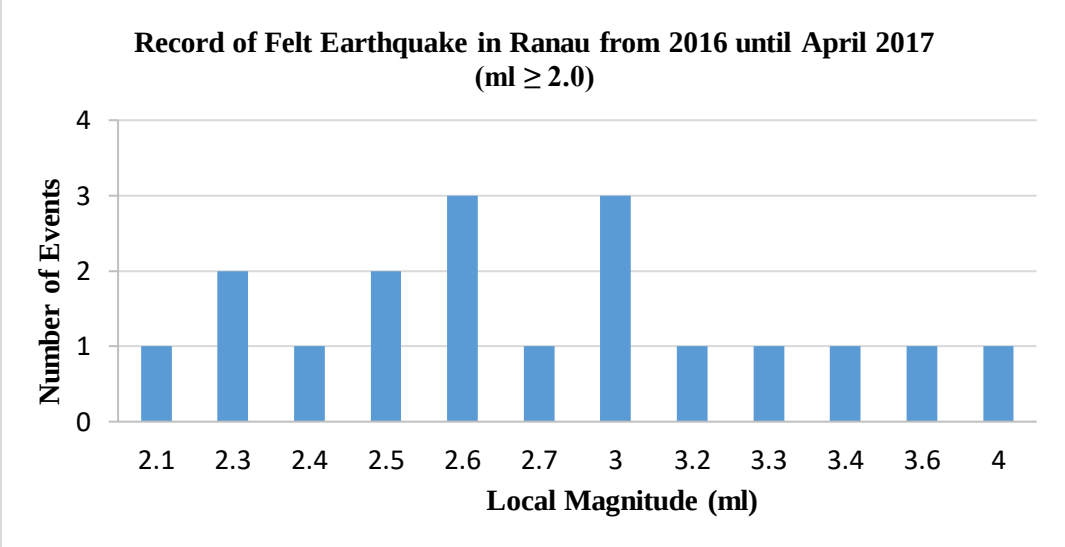

Figure 4.25 record of felt earthquake observed in Ranau from 2016 to May 2017.

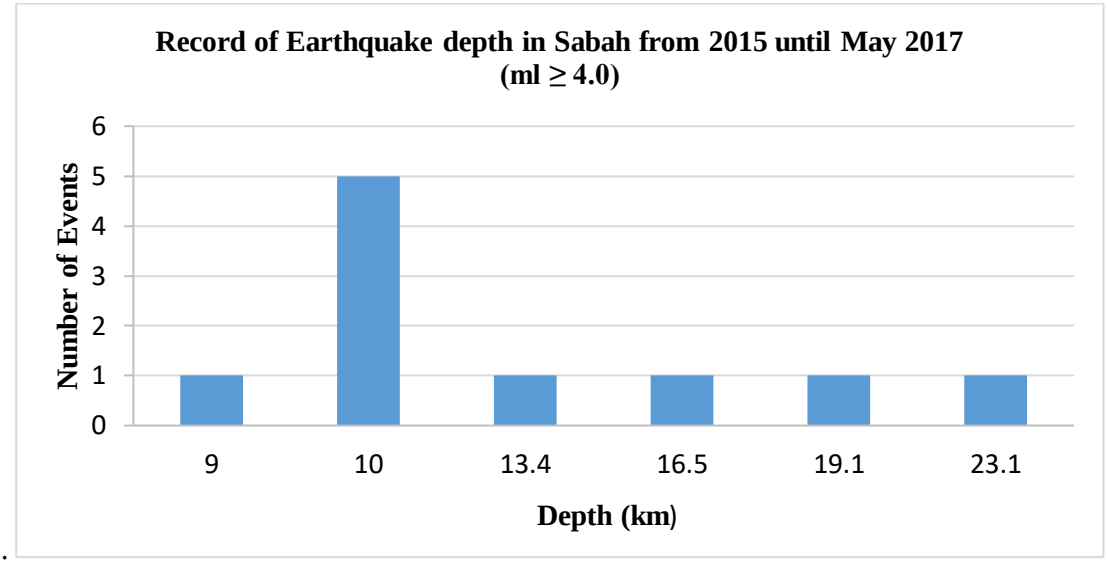

Figure 4.26 record of earthquake depth in Sabah from 2015 to May 2017.

Based on statistical records, the 5th June 2015 earthquake in Sabah is the only recorded earthquake which measures Mw 6. However, the scale of felt earthquakes in Sabah varies across this region as most aftershock display between Mw 4 and 5. According to Figure 4.24, the Mw 4 earthquake occurred at least 3 three times within a period of 2 years, which is unusual for an area like Sabah, specifically in the Ranau and Kundasang region. To further validate the results, detailed records of felt earthquakes in Ranau was shown in Figure 4.25. The spatiotemporal distribution of intraplate earthquakes mainly indicate a reading of Mw 2.6 and 3, which occurred at least three times over the 2 years span. Also, most of the earthquakes tend to form at a shallow depth of 10km. Due to this, the ground deformation and rate of shaking increases abundantly across this region. Therefore, we can classify Ranau and Kundasang region as seismically active despite being away from active plate boundaries.

4.5. Peak Ground Acceleration value for felt earthquake in Ranau (ml ≥ 4.0)

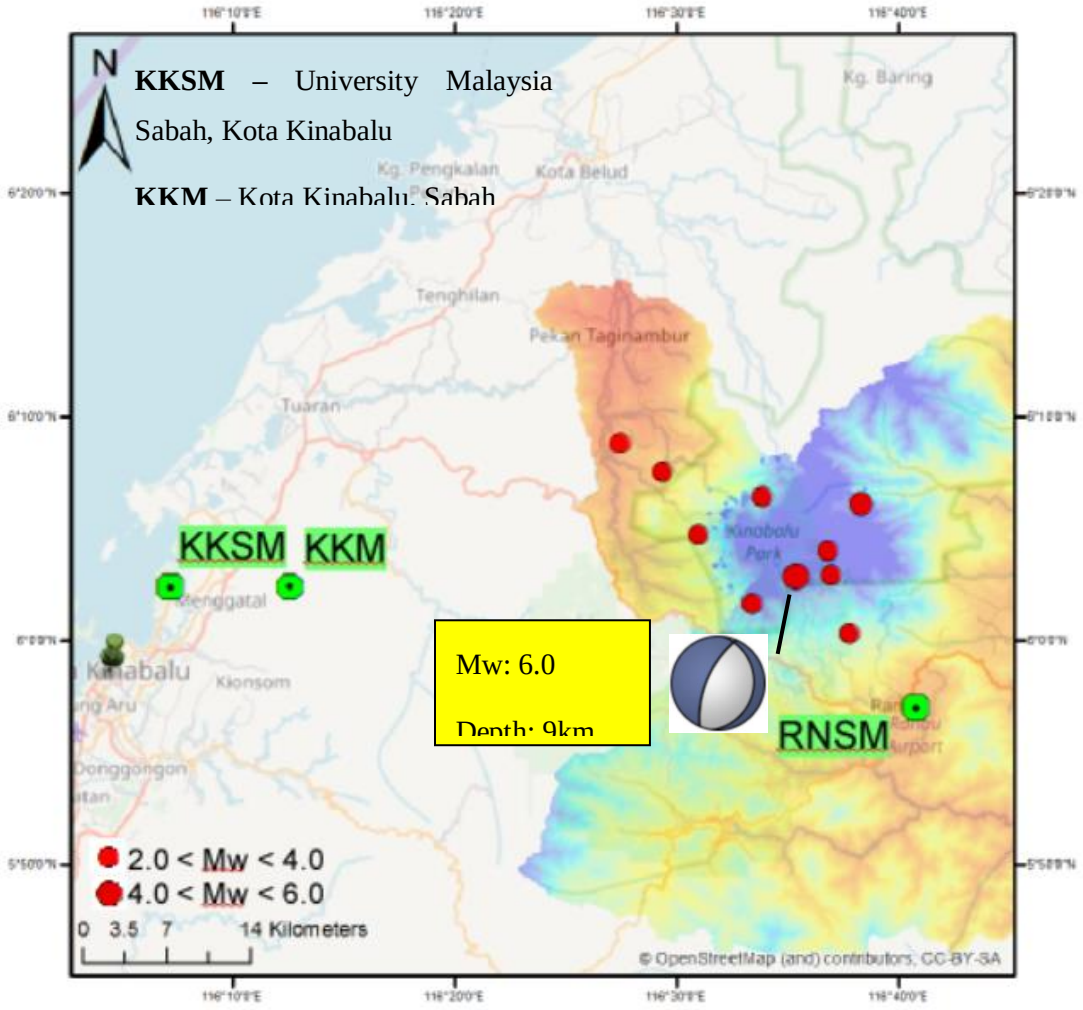

Figure 4.27 the location of seismic stations across the study area.

Table 4.7
Peak Ground Acceleration (PGA) of recent earthquakes in Ranau region.

Date	Station	Magnitude(ml)	Depth(km)	Acceleration(cms^{-2})			g - value		
				Z	N	E	Z	N	E
5/6/2015	KKM	6	9	-53.2973	-132.36958	-121.55724	-0.054385	-0.135071	-0.124038
5/6/2015	KKM	4	23.1	2.52644	-11.1524	9.7804	0.002578	-0.01138	0.00998
5/6/2015	KKM	4.2	10	1.18972	3.6848	-4.87354	0.001214	0.00376	-0.004973
5/6/2015	KKM	4.3	19.1	1.18972	3.6848	-4.87354	0.001214	0.00376	-0.004973
6/6/2015	KKM	4.8	10	-3.42902	-12.52832	-14.16394	-0.003499	-0.012784	-0.014453
12/6/2015	KKM	5.1	10	-11.05342	47.45846	43.37382	-0.011279	0.048427	0.044259
12/6/2015	RNSM	5.1	10	-41.19528	-68.33246	79.8063	-0.042036	-0.069727	0.081435
17/6/2015	KKM	4	10	3.29378	-13.42208	8.62008	0.003361	-0.013696	0.008796
17/6/2015	RNSM	4	10	-12.84584	9.61086	-10.62712	-0.013108	0.009807	-0.010844
23/6/2015	KKM	4.3	13.4	4.90294	-20.37322	16.33268	0.005003	-0.020789	0.016666
23/6/2015	RNSM	4.3	13.4	-10.5938	15.99752	9.52364	-0.01081	0.016324	0.009718
26/7/2015	KKM	4.4	10	2.19422	6.23574	-7.87528	0.002239	0.006363	-0.008036
26/8/2016	KKM	4	16.5	-0.5243	-0.3724	0.40376	-0.000535	-0.00038	0.000412
26/8/2016	RNSM	4	16.5	-15.00576	-15.19294	15.50084	-0.015312	-0.015503	0.016123
26/8/2016	KKSM	4	16.5	-0.5243	0.2548	0.3724	-0.000535	0.00026	0.00038

From Table 4.7, it is obvious that the highest recorded PGA is during the 5th June 2015 earthquake, which measured at Mw 6 in the Ranau region, based on the information provided by Kota Kinabalu seismic station. It is located at least 200 km away from the epicentre. Any nearby seismic stations could have recorded much higher PGA than (Kota Kinabalu) KKM station. Earthquake related data was available from the seismic stations, immediately after the 5^{th} June 2015 earthquake. Such urgency is necessary as detailed study is required to record ground deformation data across the region.

Table 4.8
The velocity recorded by seismic stations in Kota Kinabalu and Ranau.

Date	Station	Magnitude(ml)	Velocity (cm/s)			Perceived shaking	Potential Damage	remarks
			Z	N	E			
5/6/2015	KKM	6	0.89	2.2	2.03	Light	None	SW of KKM
5/6/2015	KKM	4	0.04	0.19	0.16	Weak	None	SE of KKM
5/6/2015	KKM	4.2	0.02	0.06	0.08	Not felt	None	NW of KKM
5/6/2015	KKM	4.3	0.02	0.06	0.08	Not felt	None	NW of KKM
6/6/2015	KKM	4.8	0.06	0.21	0.24	Weak	None	SW of KKM
12/6/2015	KKM	5.1	0.18	0.79	0.72	Weak	None	NE of KKM
12/6/2015	RNSM	5.1	0.69	1.14	1.33	Weak	None	SE of RNSM
17/6/2015	KKM	4	0.05	0.22	0.14	Weak	None	SE of KKM
17/6/2015	RNSM	4	0.21	0.16	0.18	Weak	None	NW of RNSM
23/6/2015	KKM	4.3	0.08	0.34	0.27	Weak	None	SE of KKM
23/6/2015	RNSM	4.3	0.18	0.27	0.16	Weak	None	NE of RNSM
26/7/2015	KKM	4.4	0.04	0.1	0.13	Weak	None	NW of KKM
26/8/2016	KKM	4	0.009	0.006	0.007	Not felt	None	SE of KKM
26/8/2016	RNSM	4	0.25	0.25	0.26	Weak	None	SE of RNSM
26/8/2016	KKSM	4	0.009	0.004	0.006	Not felt	None	NE of KKSM

From the information above, the highest velocity across the region is recorded during the 5th June 2015 earthquake, which experienced light shaking and no potential damage in Kota Kinabalu. The shaking intensity was enormous in the Ranau and Kundasang region, as it triggered rock falls along the Mt. Kinabalu area. It seems that intense shaking occurred in SW in the KKM seismic stations. However, the aftershocks of 5th June 2015 earthquake posed no threat, as most of the recorded data experienced weak shaking and no potential damage. The new seismic stations in Ranau area is helping geoscientist to understand more on the potential damage and acceleration data. Such interpretation seems to be accurate because the variation between the stations can be observed clearly.

4.6. Field Evidence and GPR survey

A series of ~SE dipping normal faults (outcrop A) are mapped (Figure 4.29) in the field. These faults have displaced and the displacement varies from few centimeters to meters (Figure 4.32) shows such examples, and GPR investigation is carried out to map the subsurface geometry of the faults. It appears to correlate with the GPR survey and even found new faults in the GPR profile (Figure 4.30). The faults in the GPR profile seems to have formed a horst and graben structure on the NW section of the profile and as it proceeds to SE direction, it begins to form a listric fault. Moreover, a minor horst and graben structure was observed in outcrop F. This particular structures appear to have NW and SE dipping directions, which accommodate NW – SE extension. The uplifted section (horst) has an antithetic nature. However, these structures are linked to a major normal fault with SE dipping direction. On the other hand, folded beds in this region appear to have SSE dipping direction with ENE – WSW striking trend. This provides vital information on the compressional trend. Also, overturned features such as recumbent and more complicated folding structures was observed with NE – SW trend. Therefore, the structures have undergone high compressive intensity which led to a 90° rotation. This interpretation implies that it could have initially formed either as an anticline or syncline with NE – SW compressional trend. The distance between each fold is very short and this suggest it could have formed under local compression.

4.6.1. Structural Map

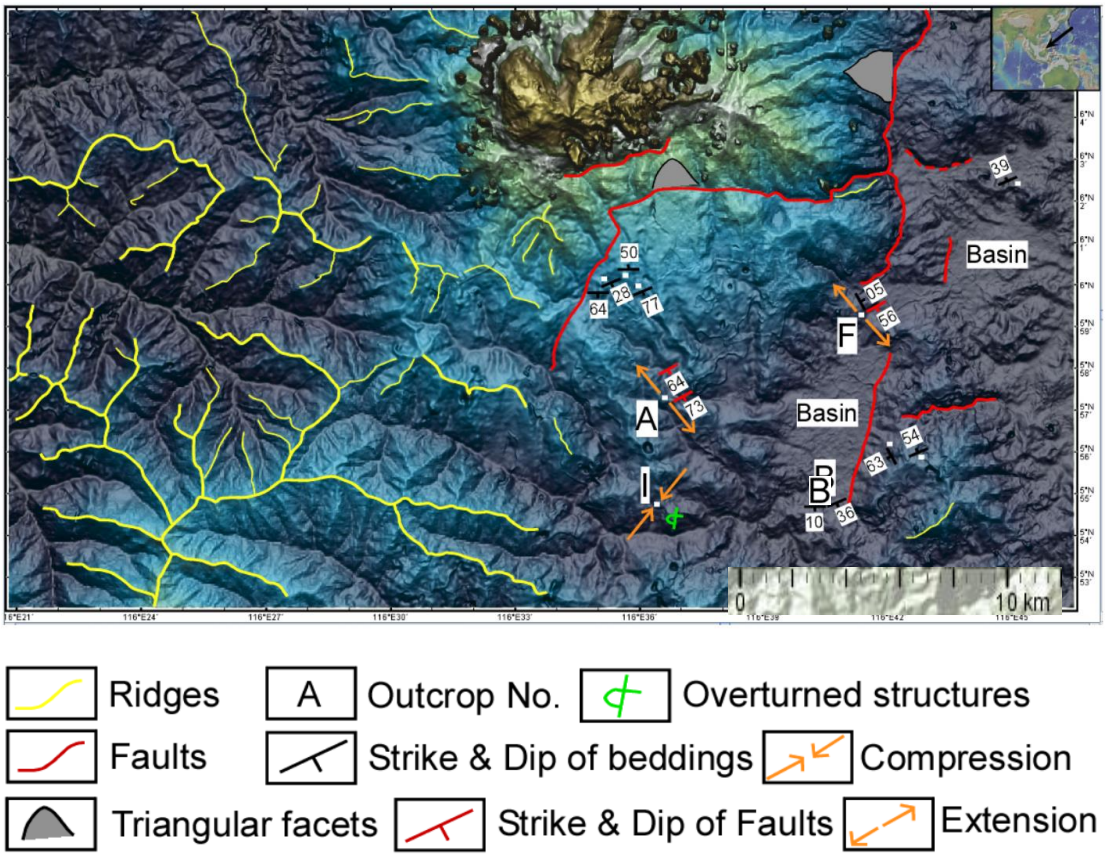

Figure 4.28 demonstrates the field survey around Kundasang and Ranau region. (Modified from geomap software).

From the field evidence, a series of faults and overturned features are observed. This particular structures exhibits a complex nature of faulting which accommodates NW – SE extension and NE – SW compression. Such interpretation implies it could have formed under two different tectonic events or localized event that formed in a single movement as a result of simple shear mechanism (Shah et al., 2018).

4.6.2. Normal Faults

Outcrop A (Latitude: 05.956 Longitude: 116.608)

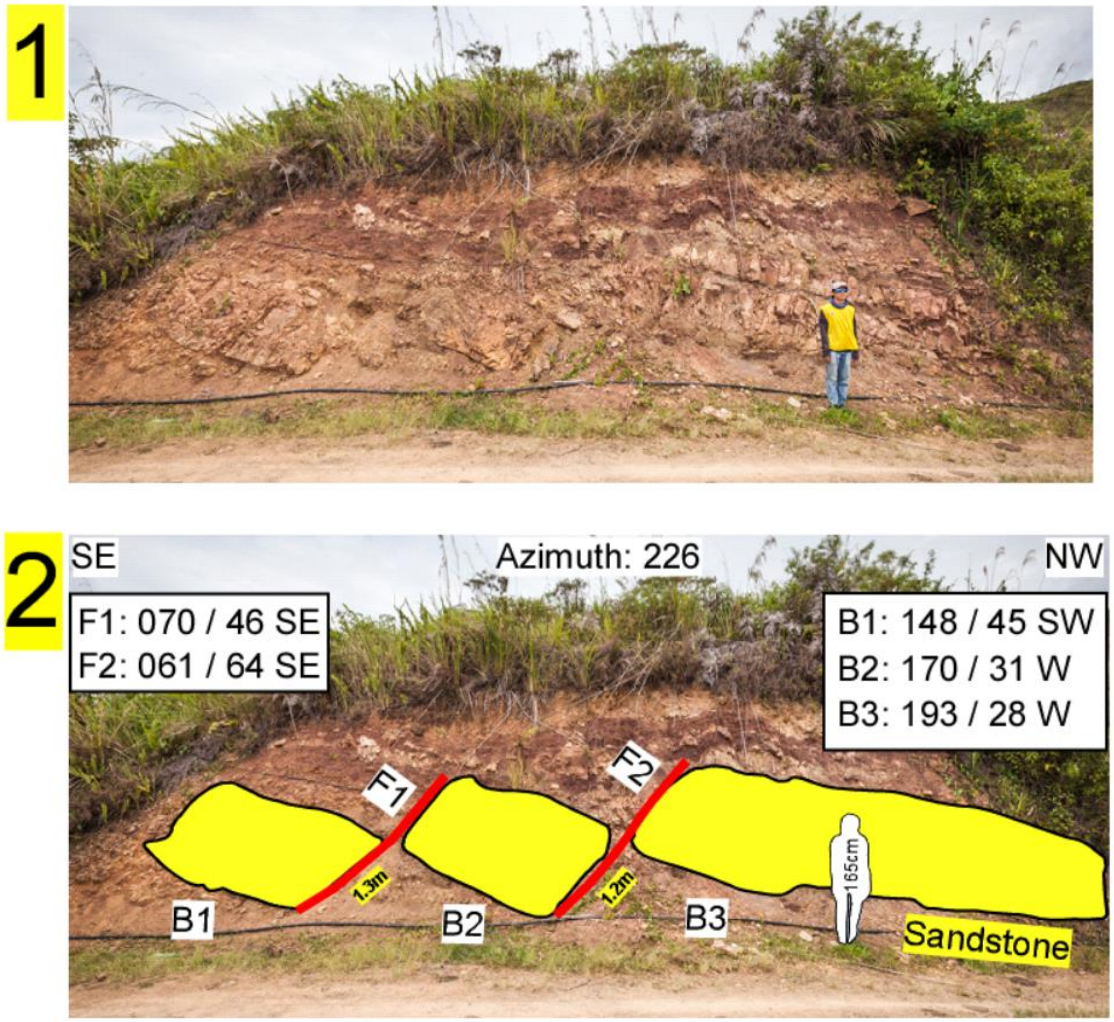

Figure 4.29 (1) Un – interpreted field photo. (2) Example of a series of normal faulting with SE dipping and striking NE – SW.

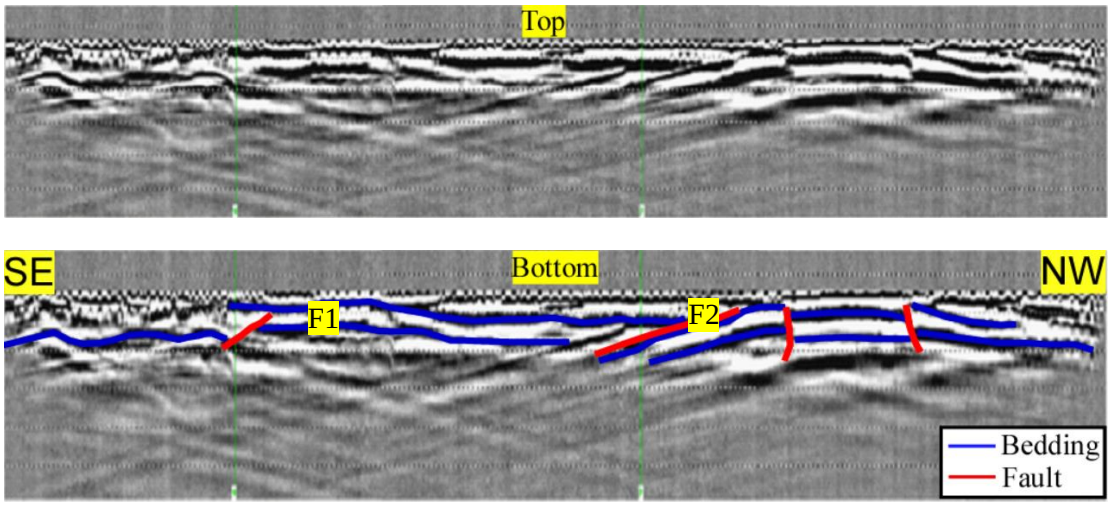

Figure 4.30 (Top): Un – interpreted GPR profile of Outcrop A. (bottom): Interpreted GPR profile of Outcrop A.

Based on Outcrop A, it is obvious that the normal faulting formed under NW – SE extension, with NE – SW striking and dipping SE. However, it appears to dip steeply on the surface and shallower as it moves sub – surface. The evidence of normal fault with listric components can be observed via GPR profile. Also, a horst and graben structure is observed on the NW section of the GPR profile. The faulted structures are observed up to a depth of 5m.

The normal fault is located in Kundasang region, which is nearby to the epicentre of many aftershocks. In order to understand the tectonism of this area, local structures must be examined in detail, which includes normal faulting as portrayed in Figure 4.29. The displacement of F1 (1.3m) and F2 (1.2m) normal fault shows that timing of such structures is the same.

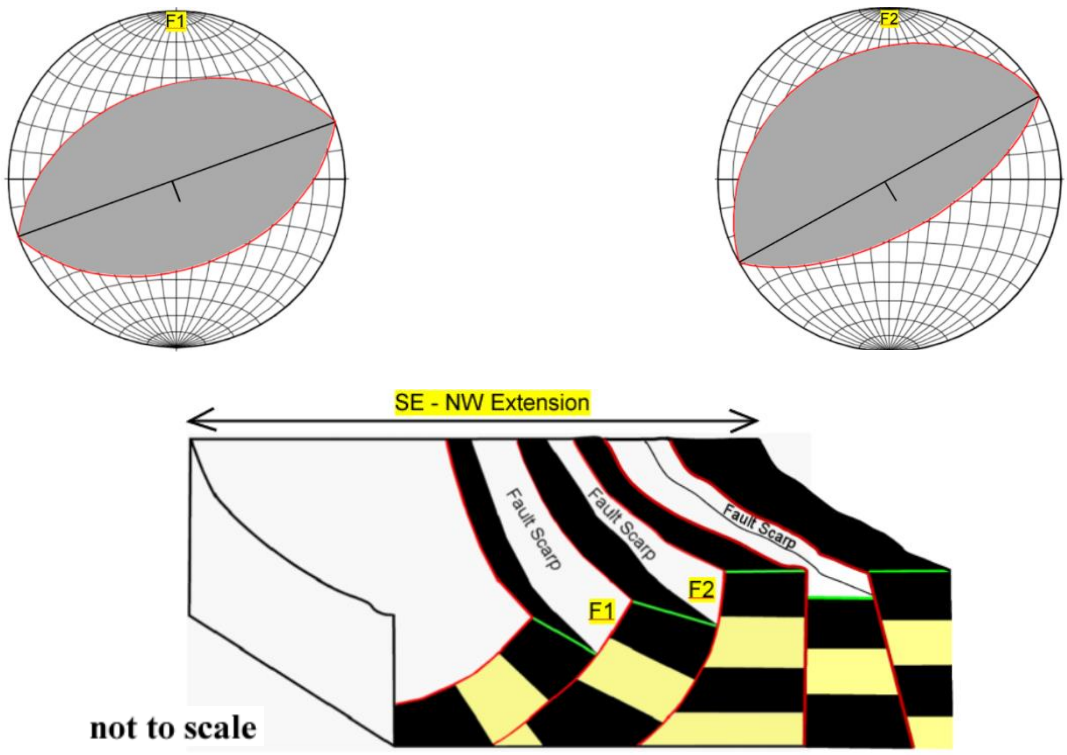

Figure 4.31 the expected fault plane solution of a future earthquake and the associated model shows the possible nature of normal faulting with listric component.

The structural model on Outcrop A shows horst and graben structure with NW and SE dipping direction. Our study reveals the localized structures are tectonically controlled by extensional domain which accommodates NW – SE extension. However, the expected fault plane solution from field evidence suggests that SE dipping normal faults are common across this region.

Outcrop F (Latitude: 05.98842 Longitude: 116.68874)

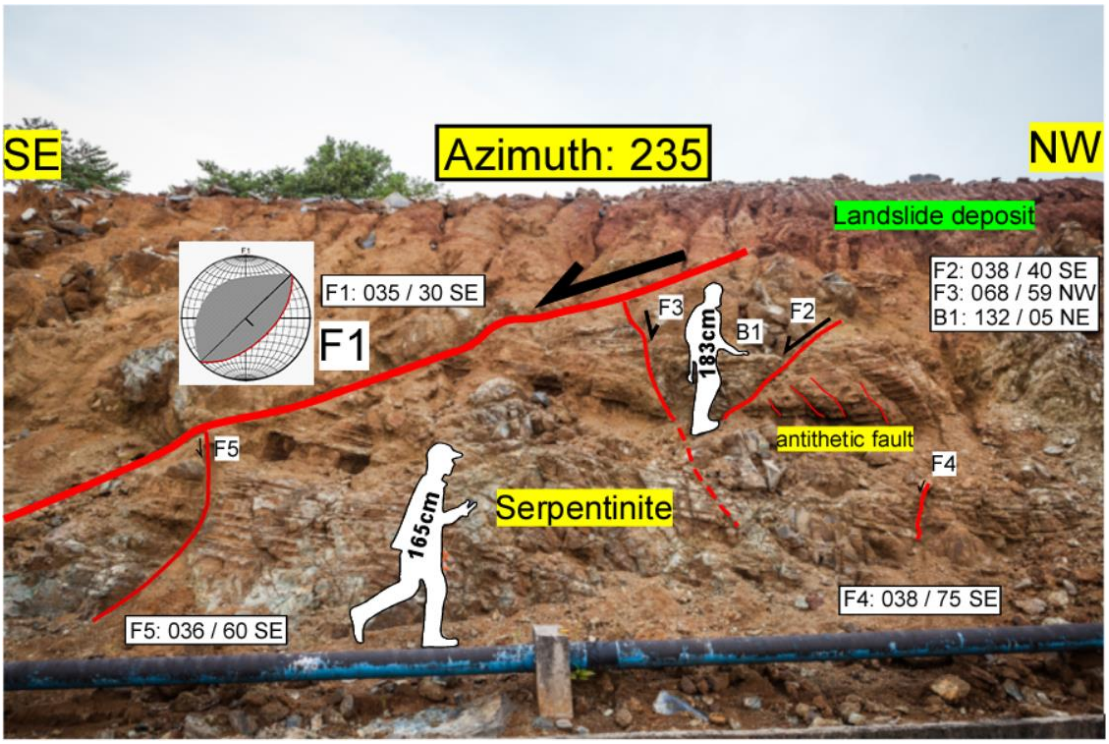

Figure 4.32 the evidence of normal faulting formed under NW – SE extension.

As illustrated in Figure 4.32, the field evidence in Ranau and Kundasang region exhibits a complex nature of faulting where extensional domain seems to structurally control the localized event. The evidence of normal faulting across Outcrop F shows subsidence of region, which explains the occurrence of major normal fault (F1) with SE dipping direction. Moreover, a minor horst and graben structure formed in response to the movement of major structures. The major fault (F1) seems to be dipping SE with an orientation between 50° and 60°. However, displaced block is not obvious due to the seismic induced landslides of the 5th June 2015 earthquake.

Outcrop F (Horst and Graben structure)

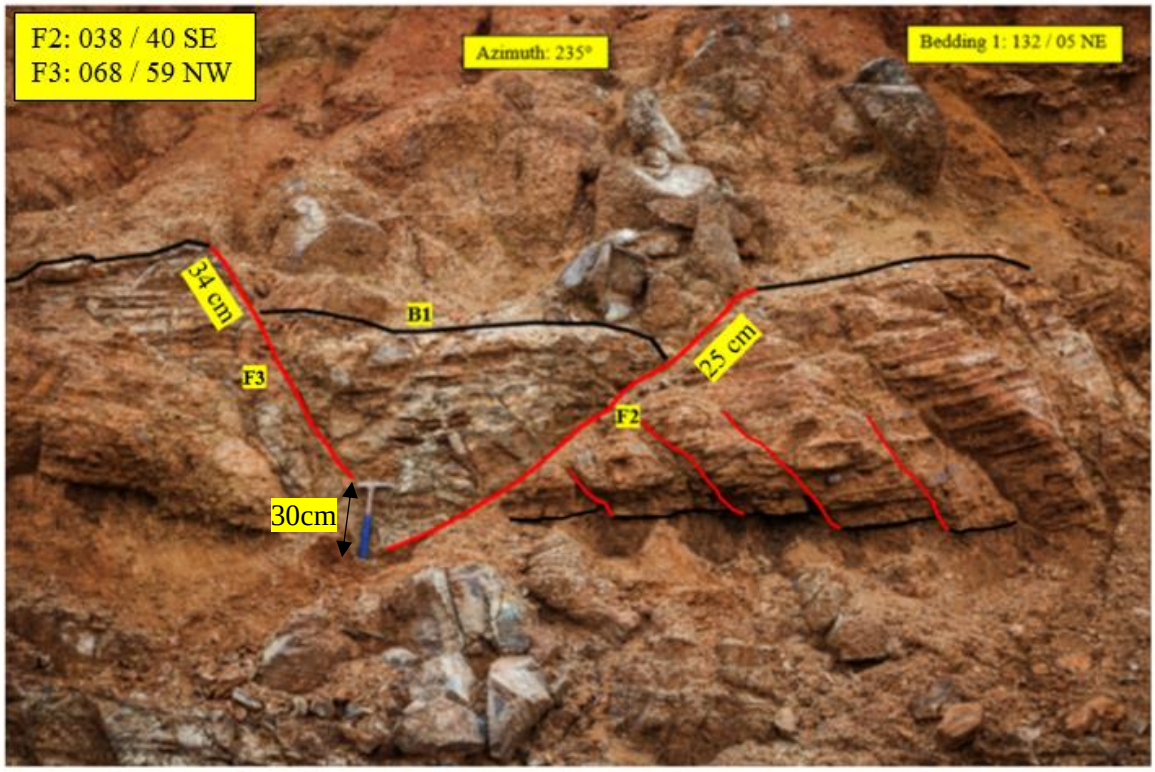

Figure 4.33 minor and horst graben structure.

The uplifted section or horst clearly shows the evidence of conjugate set or antithetic fault by its opposite dipping direction. A series of faulting is observed on the right section of the horst structure, which demonstrates a possibility of more than one event in this outcrop. These particular structures can be observed in one section of the horst while the other does not display any evidence of conjugate or antithetic set. However, there are two possibilities for such structures, firstly it could be related to major fault (F1) or minor fault (F2). It seems consistent with F2 structures as the scale of faulting is very minor. The tectonic model for Outcrop F is illustrated in Figure 4.34

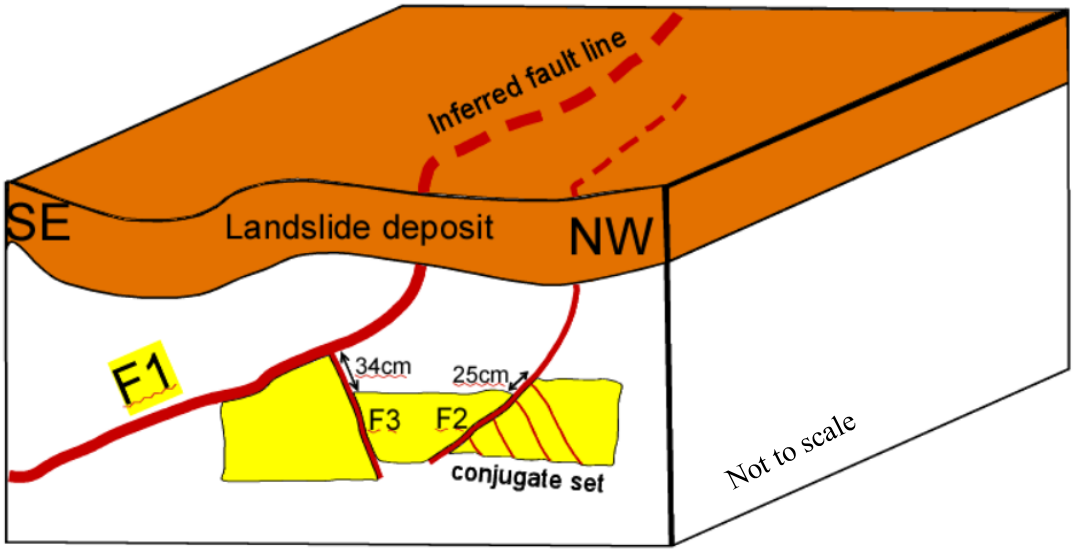

Figure 4.34 the main normal fault (F1) triggers the horst and graben structure (F2 and F3).

The remarkable faulted structure we have mapped shows a clear textbook example of horst and graben structures. Therefore, it is unlikely that non – tectonic forces produced such landforms.

4.6.3. Overturned Structures

Outcrop I (Latitude: 05.91875° Longitude: 116.60534°)

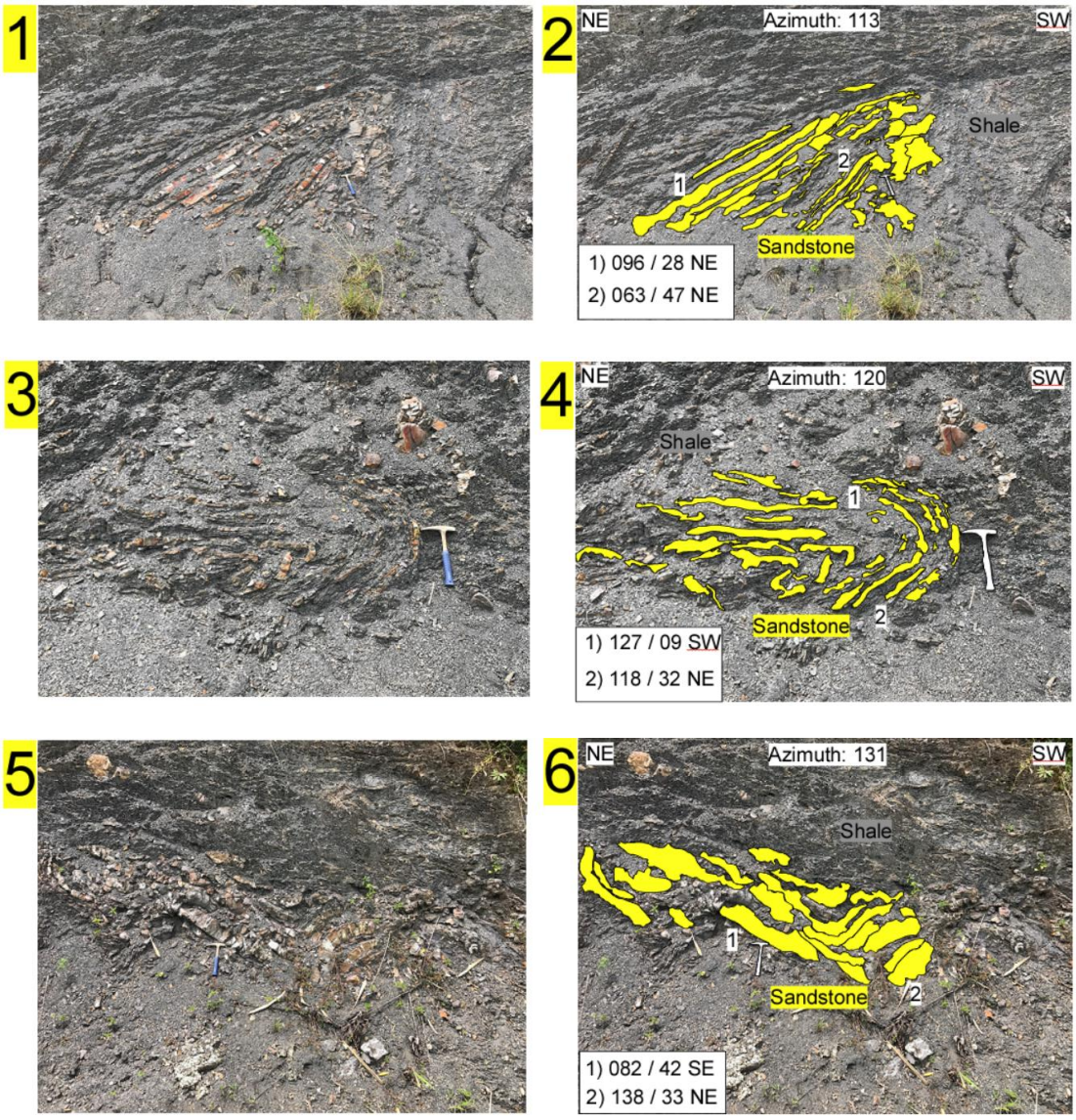

Hammer: 30cm

Figure 4.35 (left): Un – interpreted section. (Right): interpreted section.

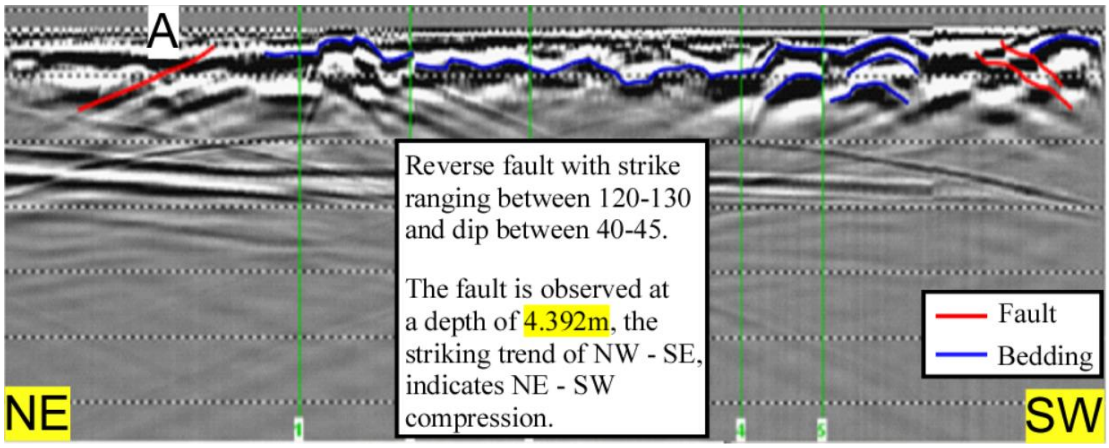

Figure 4.36 GPR profile across Outcrop I

A classic example of compression related structures such as folding and overturned features was observed in Outcrop I (Figure 4.35). Also, the sub – surface information was obtained from the 2 – Dimensional (2D) GPR survey. The evidence of reverse faulting (A in Figure 4.36) can be observed across the profile. It seems to be dipping NW with striking trend of NE – SW. Moreover, the fault is visible up to a depth of 4.392m. However, the intensity of deformation on folded sedimentary rocks seems to be increasing towards the SW direction as it coincides with the NE – SW compressional pattern. In addition, our findings suggest the entire area has undergone rotation as a result of intensive deformation. The Figure 4.37 below illustrates the possible nature of block rotation across Outcrop I.

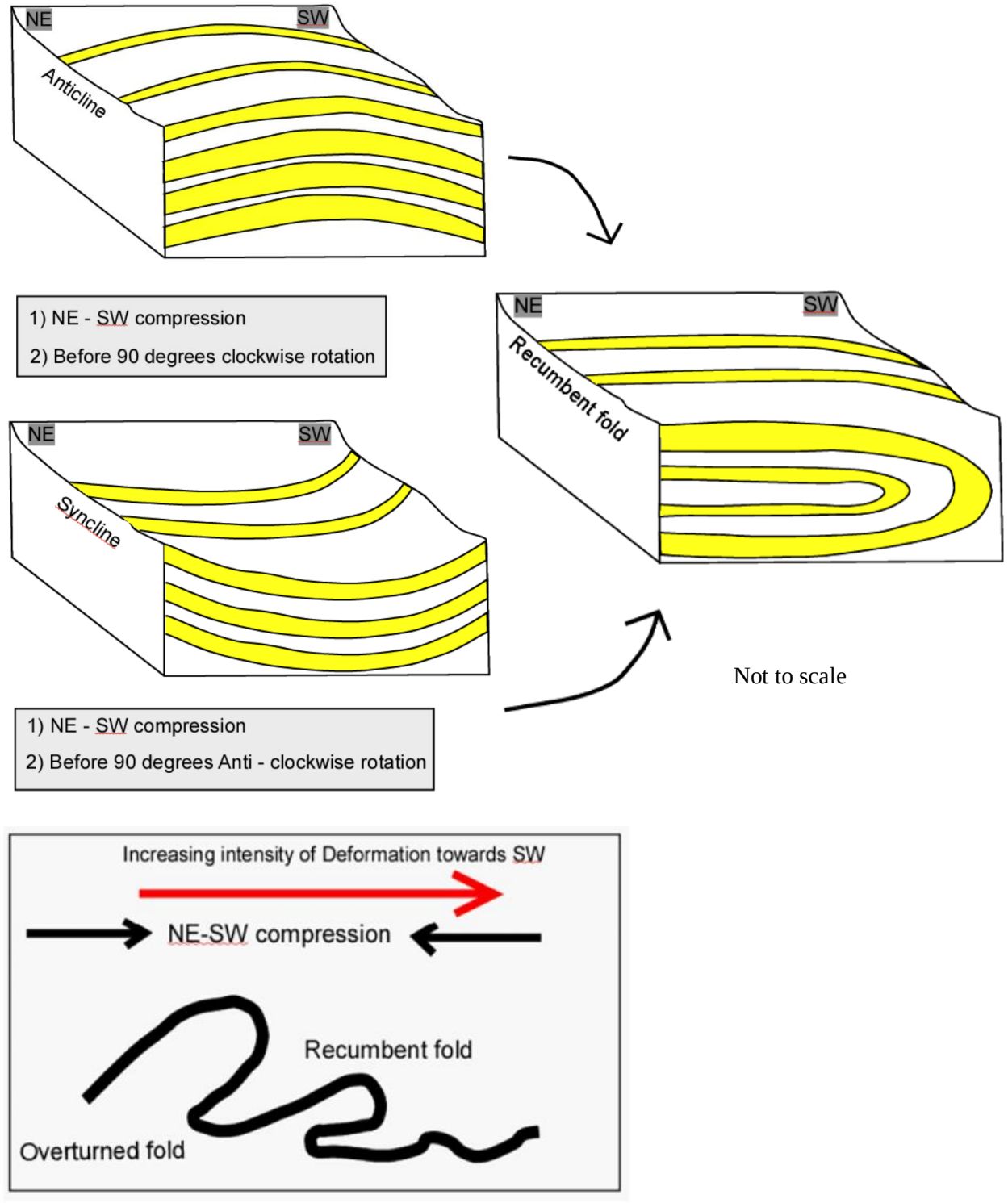

Figure 4.37 illustrate the conceptual model of Outcrop I in Ranau region.

It is obvious that the folding structures across this region has been rotated. But we are unable to determine the direction of rotation, which allows us to provide two options. From the GPR profile, no obvious structures were found. Therefore, the cartoon model was created to elucidate on such structures. Within this tectonic framework, various overturned structures and some complicated folding are also observed. This particular structures implies localized events may provide an idea of regional scale structures.

4.6.4. GPR survey in Marakau Road

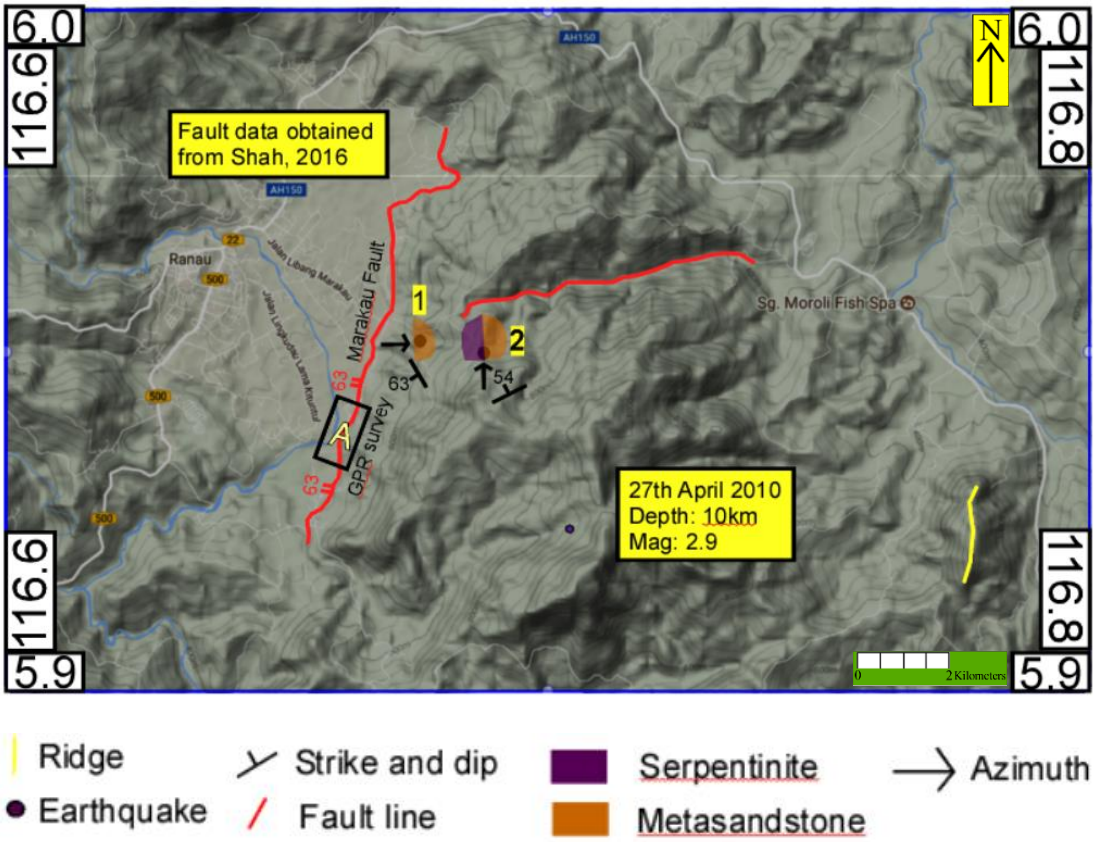

Figure 4.38 structural map of Marakau area.

The GPR survey was carried out via 2 – Dimensional (2D) and 3 – Dimensional (3D) methods, which provided a robust evidence of faulting and folded beds. However, it can be further supported with the evidence of normal faulting, which dips approximately 63° NW (Shah, 2016; Wang et al., 2017). Based on the field evidence, nearby outcrops are found to be dipping 63° SW. Such results imply that the beds are controlled by the Marakau fault, which explains the similar dipping angle. In addition, the region seems to be mainly dominated by serpentinite and metasandstone as illustrated in Figure 4.38 . The change in boundary can observed, and it

appears to be dipping 54° NW. Within localized tectonic framework, the structures exhibit a complex nature of faulting where it accommodates NW – SE extension. This interpretation is sound as the field evidence around Ranau and Kundasang area shows similar extensional pattern in response to major structures, which are complimented by the recent GPS data in a fixed NW Borneo reference frame where some stations show NW – SE extension motion (Mustafar et al., 2017). However, the localized map shows the earthquake distribution across this region. The available seismological dataset shows some low magnitude earthquakes in the study area, and these are mainly related to normal faulting.

Figure 4.39 the GPR survey along Marakau road.

Based on Figure 4.39, five waypoints was chosen to conduct 2 – Dimensional (2D) survey to determine any deformation structures that could be related to Marakau fault. The evidence of faulting is obvious in Point 2 and 4, where it appears to have formed under NE – SW extension. However, the major fault mainly shows normal slip with NW dipping plane and striking NE – SW, which truncates the metasandstone.

On the other hand, our finding postulated the folding patterns across this region seems to accommodate NE – SW compression, which can be observed in Point 1 and 3. Field evidence

suggests that the folded beds are dipping NW or SE and striking NE – SW (Rahim and Musta, 2015), which are correlated with the GPR dataset. Such results demonstrate that the area is tectonically controlled by N – S or NE – SW compressional force.

Outcrop B (Latitude: 05.91478 Longitude: 116.67197)

Figure 4.40 interbedded sandstone and shale in Marakau area.

Based on outcrop above, the folding is obvious on the left section of Figure 4.40. However, this shows NE – SW compressional trends across Marakau area and it appears to correlate with the GPR profile (Figure 4.41, Figure 4.42, Figure 4.43, Figure 4.44 and Figure 4.45) which shows similar trending direction.

Point 1

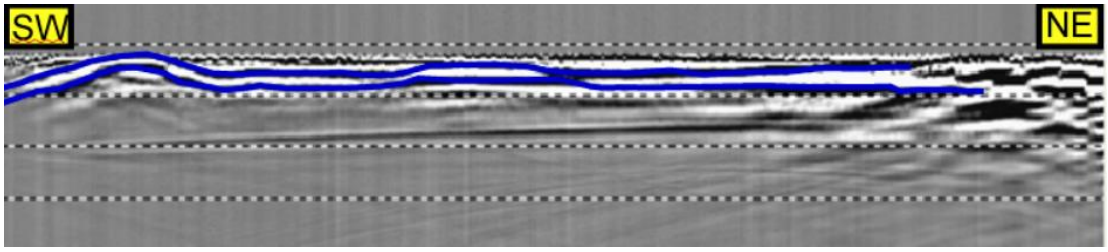

Figure 4.41 the evidence of SW – NE compressional pattern.

Point 3

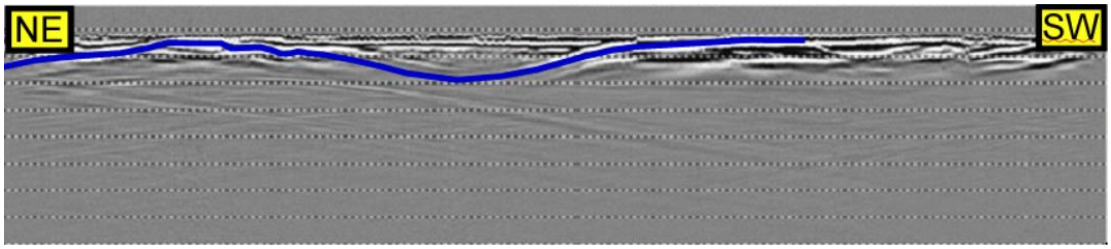

Figure 4.42 Folded structures across the Marakau road

Point 2

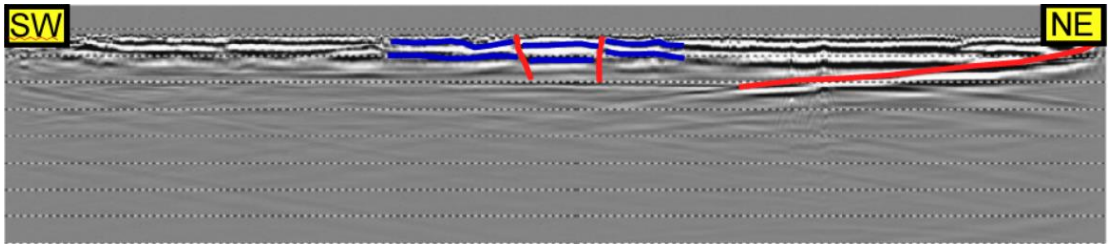

Figure 4.43 SE dipping normal faults and minor horst & graben structure

Point 4

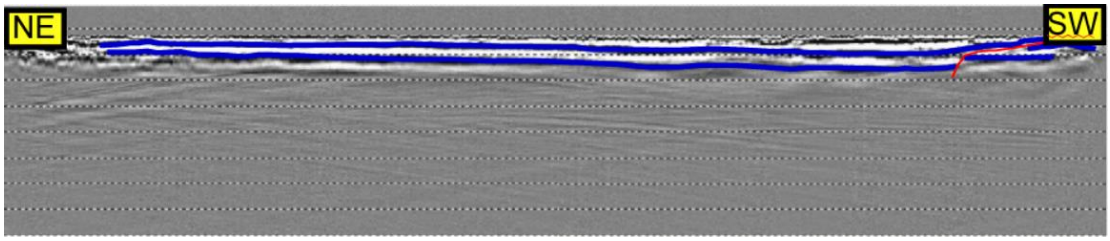

Figure 4.44 Minor normal faulting observed.

Point 5

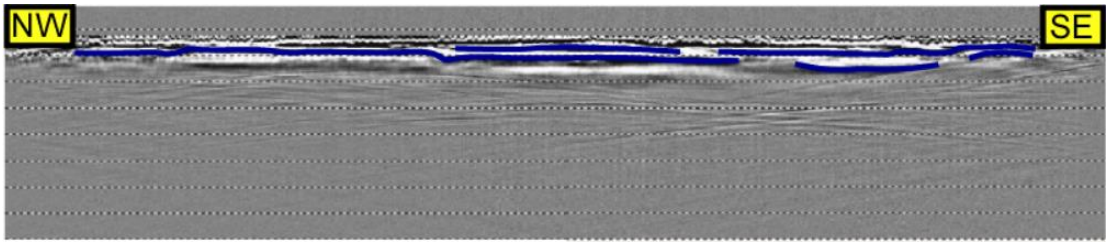

Figure 4.45 no obvious structures across this GPR profile.

3D survey of Point 3

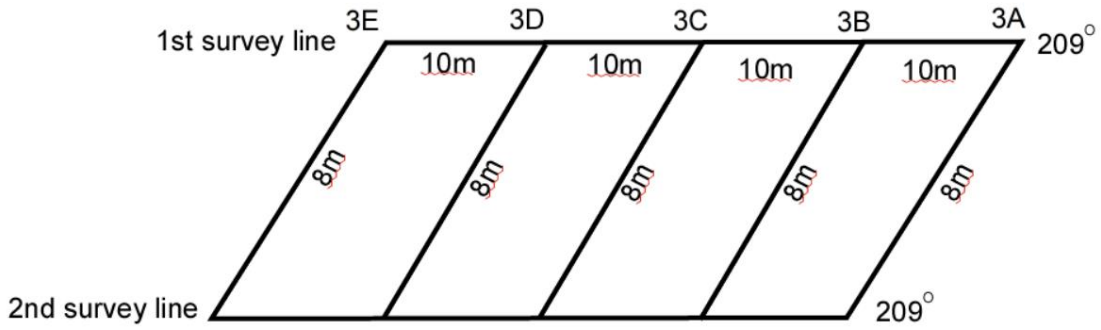

Figure 4.46 3D survey of Point 3 along Marakau road.

Based on Figure 4.46, five 3D survey lines 8m long were considered to determine the deformation pattern across Marakau road. Each lines are separated by 10m interval along the first survey line. Our findings suggest that each survey line shows the evidence of minor normal faulting (Figure 4.47 and Figure 4.48) across the folded beds. This results are comparable with other previous works by Rahim & Musta (2015). However, most of the faults (Figure 4.49, Figure 4.50 and Figure 4.51) are observed at a depth of 1m, which implies the deformation is close to surface. Also, some of the faults display steep dipping (e.g. Point 3A and 3C). The normal faults appear to be dipping SE with NE – SW striking trend. This contradicts with the Marakau fault, which dips NW and accommodates NW – SE extension. In addition, extension across folded beds implies the beds are collapsing in NW direction.

3A

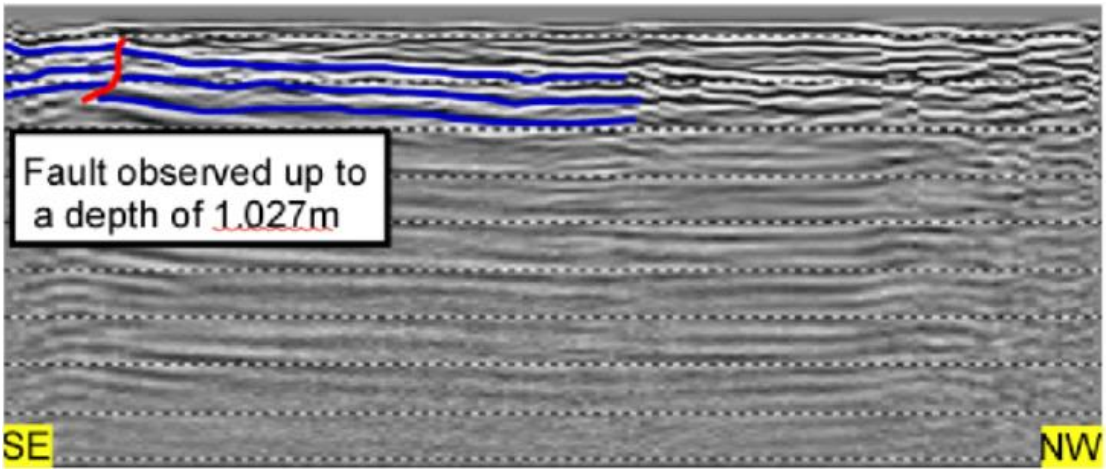

Figure 4.47 steep normal fault with SE dipping at a depth of 1.027m

3B

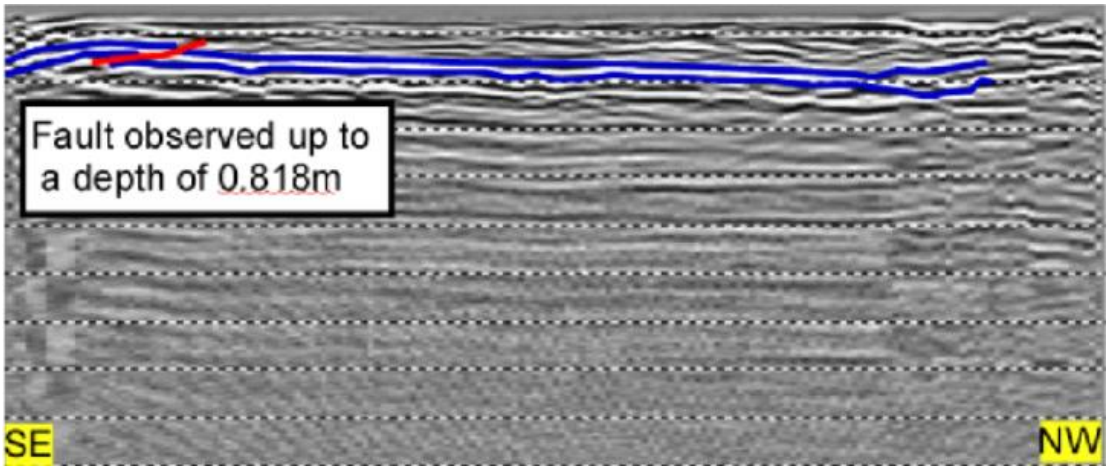

Figure 4.48 SE dipping normal fault at a depth of 0.818m

3C

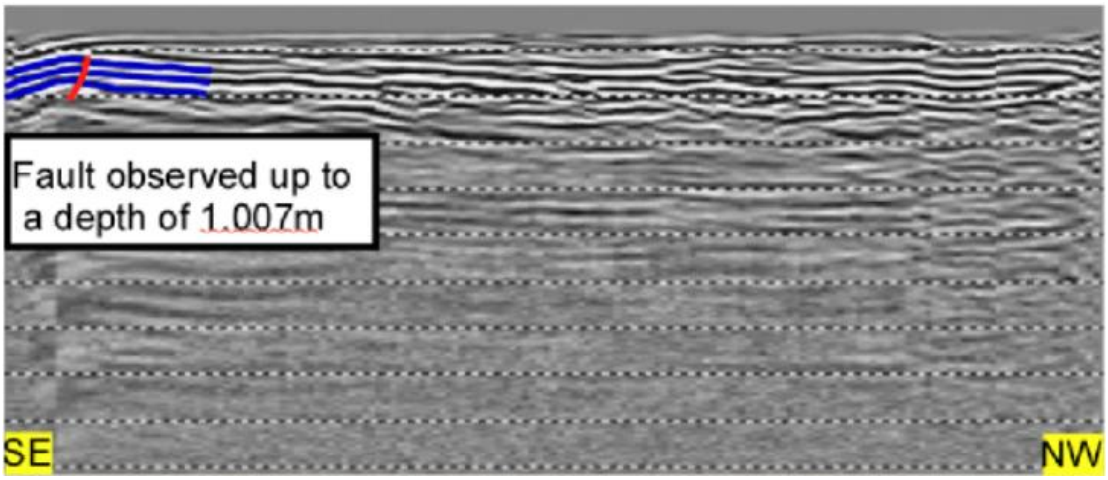

Figure 4.49 steep normal fault with SE dipping at a depth of 1.007m

3D

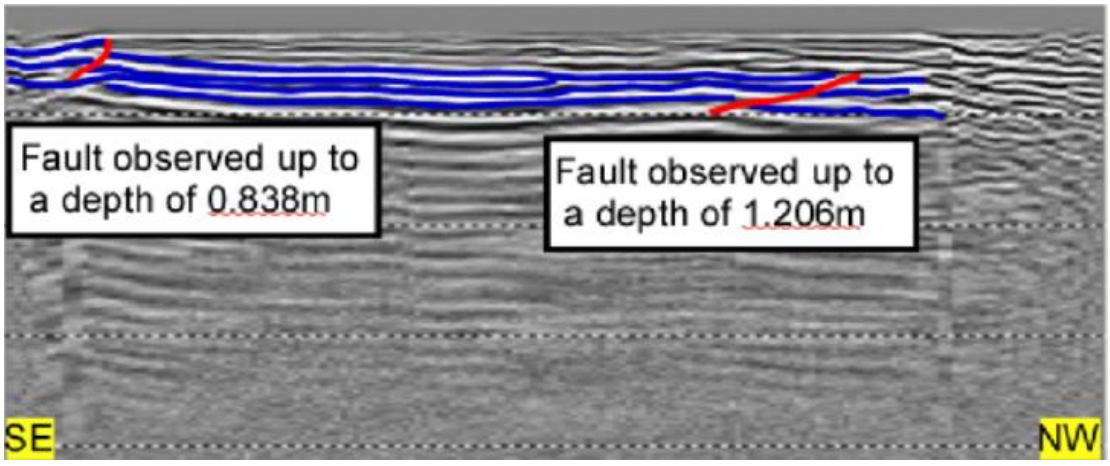

Figure 4.50 SE dipping normal faults observed at a depth of 0.838m and 1.206m

3E

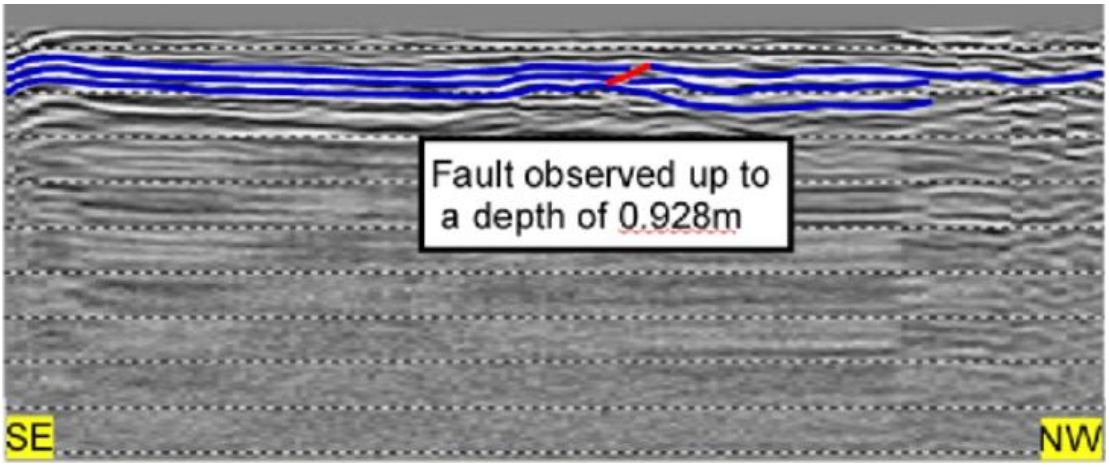

Figure 4.51 SE dipping normal fault observed at a depth of 0.928m

3D survey of Point 4

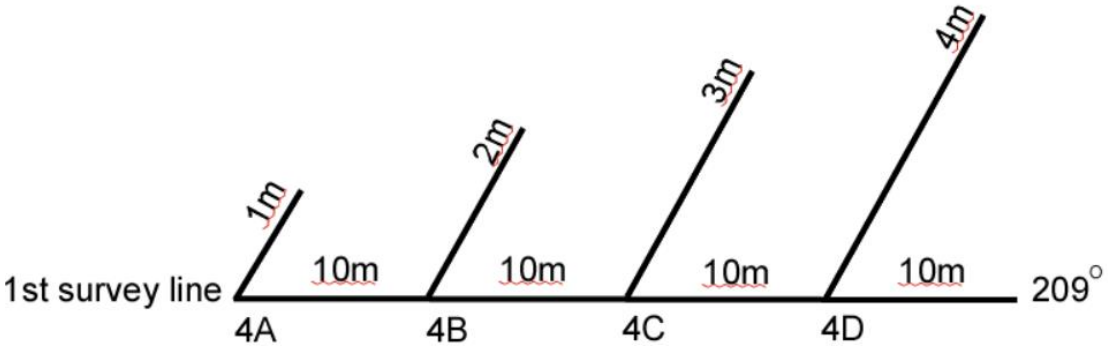

Figure 4.52 3D survey of Point 4 along Marakau road.

Figure 4.52 illustrates four 3D survey lines with varying length, progressively increasing by 1m from the starting point 4A. Each of the survey line was separated by 10m interval along the first survey line. However, due to unavoidable circumstances only two survey points were retrieved. From the available dataset, normal fault with NW dipping direction (Figure 4.53 and Figure 4.54) was observed approximately at a depth of 0.9 m, possibly related to localized events. Such interpretation implies minor faulting across Marakau road could be linked to extensional events, which is consistent with the occurrence of major faults across this region. Such minor structures across the folded region explains the extensional features to be relatively younger and could be linked to nearby seismicity. The evidence of normal faulting as an earthquake generating fault is obvious across this entire area. However, lack of field evidence suggest that this may be due to frequent occurrence of landslides along the Marakau road.

4C

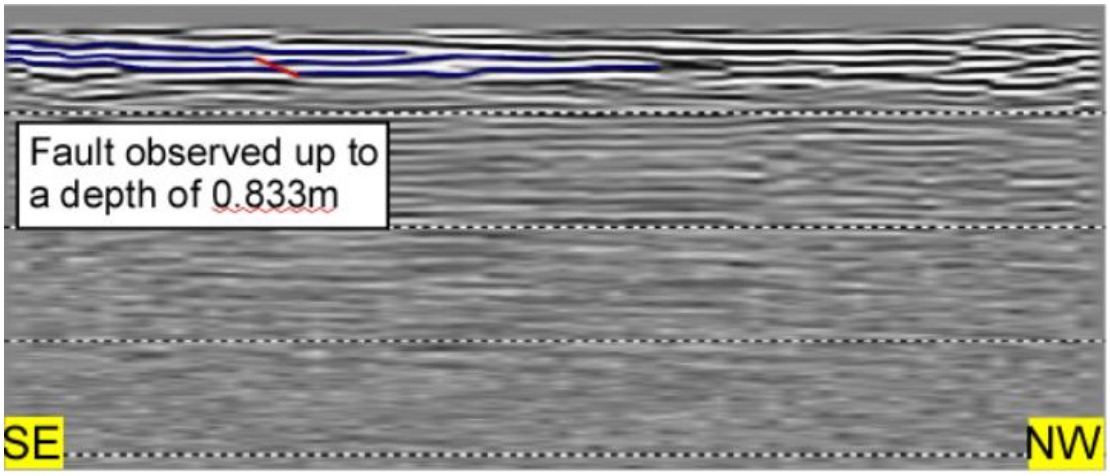

Figure 4.53 NW dipping normal fault visible at a depth of 0.833m.

4D

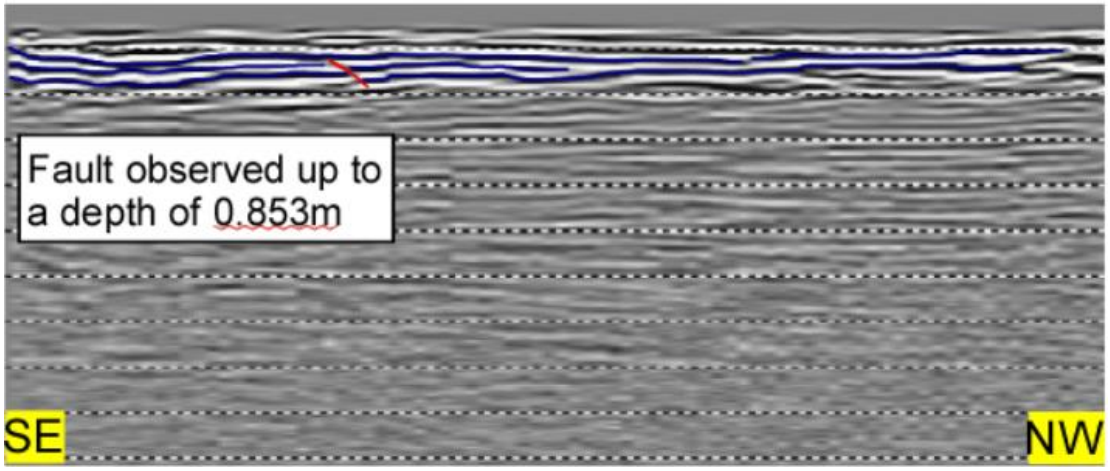

Figure 4.54 NW dipping normal fault visible at a depth of 0.853m.

Chapter 5
Discussion

5.1 Intraplate deformation in NW Borneo

The occurrence of intraplate earthquake in the Northwest Borneo has initiated interest in research community to understand the occurrence of earthquakes in Borneo (Tongkul, 2015; 2017; Shah, 2016; Wang et al., 2017; Shah et al., 2018). The work presented here shows multiple evidence of normal faulting in Ranau region, but, all these fault belongs to an older fault systems, and no evidence of recent faulting has ever been reported from the region (Wang et al., 2017), and we were also unable to observe the displacement of younger stratigraphic markers. This is interesting because it could mean that active faulting in this region is mostly occurring on blind faults, which have no surficial expression. However, the previous geomorphic works have demonstrated a number of active fault systems do exist in the region, and those are reported to have formed during the Holocene to Recent times but are now completely buried under the sediments due to the accelerated rates of erosion in the tropical environment (Hall, 2002; Mathew et al., 2016a; 2016b; Menier et al., 2017). The work presented herein suggest that some of the old fault systems could have been reactivated because the evidence of Holocene to Recent surface rupturing is not observed, and instead a number of old faults are reported in Sabah previously, and herein (Shah, 2016; Wang et al., 2017; Shah et al., 2018). The geomorphic analysis and field based studies that are carried out in Kundasang and Ranau region to fully comprehend the structural details of previous and recent faulting episodes. Most of the field locations are in the vicinity of the famous tourist destination in Sabah, the Mt. Kinabalu, which is a granite, and the June 2015 earthquake (Figure 5.1) occurred on a normal fault that runs under it. The ~NE-SW strike of the fault ruptured the ~10 km depth patch of the fault system that dips ~NW (Shah, 2016). Moreover, the recent 8th March 2018 (Figure 5.2) earthquake also seems to have ruptured a similar fault, which indicates active extension in the region. The Mw 5.2 has either ruptured the same faults as on 5th June 2015 or SE dipping normal faults. However, it seems more consistent with NW dipping plane. In addition, the clustering of earthquake hypocentres within NW Borneo is very prominent and reflects the occurrence of a major fault system (Shah et al., 2018). Earthquake records from Sabah region demonstrates active seismicity since 1897, which is related to both shortening and extensional regime (Wilford, 1967; Leyu et al., 1985; Lim, 1985; 1986). These particular areas are dominated by both NW – SE extension and NE – SW compression event. Within this

tectonic framework, we can conclude that extension in Kundasang and Ranau areas strongly backs a tectonics origin and is responsible for the intraplate earthquakes in NW Borneo. Therefore, this work substantiated the oblique compression model of Shah et al (2018).

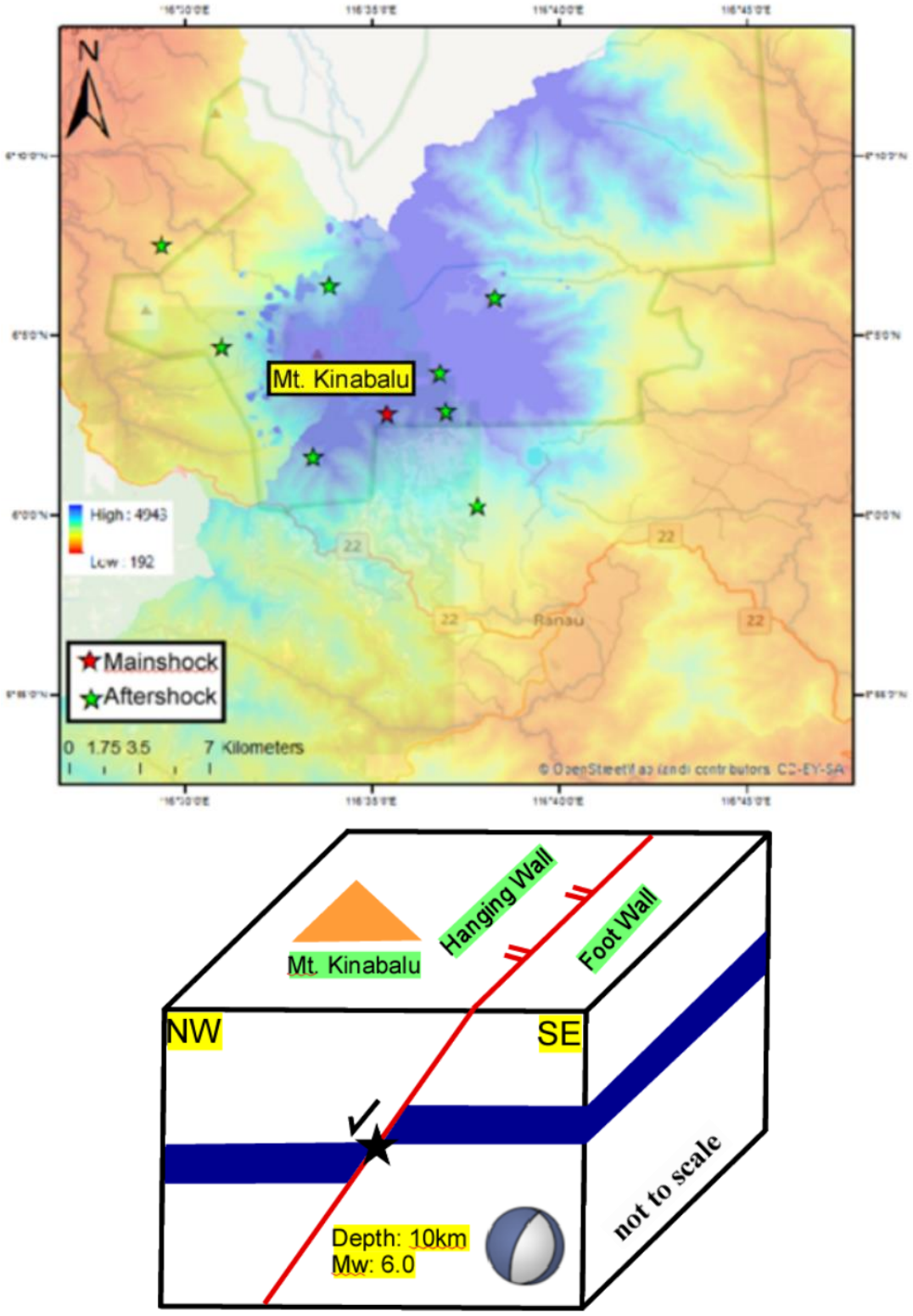

Figure 5.1 Earthquake distribution of 5th June 2015 event and 3D model of normal faulting.

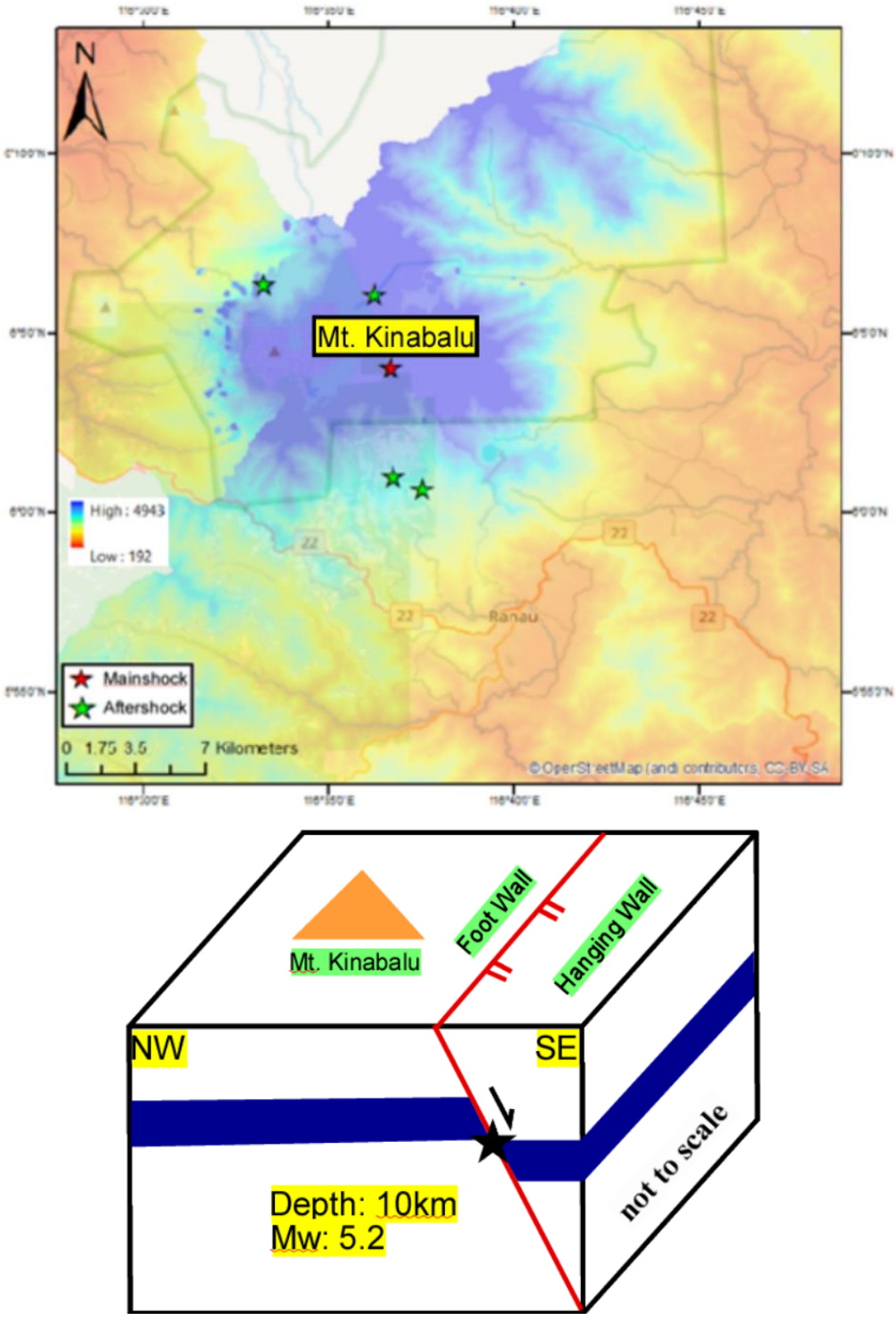

Figure 5.2 Earthquake distribution of 8th March 2018 event and 3D model of normal faulting.

5.2 Tectono – Geomorphic Assessment

Morphometric analysis across this region suggested rapid erosion, tectonic movements and climatic perturbations as changes to topographic landforms in NW Borneo (Mathew et al., 2016a, 2016b; Menier et al., 2017). Such analysis is required especially in regions like Borneo Island, which is covered with thick vegetation and intensive weathering. Our studies mainly focus on areas which are tectonically unstable such as Kundasang and Ranau. A variety of morphometric methods were used, specifically on SL index, elongation ratio, and hypsometric integral. Each analysis provided a different set of results that discusses on spatiotemporal distribution of intraplate earthquakes and pre – existing structures in Mt. Kinabalu areas. The SL index clearly demonstrates the effects of geological process along the longitudinal profile of Sg. Mesilou A, B and C. Knickpoints along those rivers coincides with pre – existing faults, which might be related to recent earthquake events. However, the dataset from elongation ratio suggest that this is mainly on Basin 6. It indicates that tectonic activity is relatively lesser in areas with earthquake recurrence and shows the surrounding regions as tectonically unstable. To further validate our findings, hypsometric integral was carried out to understand erosional processes across this region. This clearly shows that the eastern portion of Mt. Kinabalu displays young topography with slight erosion, while western portion display both old and mature landforms. And, inconsistency of hypsometric curves shows complex geological processes. Presence of near - vertical major slope breaks along Sg. Mesilou B exhibits remarkable differential uplift process. Moreover, the 5th June 2015 and 8th March 2018 earthquakes mostly likely ruptured a pre – existing normal fault and possibly occurred on the same fault line. This study reveals that the seismicity is mainly because of reactivation of ancient fault lines in response to sudden sub – crustal collapse due to oblique compression or present – day plate boundary forces. Such interpretation implies the NW Borneo as tectonically active and unstable. Therefore, we argue that the NW or SE dipping normal fault is associated with a major left lateral strike slip fault, which extends for more than 900 km long (Figure 5.3) (Shah et al., 2018).

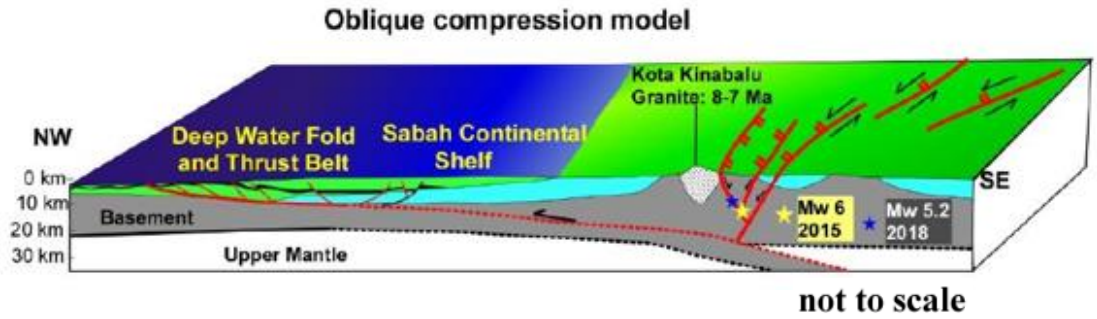

Figure 5.3 oblique compression model for NW Borneo region (Modified from Shah et al., 2018)

5.3 Field investigation

Understanding the deformation pattern in Kundasang and Ranau region is important because it suggests a strong structural control, which could be related to recent earthquake events. The tectonic system across this area remains uncertain due to the occurrence of both extensional and compressional settings. However, the major structures in NW Borneo is a well – studied NE – SW trending fold and thrust belt to the west of Sabah (Sandal, 1996; Hesse et al., 2009; Morley, 2009; Cullen, 2010; King et al., 2010a, 2010b; Sapin et al., 2013), that indicates NW – SE compression. This is attributed to large crustal scale gravity driven mechanism and the orogenic collapse of NW Borneo since 1.9 Myr (Sapin et al., 2013). But the recent recorded GPS data does not illustrate such movement across this region (Mustafar et al., 2017).

The presented work herein demonstrates the evidence of folding, reverse faulting and normal faulting in Ranau region via GPR. Based on the folded structures, evidence of NE – SW compression was determined while normal faulting suggest NW – SE extension across this area. However, the timing of deformation is unknown, this is primarily due to lack of sediment dating methods. The normal faults in Outcrop A shows listric nature of faulting, where it can be observed in sub surface as well. The GPR clearly demonstrates the evidence of horst and graben structures (Outcrop A and F). All this structural features is following the NW – SE extensional trend. Also, the 5th June 2015 earthquake occurred on similar extensional trend, therefore this indicates any deformation structures with such pattern is most likely to be active currently. This is because most of the mapped structures are located relatively close to the 5th June 2015 earthquake hypocenters. Also, Mt. Kinabalu sits on top of the fault, which shows evidence of subsidence in this area. The discovery of large scale landslides and traces of old

normal faults suggests a possibility of some old extensional fault lines? That might have reactivated during the recent earthquakes. Most importantly, we were unable to find the surface rupture / break of the 5th June 2015 earthquake, however it proves the possibility of a blind fault (Wang et al., 2017).

Folded sedimentary sequence was observed in South of Ranau region (Figure XX). The structures exhibits NE – SW compressional trend, which coincides with the bedding directions. The discovery of overturned structures (outcrop I) strongly lends support to a tectonic origin compared to gravity driven mechanism. However, the timing of deformation is unknown. Field evidence clearly shows that the intensity of deformation is increasing towards the SW of Ranau region. Such observation implies the compressive force is greater in that direction and complex folding like recumbent can be expected in SW of Ranau region. The folded structures in Outcrop I have undergone high compressive stress that led to 90° rotations. It could have initially formed either as an anticline or syncline. Also, some amount of thrusting and reverse faulting was identified via GPR section, but most likely to be inactive. However, this faults are not related to the 5th June 2015 and 8th March 2018 earthquake because it occurred on a normal fault.

5.1. Project Limitation

This research serves as an optional future reference on the GPR survey and tectono-morphometric analysis in Ranau region. Data collected in this localities can assist in similar research in the near future. Previously, GDEM and STRM have been generally used for topographic and terrain imagery while GPR has been carried out to identify subsurface deformation. This study however, utilizes GPR and GDEM for the purpose of identifying earthquake generating faults and determine its displacement in the Ranau region.

5.1.1. Limitation of Google maps

The freely available Google satellite data are widely distributed across the globe and are being. used by many researchers for different purposes, primarily because it is easy to obtain, free of cost and better visualization of scientific data at certain times (Butler, 2006; Benker et al., 2011). However, most of the Google satellite data is lacking in accuracy information and image processing methods (Potere, 2008) and this remains a major challenge in mapping of lush green rainforest such as Borneo Island. On the other hand, previous studies have raised this concern and shown that the accuracy of information obtained from Google maps could be vastly used by many geoscientist in remote sensing studies in near future (Butler, 2006). Also, freely available Google maps provides a much better platform to map geomorphic landforms such as triangular facets, topographic breaks, displaced ridge axes, deflected drainages and fault rupture scarps (Schumm, 1956; Yeats et al., 1997; Burbank and Anderson, 2001; Wang et al., 2017; Shah and Malik, 2017). Therefore, the scientific community and Google developers should work together to make the freely available dataset better and more robust to ensure better visualization and dissemination of scientific data (Butler, 2006).

5.1.2. Limitation of Ground Penetrating Radar (GPR)

Some limitations were encountered during the Ground Penetrating Radar (GPR) survey. Firstly, uncontrollable weather during the survey affected the effectiveness of the GPR. To avoid such circumstances, the weather forecast was regularly checked prior to the fieldwork. Also, inaccessible outcrops due to the logging activity was a major issue, as this limits the pathway to transport GPR equipment. However, alternative access to the outcrop was found by checking the area while ensuring the pathway is safe to transport the equipment. The GPR equipment which includes the Fibre Optic wires are fragile, thus the possibility for the equipment to be damaged are high. Moreover missing parts could disrupt the GPR survey altogether. To prevent such matters, the equipment is well maintained by checking all the parts and testing the GPR before conducting the actual survey.

Chapter 6
Conclusion

Understanding the occurrence of intraplate earthquake in Sunda plate remains a challenge and particularly in regions which are considered tectonically very stable. The notion of this is vigorously debated on post 5th June 2015 earthquake that caused significant damage and loss of life (Wang et al., 2017). The geomorphic, geologic, and structural mapping reported herein clearly demonstrate that Sabah region is tectonically active. Although the geomorphic analysis indicates the presence of active tectonic fault scarps, however, such evidence are not observed in the field locations (Mathew et al., 2016a; 2016b; Menier et al., 2017; Wang et al., 2017). The evidence of old normal faults are almost everywhere but the lack of Holocene to Recent breaks, which includes the June 2015 event, suggests either the faulting is blind or the evidence of past events have been erased in the tropical conditions of the Island. The GPR survey further illustrates the presence of old fault system in the region. Regionally, the ~NW-SE extension is currently occurring in the region, and it seems the deformation is controlled at depth by the major strike-slip fault (Shah et al., 2018) that runs through the backbone of the Island. This means that the deformation is a product of oblique convergence, and if that is true, then this part of Sunda plate is undergoing active extension, and since the region is not influenced by the nearby subduction systems therefore this kind of deformation is related to intra-plate deformation process. The origin of such forces is not clear yet but it could originate from the Palawan trough, which may be actively subducting (Wang et al., 2017).

Reference

Balaguru, A., Nichols, G. & Hall, R. (2003). The origin of the 'circular basins' of Sabah, Malaysia. *Geological Society of Malaysia*, 335 - 351.

Banda, R. M., & Honza, E. (1996, June 8 - 9). Miocene stratigraphy of northwest Borneo Basin. *Geological Society of Malaysia*, pp. 1 - 11.

Bull, W.B. & McFadden, L. (1977). Tectonic geomorphology North and South of the Garlock fault, California. In: Dohering, D.O. (Ed.), *Geomorphology in Arid Regions*. Geomorphology, State University of New York, Binghamton, 115 - 138.

Burbank, D. W. & Anderson, R. S. (2001). *Tectonic Geomorphology*. Blackwell Science, 274.

Burdette, K. E.; Rink, W. J.; Lopez, G. I.; Mallinson, D. J.; Parham, P. R. & Reinhardt, E. G. (2012). Geological investigation and optical dating of Quaternary siliciclastic sediments near Apalachicola, North-west Florida, USA. *Sedimentology*, 59(6), 1836-1849. doi:10.1111/j.1365-3091.2012.01328.x

Butler, D. (2006). The web – wide world. *Nature*, 439, 776 – 779.

Cullen, A. (2010). Transverse segmentation of the Baram – Balabac Basin, NW Borneo: refining the model of Borneo's tectonic evolution, *Petroleum Geoscience*, 16, 3 – 19.

Darman, H. & Sidi, F. H. (2000). *An outline of the geology of Indonesia*. Indonesian Association of Geologists, 192.

Dar, R. A.; Romshoo, S. A.; Chandra, R. & Ahmad, I. (2014). Tectono – geomorphic study of the Karewa Basin of Kashmir Valley. *Journal of Asian Earth Science*, 92, 143 – 156.

Dehbozorgi, M.; Pourkermani, M.; Arian, M.; Matkan, A.; Motamedi, H. & Hosseiniasl, A. (2010). Quantitative analysis of relative tectonic activity in the Sarvestan area, central Zagros, Iran. *Geomorphology*, 121, 329 – 341.

Dentith, M.; O'Neill, A. & Clark, D. (2010). Ground penetrating radar as a means of studying paleo fault scarps in a deeply weathered terrain, southwestern Western Australia. *Journal of Applied Geophysics*, 92-101.

Dietrich, W. E.; Wilson, C. J.; Montgomery, D. R. & McKean, J. (1993). Analysis of erosion thresholds, channel networks, and landscape morphology using a digital terrain model. *Journal of Geology*, 101, 259 – 278.

El Hamdouni, R.; Irigaray, C.; Fernandez, T.; Chacon, J. & Keller, E. (2008). Assessment of relative active tectonics, southwest border of the Sierra Nevada (Southern Spain). *Geomorphology*, 96, 150 – 173.

Font, M.; Amorese, D. & Lagarde, J. L. (2010). DEM and GIS analysis of the stream

gradient index to evaluate effects of tectonics: the Normandy intraplate area (NW France). *Geomorphology*, 119, 172 – 180.

Fountoulis, I.; Vassilakis, E.; Mavroulis, S.; Alexopoulos, J.; Dilalos, S. & Erkeki, A. (2015). Synergy of tectonic geomorphology, applied geophysics and remote sensing tectonics reveals new data for active extensional tectonism in NW Peloponnese (Greece). *Geomorphology*, 237, 52-64.

Gao, M.; Zeilinger, G.; Xu, X.; Tan, X.; Wang, Q. & Hao, M. (2016). Active tectonics evaluation from geomorphic indices for the central and the southern Longmenshan range on the Eastern Tibetan Plateau, China. *Advancing Earth and Space Science*, 35, 1812 – 1826.

Gill, J.; Shariff, N. S.; Omar, K. & Amin, Z. M. (2015). Tectonic motion of Malaysia: analysis from years 2001 to 2013. *ISPRS Annual Photogrammetry Remote Sensing Spatial Information Science*, 199-206. doi: 10.5194/isprsannals-II-2-W2-199-2015

Hack, J. T. (1973). Stream profile analysis and stream-gradient index. *Journal of research of the U. S. Geological Survey*, 1, 421 - 429.

Haile, N. S. (1962). The geology and mineral resources of the Suai – Baram area, north Sarawak. *The Geological Survey Department, British Territories in Borneo*, 13, 176.

Hajam, R. A.; Hamid, A. & Bhat, S. (2013). Application of morphometric analysis for geo – hydrological studies using geo – spatial technology – a case study of Vishav Drainage Basin. *Hydrology: Current Research*, 4, 1 – 12.

Hall, R. (2002). Cenozoic geological and plate tectonic evolution of SE Asia and the SW Pacific: Computer-based reconstructions, model and animations, *Journal of Asian Earth Science*, 20, 353–431, doi: 10.1016/S1367-9120(01)00069-4.

Hall, R. (2013). Contraction and extension in northern Borneo driven by subduction rollback. *Journal of Asian Earth Sciences*, 399-411.

Hesse, S.; Back, S. & Franke, D. (2009). The deep-water fold-and-thrust belt offshore NW Borneo: gravity-driven versus basement-driven shortening, *Bulletin of Geological Society of Amsterdam*, 121, 939–953.

Hinz, K. & Schlüter, H. U. (1985). Geology of the Dangerous Grounds, South China Sea and the continental margin off southwest Palawan: Results of SONNE cruises SO-23 and SO-27. *Energy*, 10, 297–315, doi: 10.1016/0360-5442(85)90048-9.

Hurtgen, J.; Rudersdorf, A.; Grutzner, C. & Reicherter, K. (2013). Morphotectonics of the Padul- Niguelas Fault Zone, Southern Spain. *Annals of Geophysics*, 6, 56.

Hutchison, C.S. (2005). Geology of North-West Borneo: Sarawak, Brunei and Sabah. Amsterdam. *Elsevier*, 421.

Ichikawa, M. (2007). Degradation and Loss of Forest Land and Land – use changes in Sarawak, East Malaysia: a study of Native Land Use by the Iban. *Journal of Ecological Research*, 22, 403-413.

John, B. & Rajendran. C. (2008). Geomorphic indicators of Neotectonism from the Pre – Cambrian terrain of Peninsular India: a study from the Bharathapuzha Basin, Kerala. *Journal of Geological Society of India*, 71, 827 – 840.

Kale, V.S.; Sengupta, S.; Achyuthan, H. & Jaiswal, M.K. (2014). Tectonic controls upon Kaveri River drainage, cratonic Peninsular India: inferences from longitudinal profiles, morphotectonic indices, hanging valleys and fluvial records. *Geomorphology*, 227, 153-165.

Keller, E.A. & Pinter, N. (2002). *Active tectonics: earthquakes, uplift and landscape*. Prentice Hall incorporation, New Jersey, 362.

King, R.C.; Backe, G.; Morley, C.K.; Hillis, R.R. & Tingay, M.R.P. (2010a). Balancing deformation in NW Borneo: quantifying plate-scale vs. gravitational tectonics in a delta and deepwater fold-thrust belt system. *Marine and Petroleum Geology*, 27, 238–249.

King, R.C.; Hillis, R.R.; Tingay, M.R.P. & Damit, A. R. (2010b). Present day stress and neotectonic provinces of the Baram Delta and deep-water fold-thrust belt. *Journal of Geological Society*, 166, 197–200.

King, R. C.; Tingay, M. R. P.; Hillis, R. R.; Morley, C. K. & Clark, J. (2010c). Present- day stress orientations and tectonic provinces of the NW Borneo collisional margin. *Journal of Geophysical Research*, 1-15.

Lambiase, J. J.; Rahim A. A. A. & Peng, C. Y. (2002). Facies distribution and sedimentary processes on the modern Baram Delta: Implications for the reservoir sandstones of NW Borneo, *Marine and Petroleum Geology*, 19, 69-78, doi: 10.1016/S0264-8172(01)00048-4.

Leyu, C. H.; Chang, C. F.; Arnold, E. P.; Kho, S. L.; Lim, Y. T.; Subramaniam, M.; Ong, T. C.; Tan, C. K.; Yap, K. S. & Goh, H. L. (1985). Southeast Asia Association of Seismology and Earthquake Engineering Series on Seismology, 3.

Lim, P. S. (1985). *History of earthquake activities in Sabah, 1897 - 1983*. Geological Survey Malaysia Annual Report 1983, 350 – 357.

Lim, P. S. (1986). *Seismic activities in Sabah and their relationship to regional tectonics*. Geological Survey of Malaysia Annual Report 1985, 465 – 480.

Malik, J. N.; Sahoo, A. K. & Shah, A. A. (2007). Ground-penetrating radar investigation along Pinjore Garden Fault: Implication toward identification of shallow subsurface deformation along active fault, NW Himalaya. *Current Science*, 1422-1427.

Malik, J. N. & Mohanty, C. (2007). Active tectonic influence on the evolution of drainage and landscape: geomorphic signatures from frontal and hinterland areas along the Northwestern Himalaya, India. *Journal of Asian Earth Science*, 29, 604 – 618.

Mathew, M. J.; Menier, D.; Pubellier, M.; Sapin, F.; Siddiqui, N. & Sautter, B. (2015). Along-strike Deformation in Quaternary Valleys of Tropical NW Borneo: Implications for Active Tectonics, Seismicity and Geomorphology. American Geophysical Union. San Francisco.

Mathew, M. J.; Menier, D.; Siddiqui, N.; Kumar, S. G. & Authemayou, C. (2016a). Active tectonic deformation along rejuvenated faults in tropical Borneo: Inferences obtained from tectono-geomorphic evaluation. *Geomorphology*, 267, 1-15. doi:http://dx.doi.org/10.1016/j.geomorph.2016.05.016

Mathew, M. J.; Menier, D.; Siddiqui, N.; Ramkumar, M.; Santosh, M.; Kumar, S. & Hassaan, M. (2016b). Drainage basin and topographic analysis of a tropical landscape: Insights into surface and tectonic processes in northern Borneo. *Journal of Asian Earth Sciences*, 124, 14-27. doi:http://dx.doi.org/10.1016/j.jseaes.2016.04.016

Menier, D.; Pierson, B.; Chalabi, A.; Ting, K.K. & Pubellier, M. (2014). Morphological indicators of structural control, relative sea-level fluctuations and platform drowning on present-day and Miocene carbonate platforms. *Marine and Petroleum Geology*, 58, 776–788.

Menier, D.; Mathew, M.; Pubellier, M.; Sapin, F.; Delcaillau, B.; Siddiqui, N. & Santosh, M. (2017). Landscape response to progressive tectonic and climatic forcing in NW Borneo: Implications for geological and geomorphic controls on flood hazard. *Scientific Reports*, 1-18.

Moglen, G. E. & Bras, R. L. (1995). The importance of spatially heterogenous erosivity and the cumulative area distribution within a basin evolution model. *Geomorphology*, 12, 173 – 185.

Mohamed, A. (2012). *Monitoring Active Faults in Ranau, Sabah Using GPS*. 19th United Nations Regional Cartographic Conference for Asia and the Pacific, 1-7.

Mohapatra, S. & McMechan, G. A. (2014). Prediction and subtraction of coherent noise using a data driven time shift: A case study using field 2D and 3D GPR data. *Journal of Applied Geophysics*, 111, 312-319. doi:http://dx.doi.org/10.1016/j.jappgeo.2014.10.018

Montgomery, D. R. & Foufoula – Georgiou, E. (1993). Channel network source representation using digital elevation models. *Water Resources Research*, 29, 3925 – 3934.

Mooney, W.D., Ritsema, J., & Hwang, Y.K. (2012) Crustal Seismicity and earthquakes catalog maximum moment magnitude (Mcmax) in stable continental regions (SCRs): Correlation with the seismic velocity of the lithosphere. *Earth and Planetary Science Letters 357 – 358*, 78 – 83.

Morley, C.K. (2009). Growth of folds in deep-water setting, *Geopshere*, 5, 59–89.

Mukherjee, S. & Koyi, H. A. (2010a). Higher Himalayan Shear Zone, Sutlej section: structural geology and extrusion mechanism by various combinations of simple shear, pure shear and channel flow in shifting modes. *International Journal of Earth Science*, 99, 1267 – 1303.

Mukherjee, S & Koyi, H. A. (2010b). Higher Himalayan Shear Zone, Zanskar Indian Himalaya: microstructural studies and extrusion mechanism by a combination of simple shear and channel flow. *International Journal of Earth Science*, 99, 1083 – 1110.

Mukherjee, S. (2013). Higher Himalaya in the Bhagirathi section (NW Himalaya, India): its structures, backthrusts and extrusion mechanism by both channel flow and critical taper mechanisms. *International Journal of Earth Science*, 102, 1851 – 1870.

Mukherjee, S., Carosi, R., Van Der Beek, P. A., Mukherjee, B. K. & Robinson, D. M. (2015). Tectonics of the Himalaya: an introduction. *Geological Society, London, Special Publications*, 412, 1 – 3.

Mustafar, M. A.; Simons, W.J.F.; Tongkul, F.; Satirapod, C.; Omar, K.M. & Visser, P.N.A.M (2017). Quantifying deformation in North Borneo with GPS. *Springer*, 1241 - 1259.

Pedrera, A., Perez – Pena, J. V., Galindo – Zaldivar, J., Azanon, J. M., & Azor, A. (2009). Testing the sensitivity of geomorphic indices in areas of low – rate active folding (eastern Betic Cordillera, Spain). *Geomorphology*, 105, 218 – 231.

Peters, G., & Van Balen, R.T. (2007). Tectonic geomorphology of the northern Upper Rhine Graben, Germany. *Global and Planetary Change*. 58, 310-334.

Potere, D. (2008). Horizontal position accuracy of Google Earth's high – resolution imagery archive. *Sensors*, 8, 7973 – 7981.

Rahim, A. I. &Musta, B. (2015). *The stability of Metasedimentary rock in Ranau, Sabah, Malaysia*. The 2nd International Conference and the 1st Joint Conference, 69 – 79.

Rockwell, T. K., Keller, E.A., & Johnson, D.L. (1984). *Tectonic geomorphology of alluvial fans and mountain fronts near Ventura, California*. In: Morisawa, M., Hack, T.J. (Eds.), Tectonic Geomorphology. Geomorphology, State University of New York, Binghamton, 183-207.

Sandal, S.T. (1996). *The Geology and Hydrocarbon Resources of Negara Brunei Darussalam*, Brunei Shell Petroleum, Bandar Seri Begawan, 243.

Sapin, F., Pubellier, M., Ringenbach, J. C. & Rives, T. (2009). *The Brunei fold-and-thrust belt: Tectonically-or Gravity-driven?* AAPG Hedberg Conference, 1-6.

Sapin, F., Pubellier, M., Lahfid, A., Janots, D., Aubourg, C., & Ringenbach, J.C. (2011). Onshore record of the subduction of a crustal salient: example of the NW Borneo Wedge. *Terra Nova, 23*, 232- 240. doi:10.1111/j.1365-3121.2011.01004.x

Sapin, F., Hermawan, I., Pubellier, M., Vigny, C., & Ringenbach, J. C. (2013). The recent convergence on the NW Borneo Wedge—a crustal-scale gravity gliding evidenced from GPS. *Geophysical Journal International*, 2, 549-556.

Schumm, S. A. (1956). Evolution of drainage systems and slopes in badlands at Perth Amboy, New Jersey. *Geological Society of Amsterdam*, 67, 597 – 646.

Shah, A. A. (2016). Understanding the recent Sabah earthquake and other seismogenic sources in North West Borneo. *Scientific Malaysian Magazine*. Retrieved from http://magazine.scientificmalaysian.com/issue-11-2015/understanding-sabah-earthquake/.

Shah, A. A., & Malik, J. N. (2017). Four major unknown active faults identified, using satellite data, in India and Pakistan portions of NW Himalaya. *Natural Hazards*, 88, 845 – 1865.

Shah, A. A., Zhafri, M. N., Delson J. & Batmanathan N. (2018). Major Strike-slip Faults Identified, Using Satellite Data, in Central Borneo, SE Asia. *Geosciences*, 8, 156.

Shyu, J. B. H., Sieh, K., Chen, Y. G. & Liu, C. S. (2005). Neotectonic architecture of Taiwan and its implications for future large earthquakes. *Journal of Geophysical Research: Solid Earth*, 110. doi: 10.1029/2004JB003251.

Silva, G.P., Goy, J.L., Zazo, C. & Bardaji, T. (2003). Fault-generated Mountain fronts in southeast Spain: geomorphologic assessment of tectonic and seismic activity. *Geomorphology*, 50, 203-225.

Simons, W. J. F., Socquet, A., Vigny, C., Ambrosius, B. A. C., Haji Abu, S., Promthong, C., & Spakman, W. (2007). A decade of GPS in Southeast Asia: Resolving Sundaland motion and boundaries. *Journal of Geophysical Research: Solid Earth*, 112. doi: 10.1029/2005JB003868.

Sklar, L., & Dietrich, W. E. (1998). River longitudinal profiles and bedrock incision models: stream power and the influence of sediment supply. *American Geophysical Union Geophysical Monograph*, 107, 237 – 260.

Slaymaker, O. (2001). The role of remote sensing in geomorphology and terrain analysis in the Canadian Cordillera. *International Journal of Applied Earth Observation and Geoinformation*, 3, 11 – 17.

Strahler, A. N. (1957). Quantitative analysis of watershed geomorphology. *Transactions – American Geophysical Union*, 38, 913 – 920.

Synder, N. P., Whipple, K. X., Tucker, G. E., & Merritts, D. J. (2000). Landscape response to tectonic forcing: Digital elevation model analysis of stream profiles in the Mendocino triple junction region, northern California. *Journal of Geological Society of Amsterdam*, 112, 1250 – 1263.

Talwani, P. (2014). *A unified model for intraplate earthquakes*. In: Talwani P (ed) Intraplate earthquakes. Cambridge University Press, 275 – 302.

Talwani, P. (2016). On the nature of intraplate earthquakes. *Springer*, 1 – 22.

Tarboton, D. G., Bras, R. L. & Rodrigues – Iturbe, I. (1991). On the extraction of channel networks from digital elevation data. *Hydrological Processes*, 5, 81 – 100.

Tongkul, F. (2015). Status of Mount Kinabalu water catchments after the June 2015 Ranau Earthquake – Lessons learned. International Conference on the Heart of Borneo, Kota Kinabalu, 1 – 67.

Tongkul, F. (2017). Active tectonics in Sabah – seismicity and active faults. *Bulletin of the Geological Society of Malaysia*, 64, 27 – 36.

Toudeshki, V. H., & Arian, M. (2011). Morphotectonic analysis in the Ghezel Ozan river basin, NW Iran. *Journal of Geography and Geology*, 3, 258.

Tucker, G. (1996). *Modelling the regional – scale interaction of climate, tectonics and topography*. Pennsylvania State University Earth System Science Center Technical Report, 96.

Viveen, W., Van Balen, R.T., Schoorl, J.M., Veldkamp, A., Temme, A.J.M., & Vidal-Romani, J.R. (2012). Assessment of recent tectonic activity on the NW Iberian Atlantic Margin by means of geomorphic indices and field studies of the Lower Mino River terraces. *Tectonophysics*, 544-545, 13-30.

Wang, P. C., Li, S. Z., Guo, L. L., Jiang, S. H., Somerville, I. D., Zhao, S. J., & Han, B. (2016). Mesozoic and Cenozoic accretionary orogenic processes in Borneo and their mechanisms. *Geological Journal*, 51, 464-489. doi:10.1002/gj.2835.

Wang, Y., Wei, S., Wang, X., Lindsey, E. O., Tongkul, F., Tapponnier, P., & Sieh, K. (2017). The 2015 Mw 6.0 Mt. Kinabalu earthquake: an infrequent fault rupture within the Crocker fault system of East Malaysia. *Springer Open*, 1-12.

Waikar, M., & Nilawar, A. P. (2014). Morphometric analysis of a drainage basin using geographical information system: a case study. *International Journal of Multidisciplinary and Current Research*, 2, 179 – 184.

Wannier, M., Lee, C., Raven, H., Sorkhabi, R., Lesslar, P., & Ibrahim, A. (2011). *Geological Excursion around Miri, Sarawak.* Miri: Eco Media Software.

Weissel, J. K., & Seidl, M. A. (1998). Inland propagation of erosional escarpments and river profile evolution across the southeast Australian passive continental margin. *Geophysical Monographs Series American Geophysical Union*, 107, 189 – 206.

Wilford, G. E. (1967). Earth tremors in Sabah. *Sabah Society Journal*, 3, 136 – 138.

Yamakura, T., Kanzaki, M., Itoh, A., Ohkubo, T., Ogino, K., Chai, E.O.K, Lee, H. S. & Ashton, P.S. (1995). Topography of a Large – Scale Research Plot Established within a Tropical Rain Forest at Lambir, Sarawak. *Journal of Tropics*, 5: 41 – 56

Yan, A. S. (2010). *Earthquake-Generating Faults In Malaysia*. Retrieved from http://www.met.gov.my/web/metmalaysia/publications/reports/presentationpaper/2010/natset2010/presentation/182521/Mr.%20Alexander%20Yan%20Sze%20Wah%20(JMG).pdf

Yeats, R. S., Sieh, K., & Allen, C. R. (1997). *The Geology of Earthquakes*, Oxford University Press, Beijing, China.

Yusoff, H. H. M., Khamarrul Azahari, R., Florence, Y., Afifi, H., Jasmi, T., Zakaria, M. & Razain, A.R. (2016). Mapping of post-event earthquake induced landslides in Sg. Mesilou using LiDAR. IOP Conference Series: Earth and Environmental Science, 37(1), 012068. Retrieved from http://stacks.iop.org/1755-1315/37/i=1/a=012068

Zygouri, V., Koukouvelas, I. K., Kokkalas, S, Xypolias, P., & Papadopoulos, G.A. (2015). The Nisi Fault as a key structure for understanding the active deformation of the NW Peloponnese, Greece. *Geomorphology*, 237, 142-156.

Appendix A Hypsometry Curves

Sub – basin of Area 1

Area A

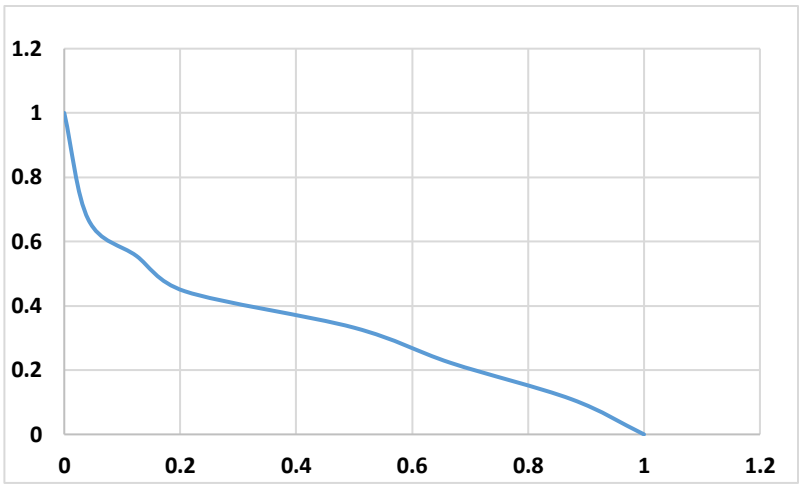

Figure A.1 the subdued peneplain stage of a basin.

Area B

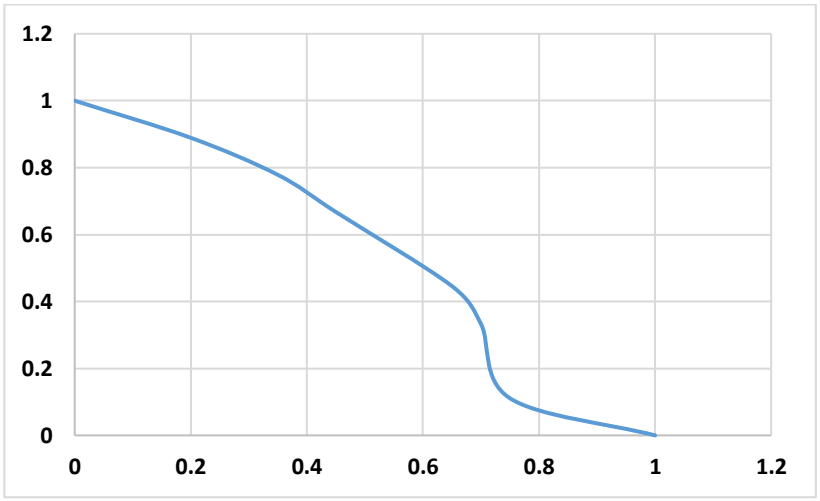

Figure A.2 the young topography on upstream region and subdues as it moves downstream.

Area C

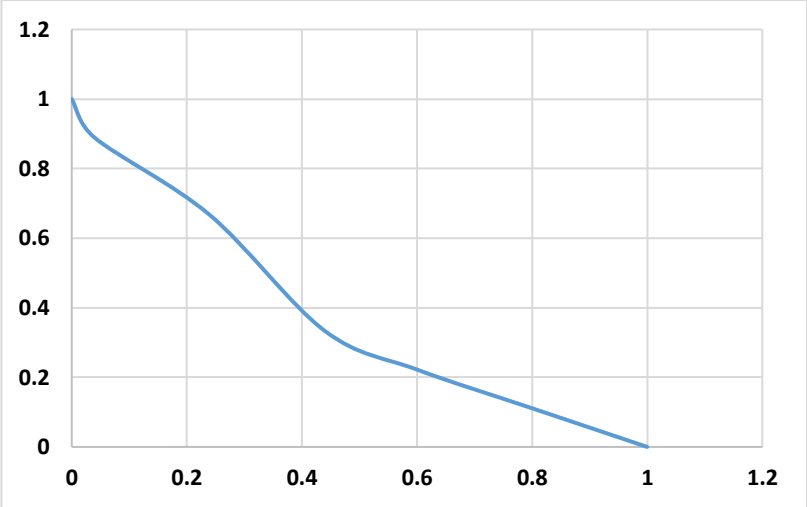

Figure A.3 the subdued peneplain stage of a basin.

Area D

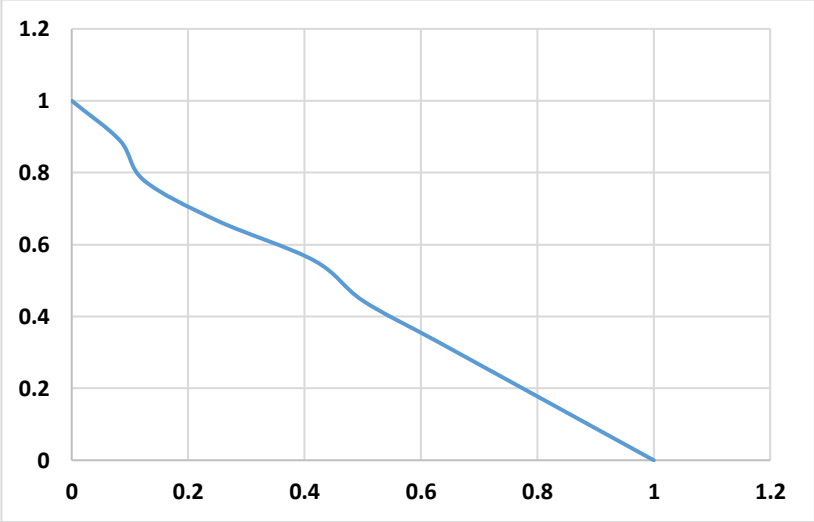

Figure A.4 increase in erosional processes as concavity increasing in upstream region.

Area E

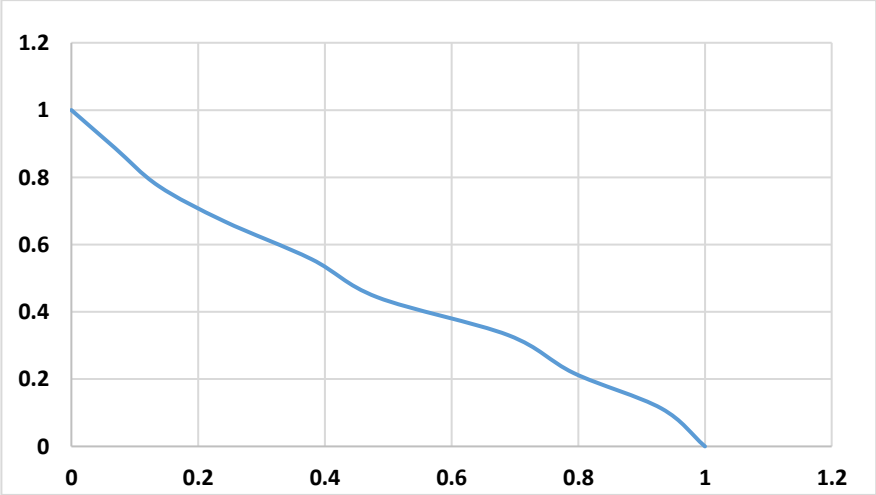

Figure A.5 variation in denudational process.

Area F

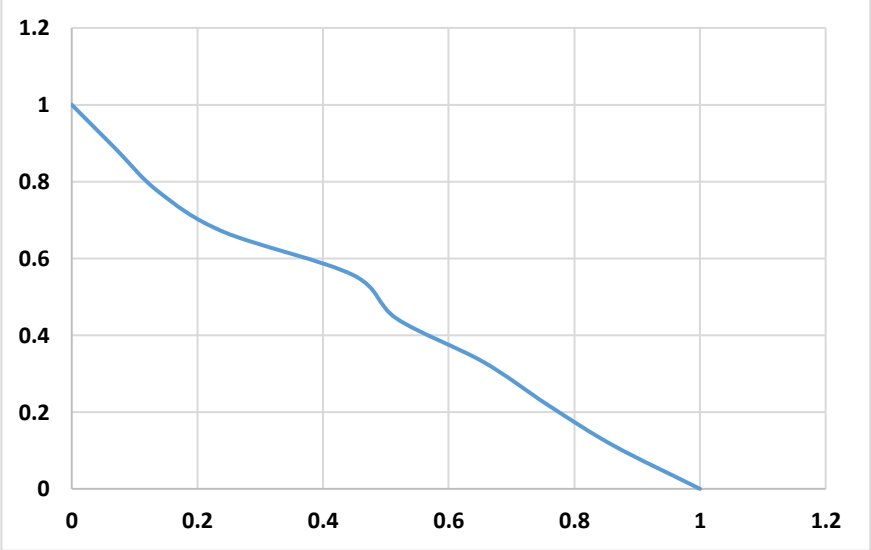

Figure A.6 increase in convexity curve at the middle of the basin.

Area G

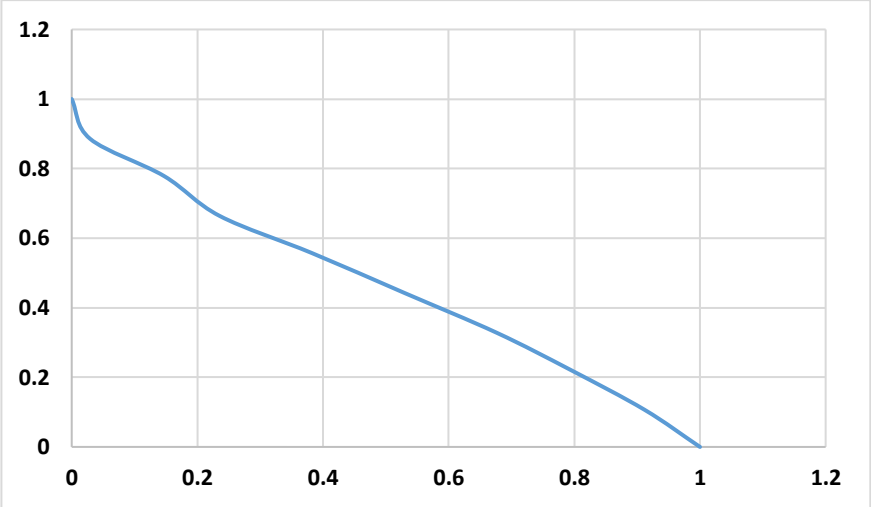

Figure A.7 the subdued peneplain stage of a basin.

Area H

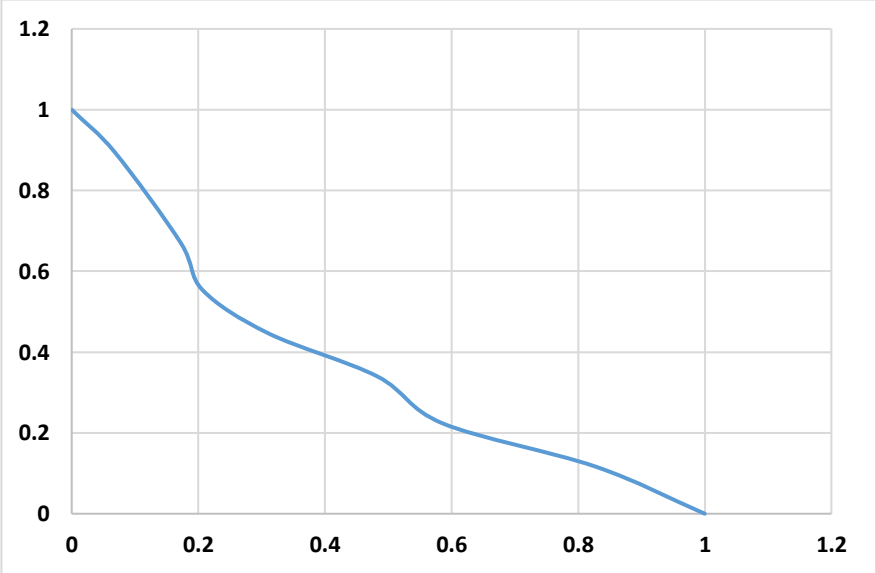

Figure A.8 increase in convexity curve at the upstream of the basin.

Area I

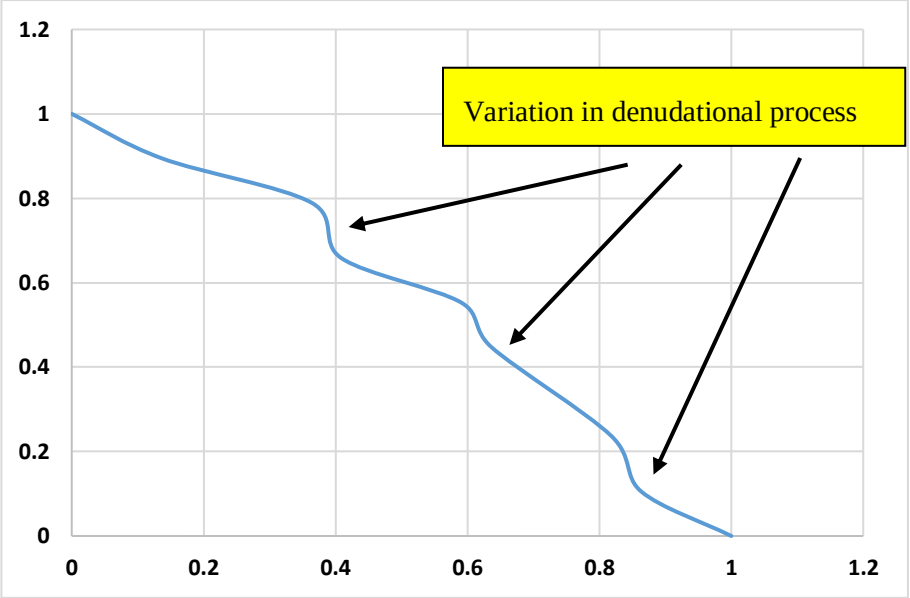

Figure A.9 complex curve in sub – basin area.

Area J

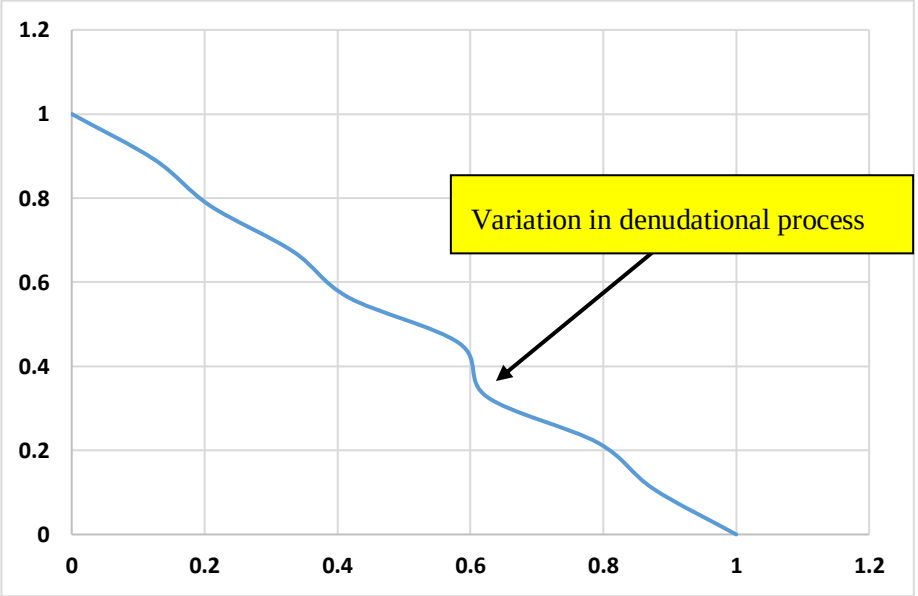

Figure A.10 complex curve in sub – basin area.

Area K

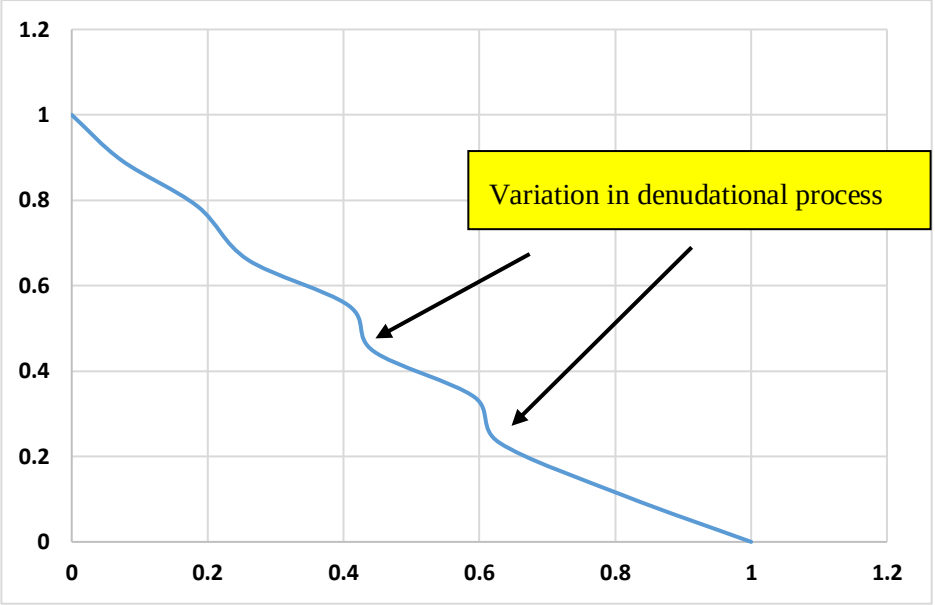

Figure A.11 complex curve in sub – basin area.

Area L

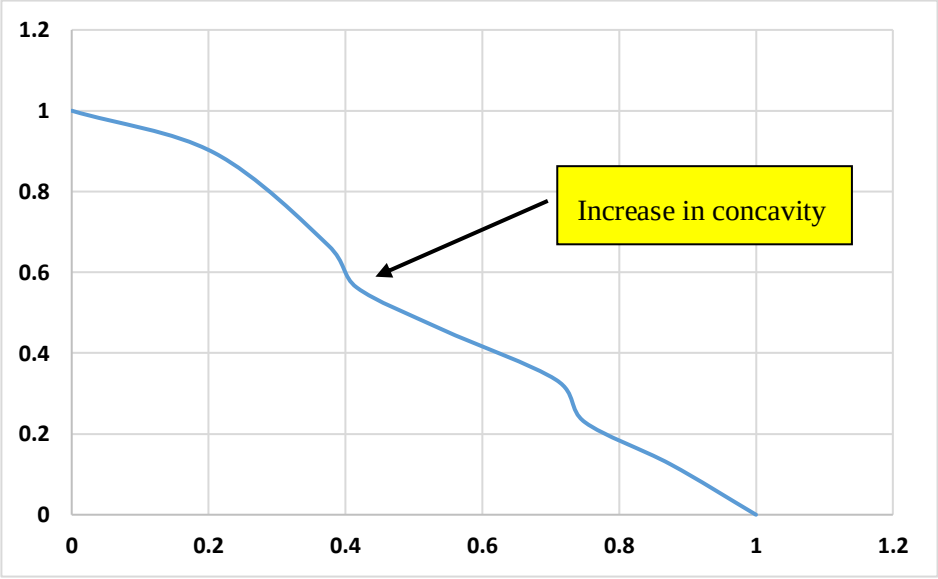

Figure A.12 young topography with variation in erosional process.

Area M

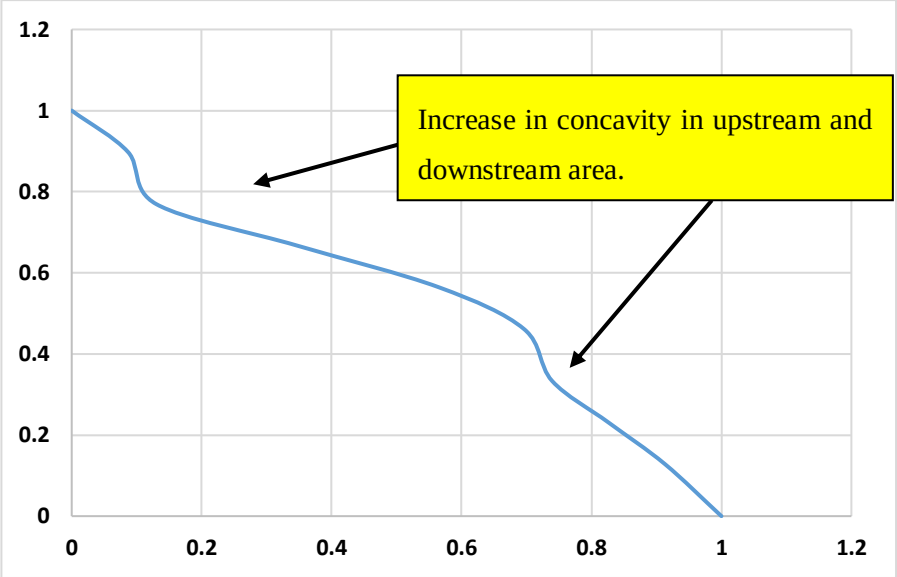

Figure A.13 complex curve in sub – basin area.

Area N

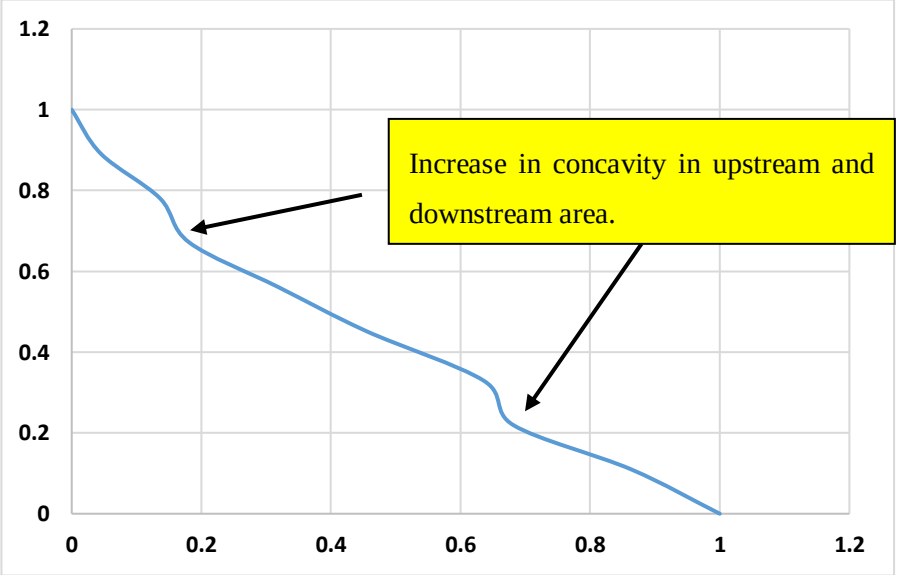

Figure A.14 complex curve in sub – basin area.

Area O

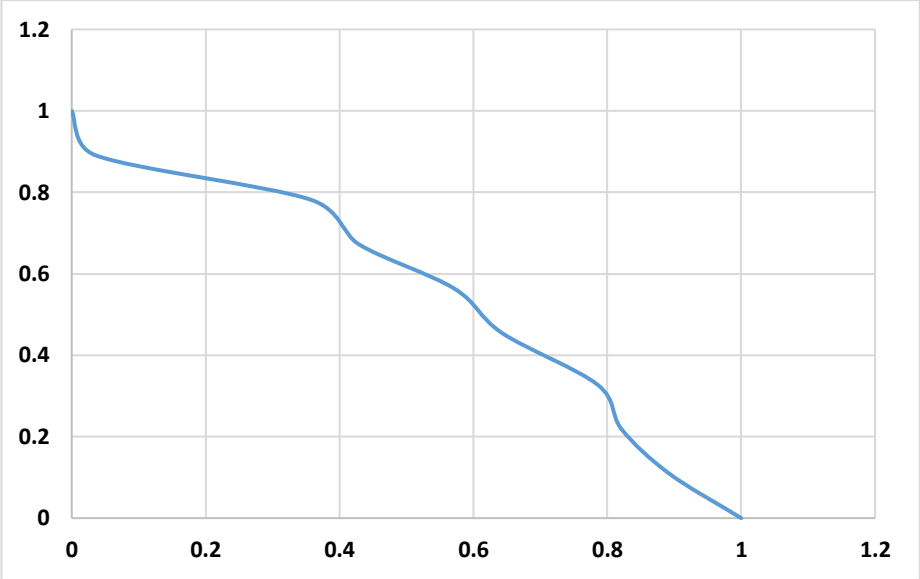

Figure A.15 variation in denudational process in upstream and downstream area.

Area P

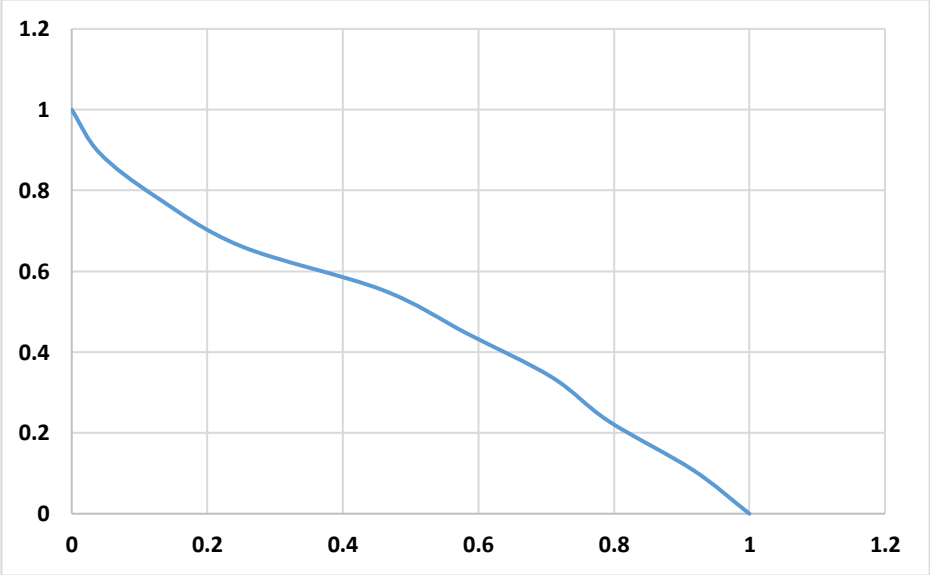

Figure A.16 moderately eroded region, forms S – shape curve.

Sub – basin of Area 2

Area A

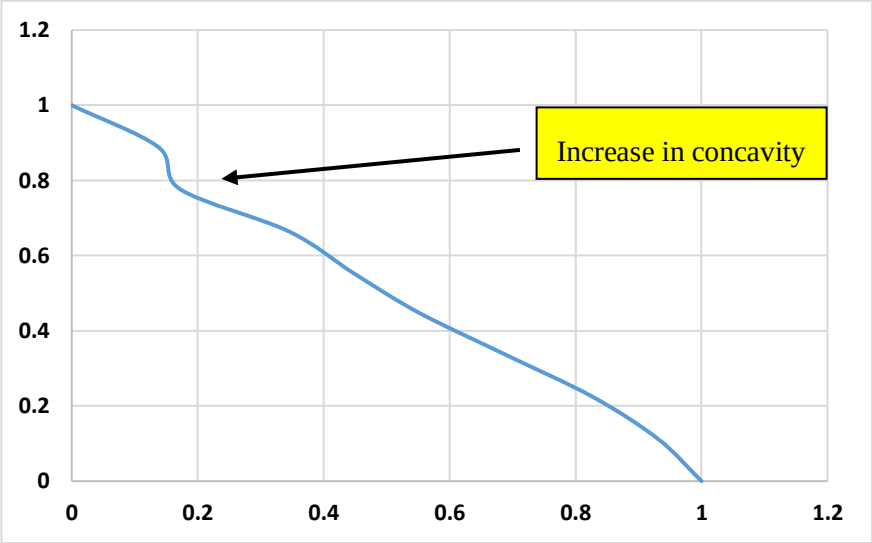

Figure A.17 young topography with slight concavity in upstream region.

Area B

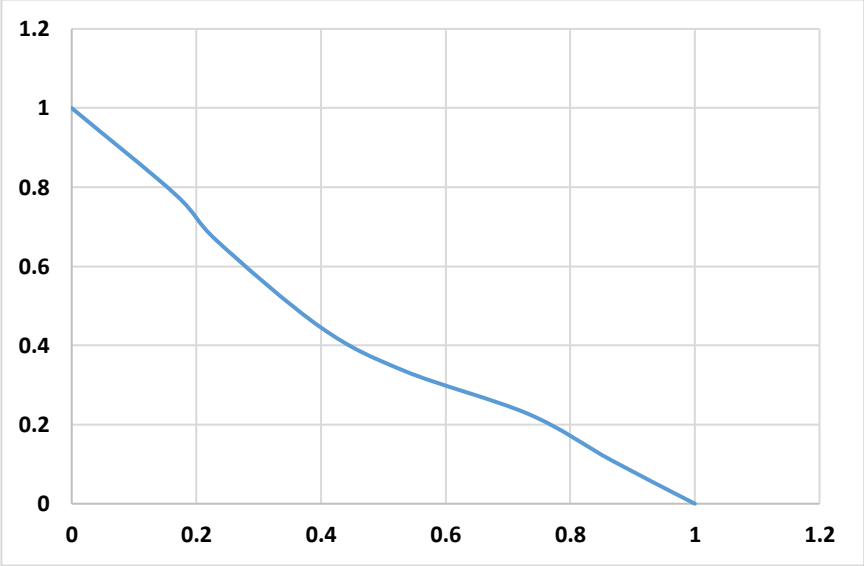

Figure A.18 increasing concavity, due to high erosion rate.

Area C

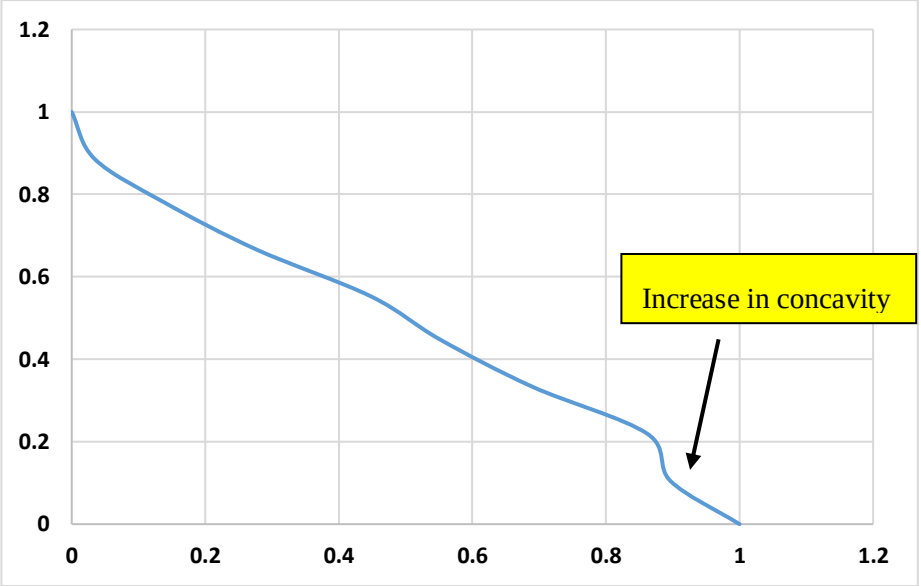

Figure A.19 old terrain with increasing concavity in downstream region.

Area D

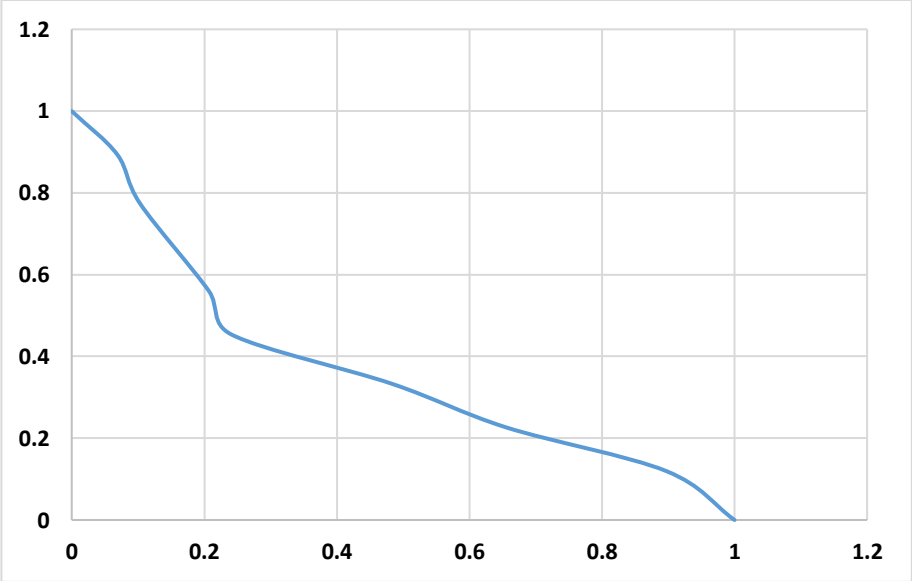

Figure A.20 the subdued peneplain stage of a basin.

Area E

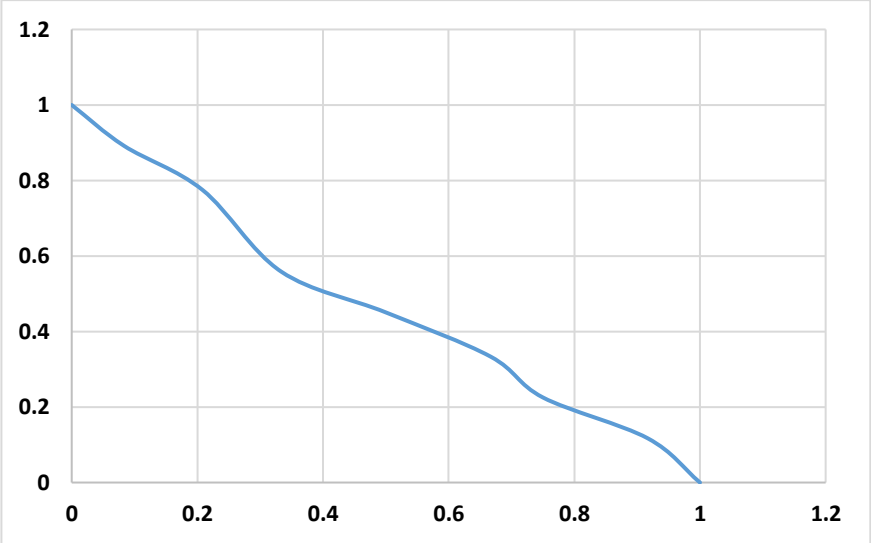

Figure A.21 complex features in sub – basin area.

Area F

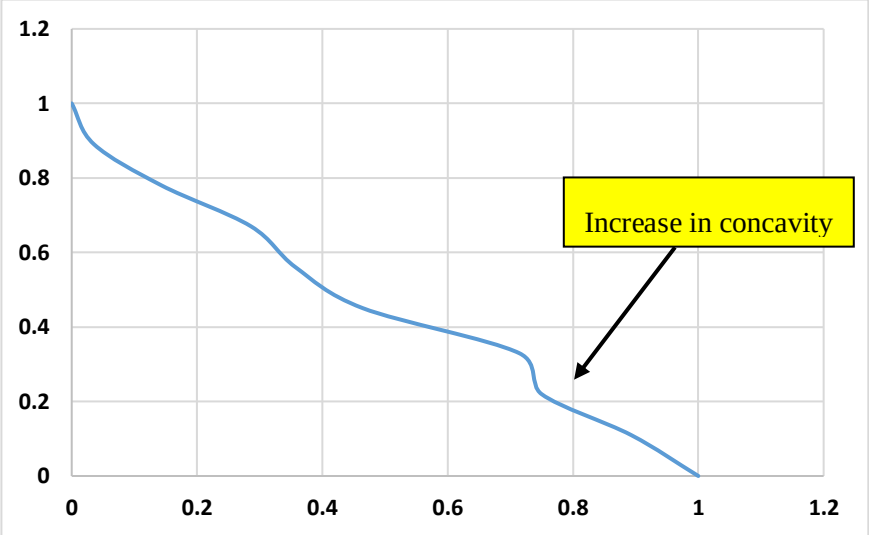

Figure A.22 complex features in sub – basin area.

Area G

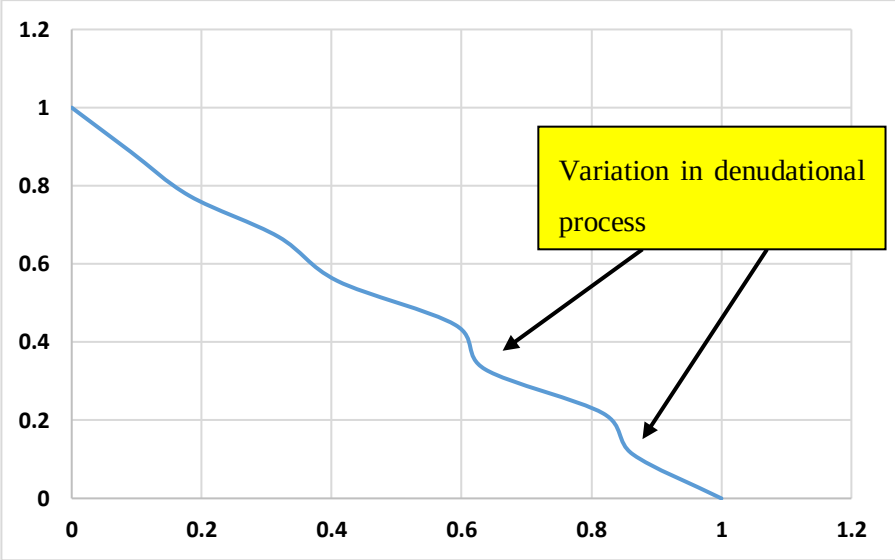

Figure A.23 complex features in sub – basin area.

Area H

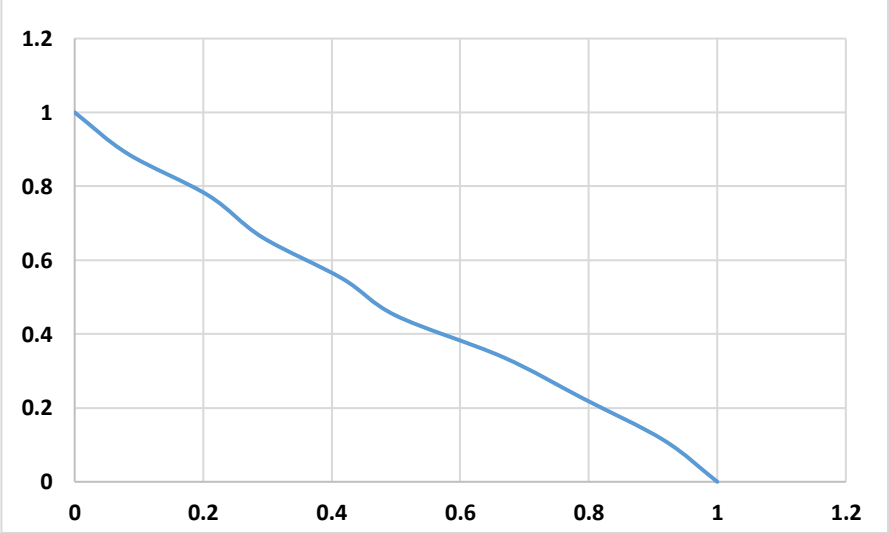

Figure A.24 steady denudational process.

Area I

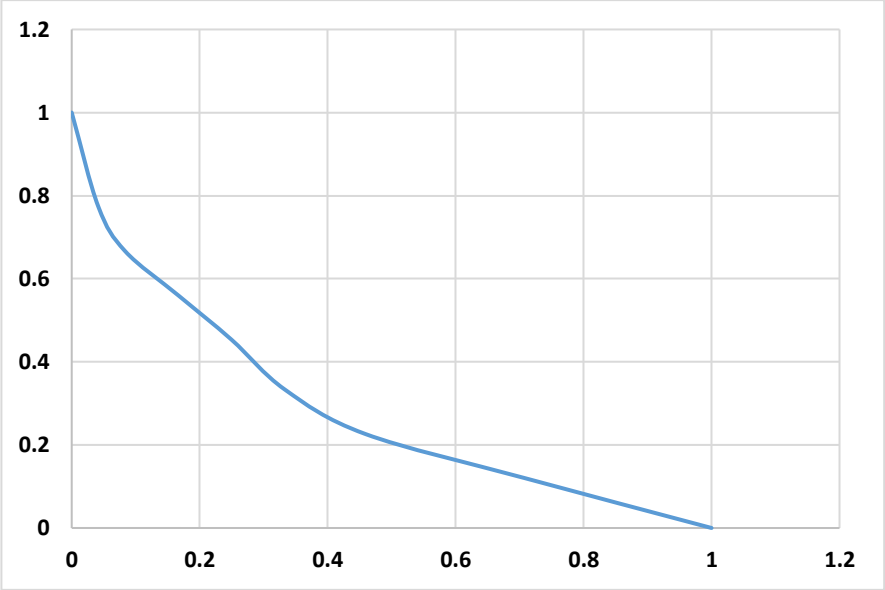

Figure A.25 subdued peneplain stage of a basin.

Area J

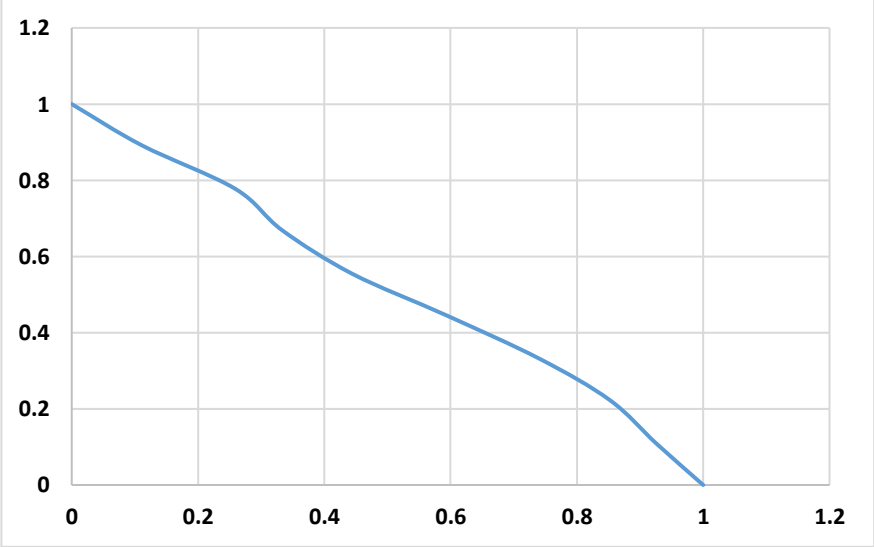

Figure A.26 young topography with increasing convexity.

Area K

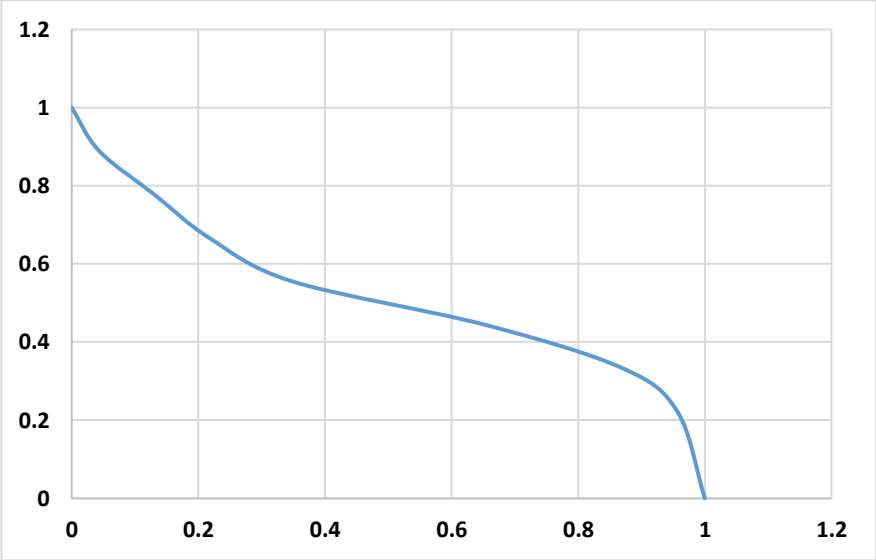

Figure A.27 textbook example of mature basin

Area L

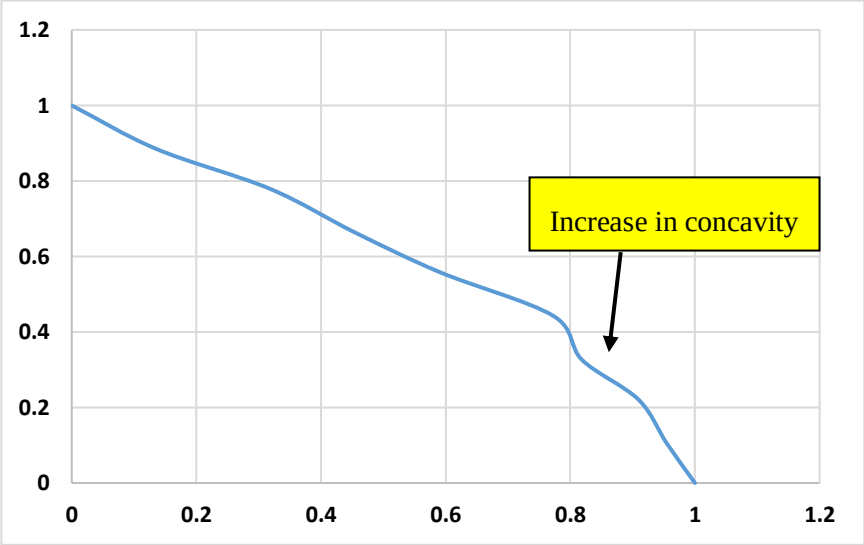

Figure A.28 young topography with increasing concavity.

Area M

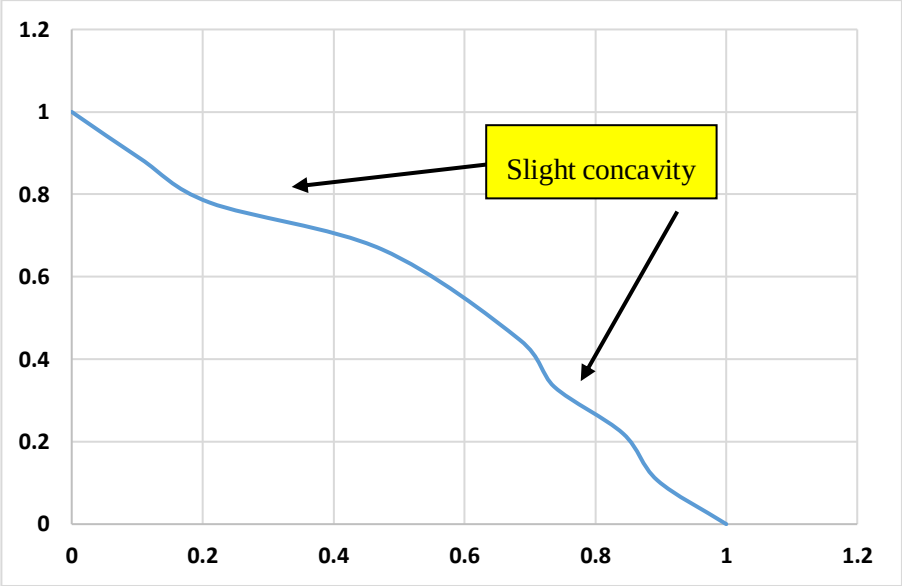

Figure A.29 young topography with slight increase in concavity.

Area N

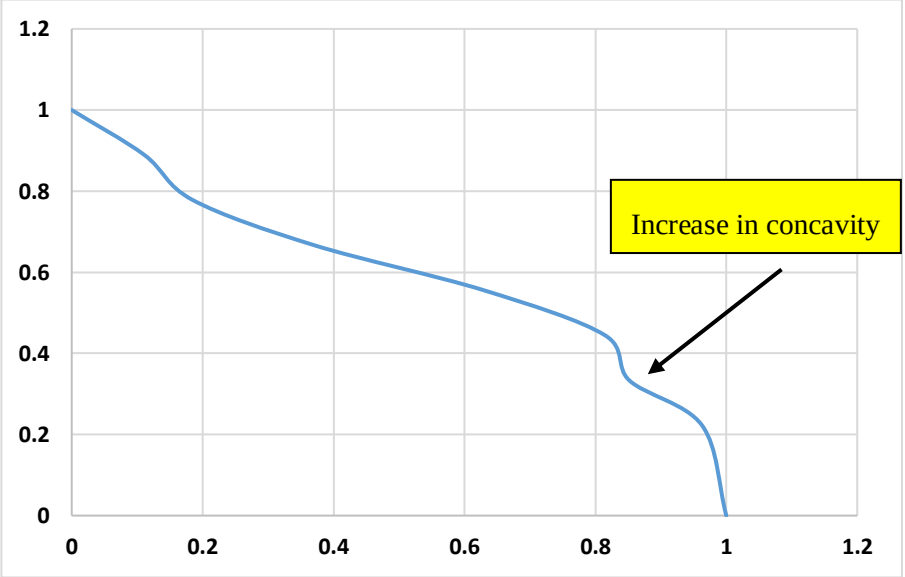

Figure A.30 young topography with slight increase in concavity.

Area O

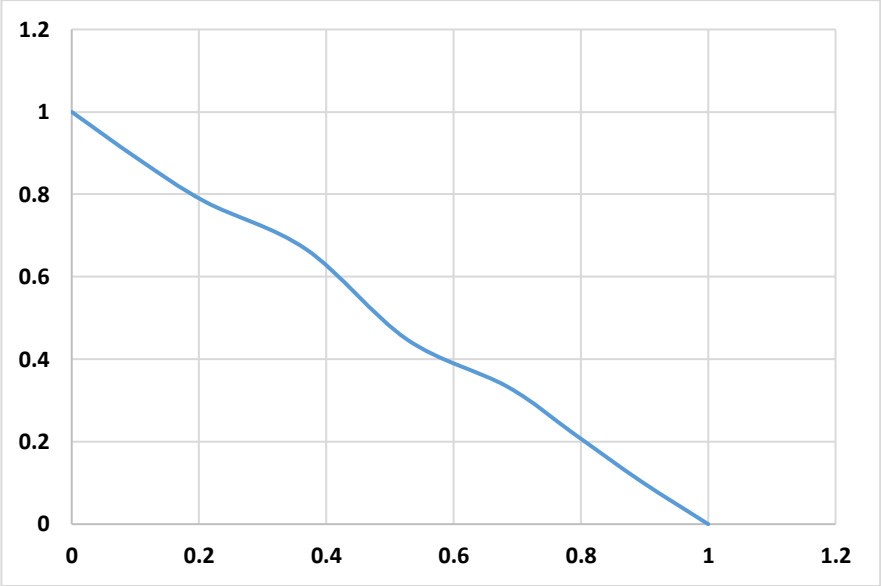

Figure A.31 steady denudational process.

Area P

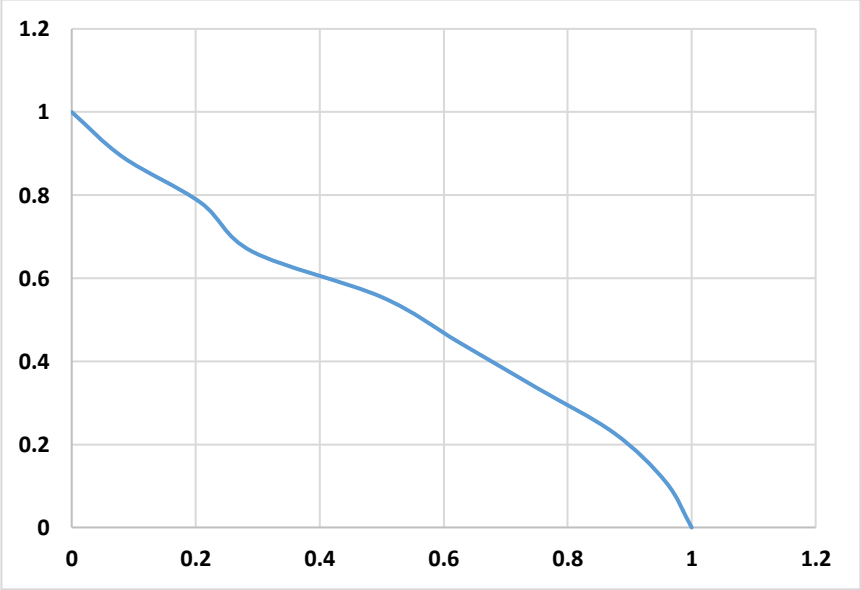

Figure A.32 increasing concavity in upstream region.

Sub – basin of Area 3

Area A

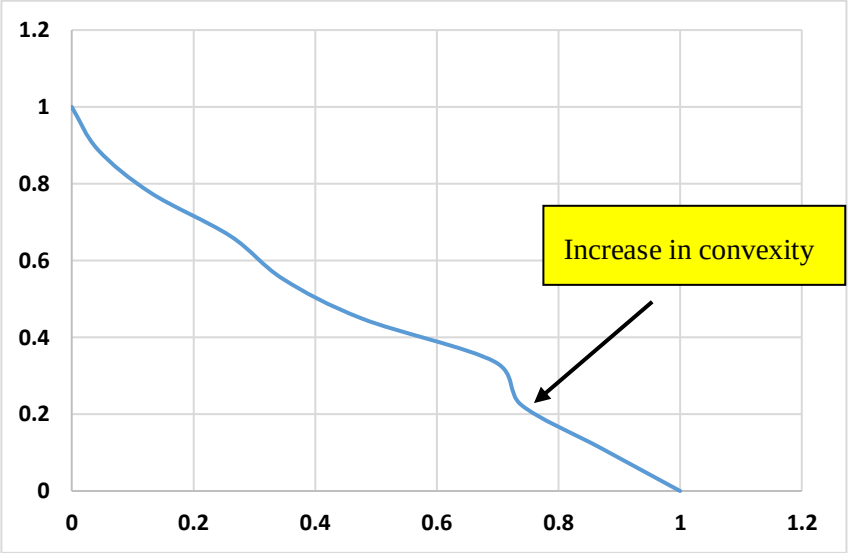

Figure A.33 increasing erosional process across this region.

Area B

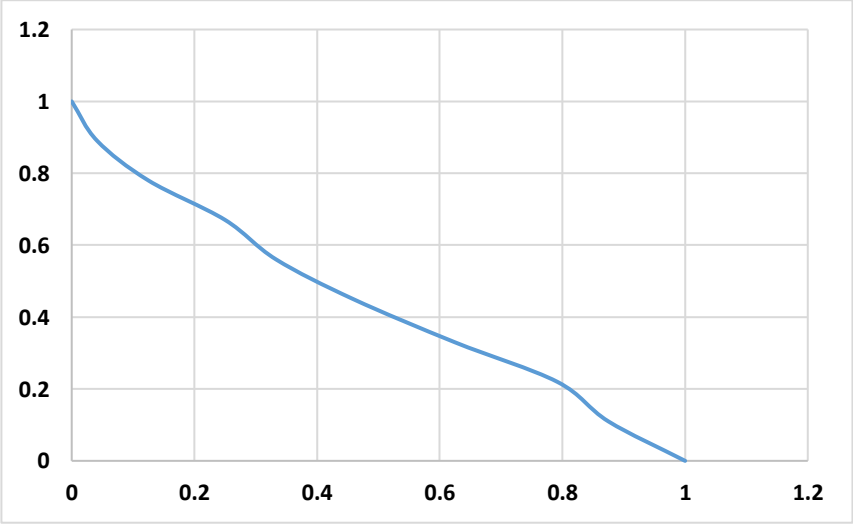

Figure A.34 increasing erosional process across this region.

Area C

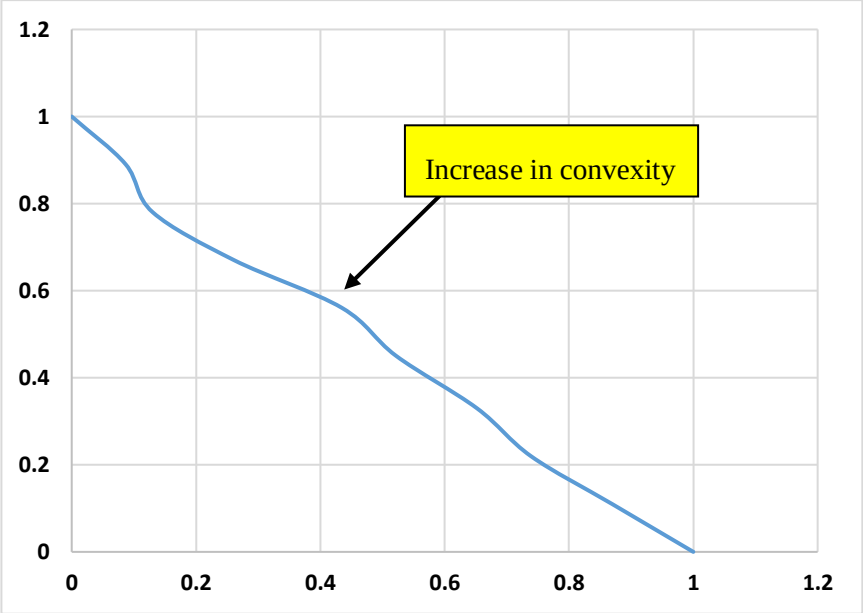

Figure A.35 increasing erosional process across this region.

Area D

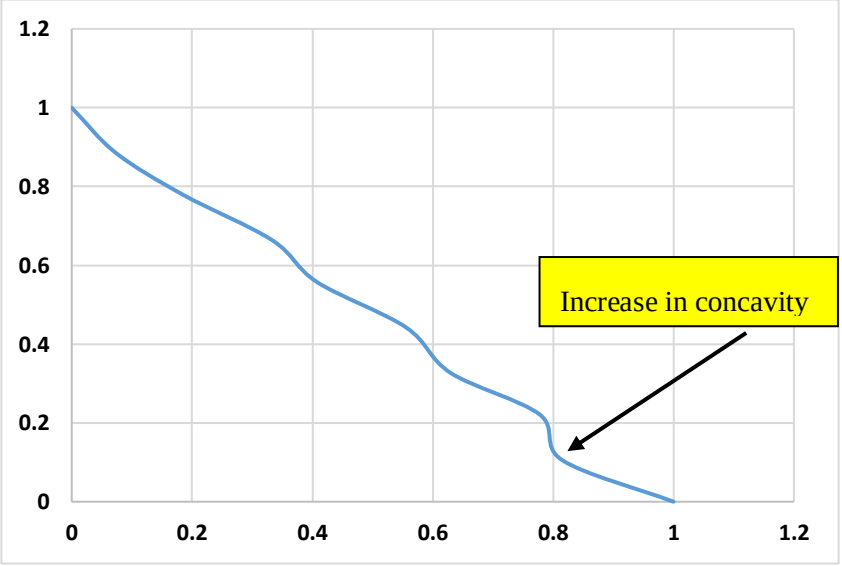

Figure A.36 increasing erosional process across this region.

Area E

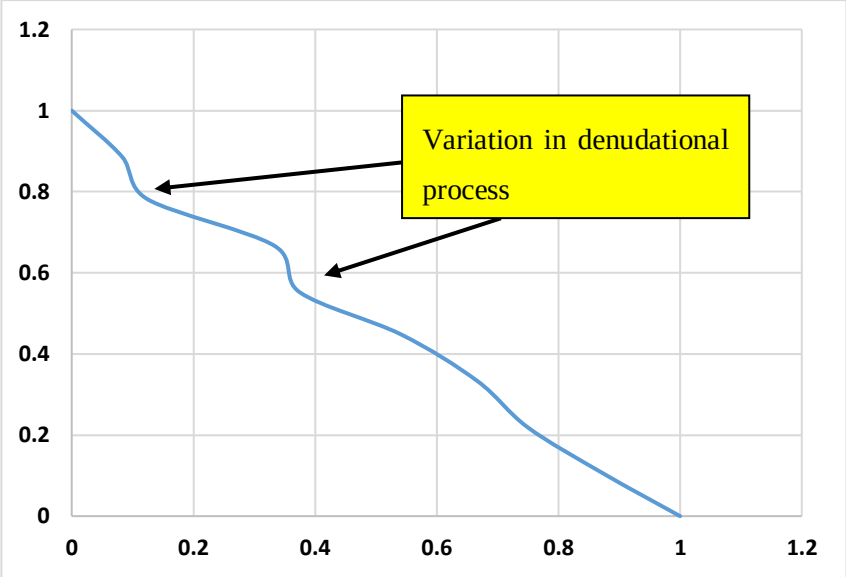

Figure A.37 complex features in sub – basin area.

Area F

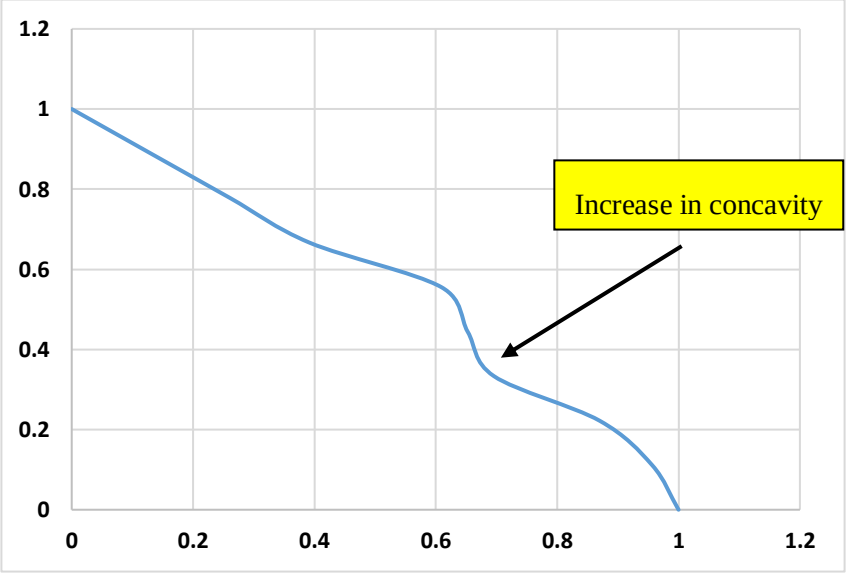

Figure A.38 young topography with slight increase in concavity.

Area G

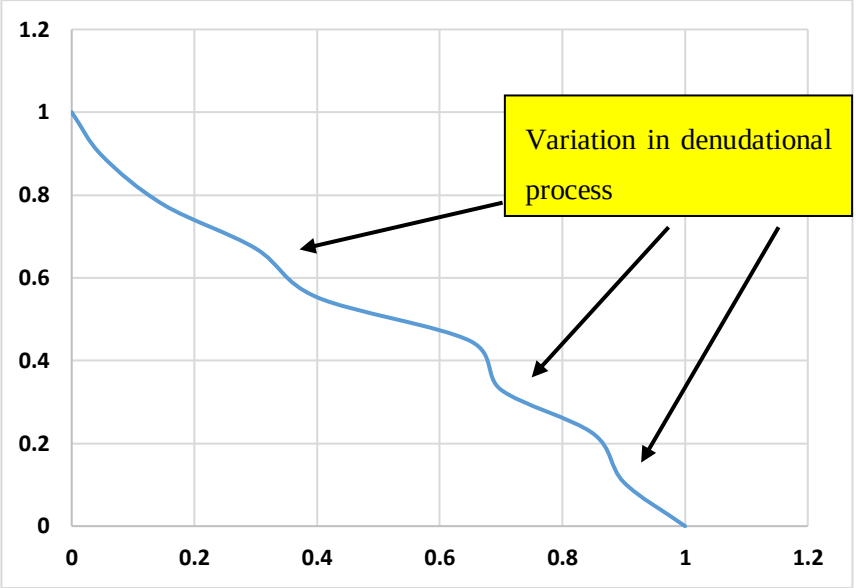

Figure A.39 complex features in sub – basin area.

Area H

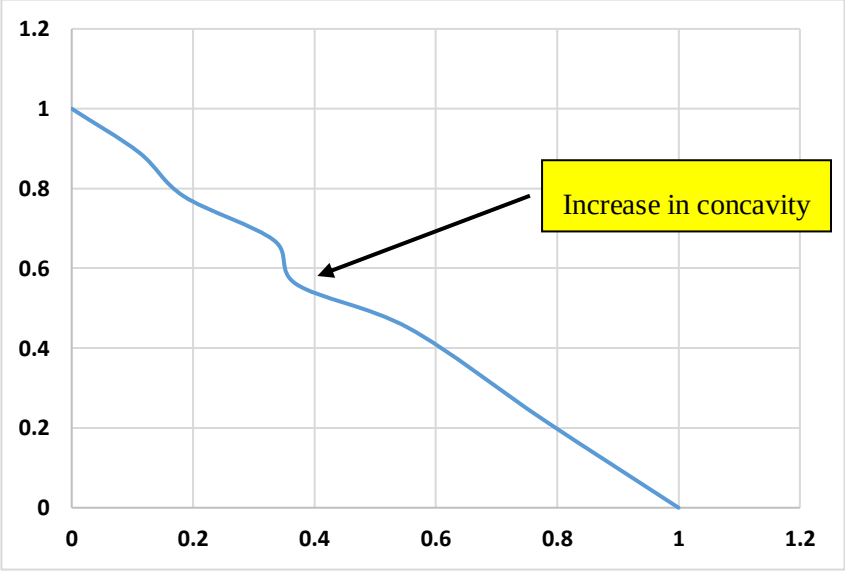

Figure A.40 increasing erosional process across this region.

Area I

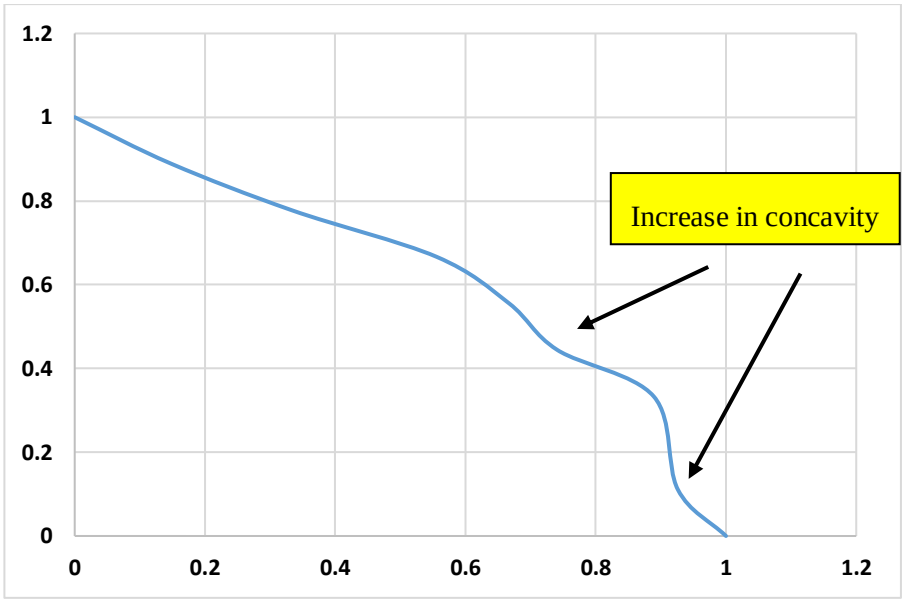

Figure A.41 young topography with slight increase in concavity.

Area J

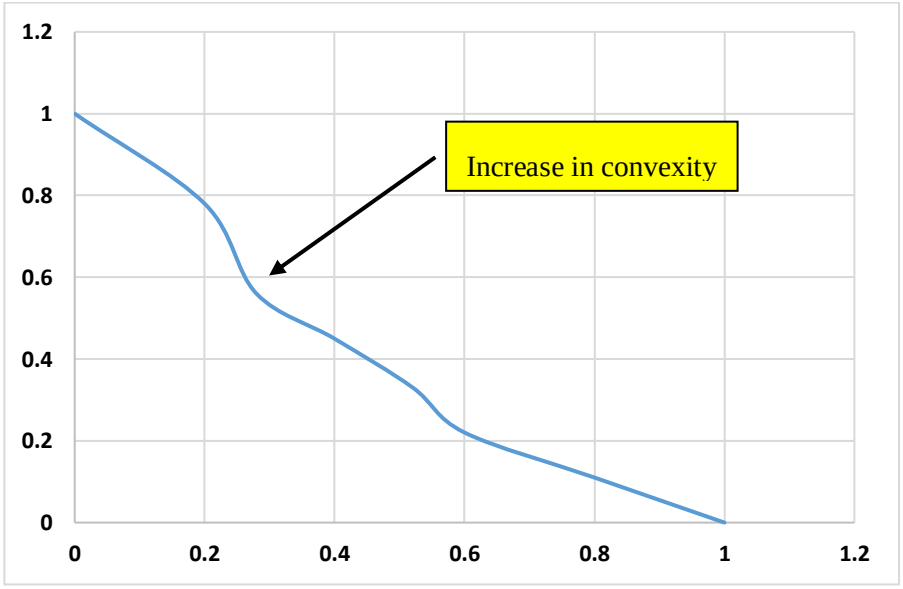

Figure A.42 increasing erosional process in downstream region.

Area K

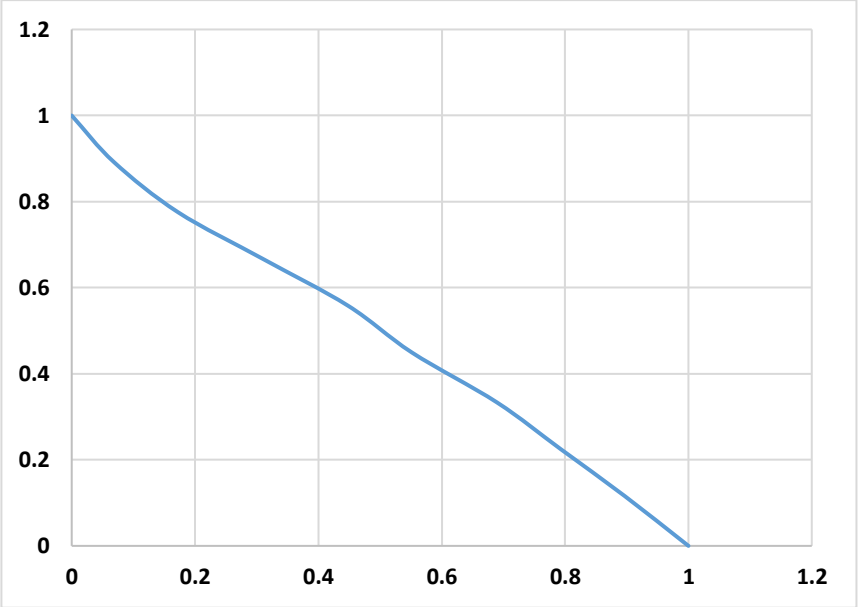

Figure A.43 steady denudational process.

Area L

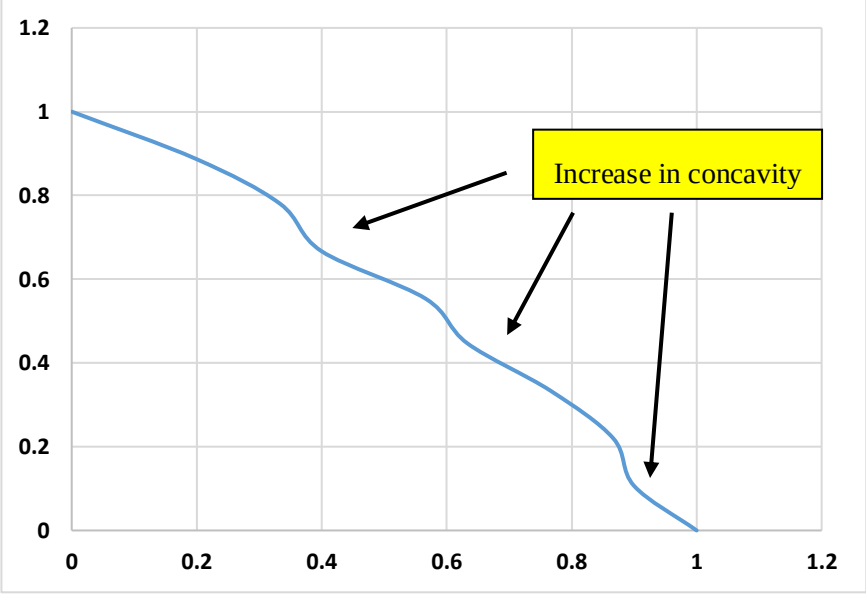

Figure A.44 young topography with slight increase in concavity.

Area M

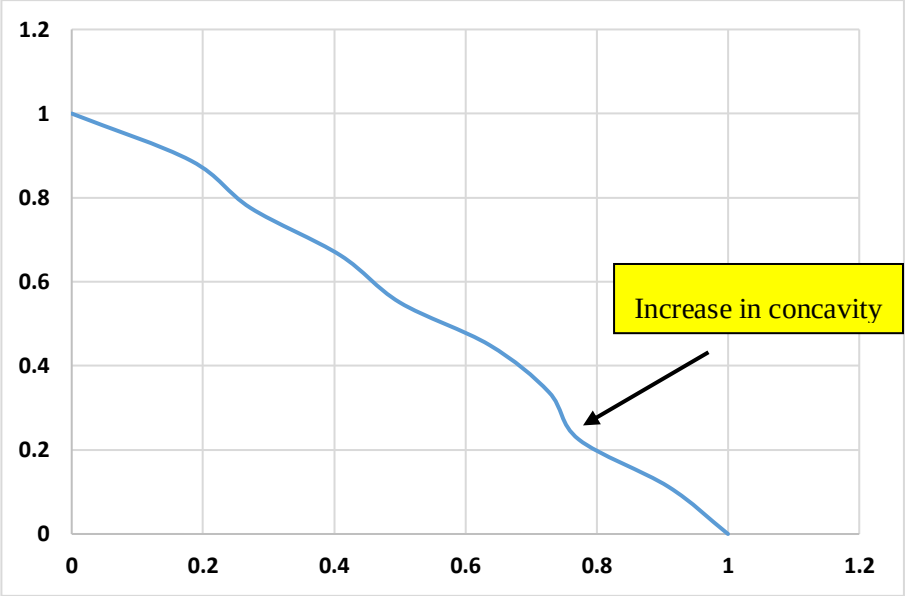

Figure A.45 young topography with slight increase in concavity.

Area N

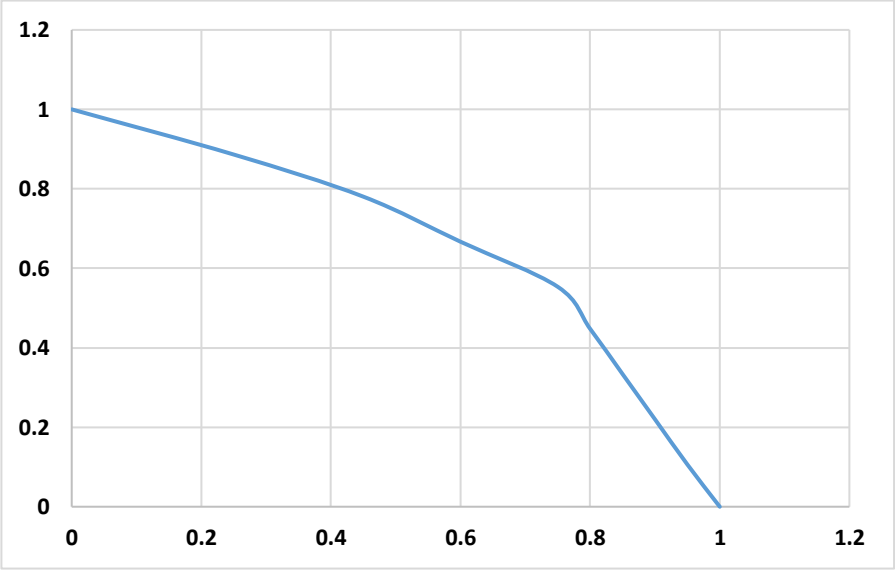

Figure A.46 the youthful stage of a basin.

Area O

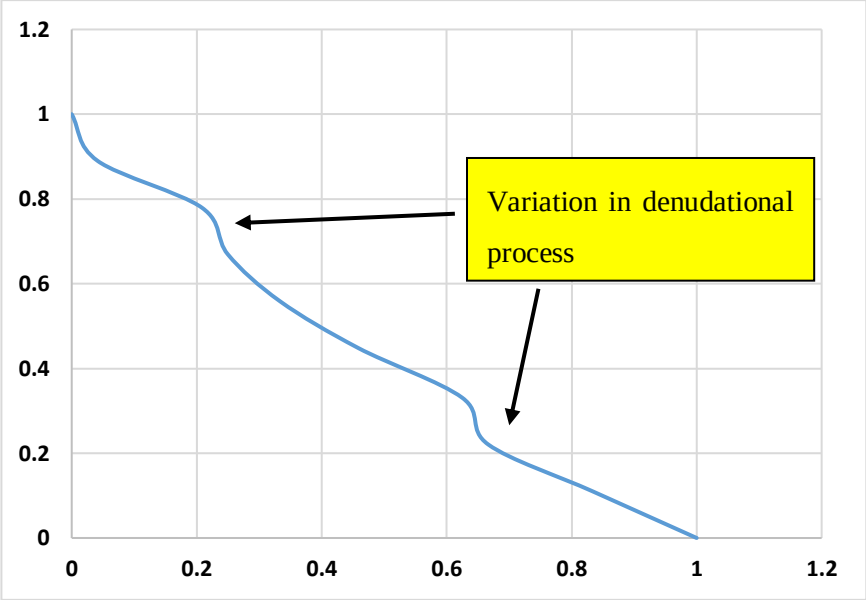

Figure A.47 complex features in sub – basin area.

Area P

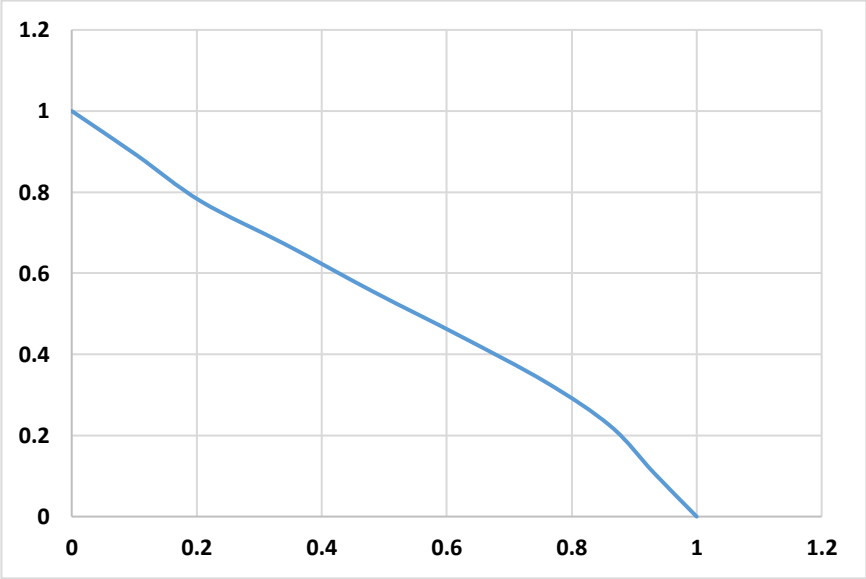

Figure A.48 youthful stage of a basin.

Sub – basin of Area 4

Area A

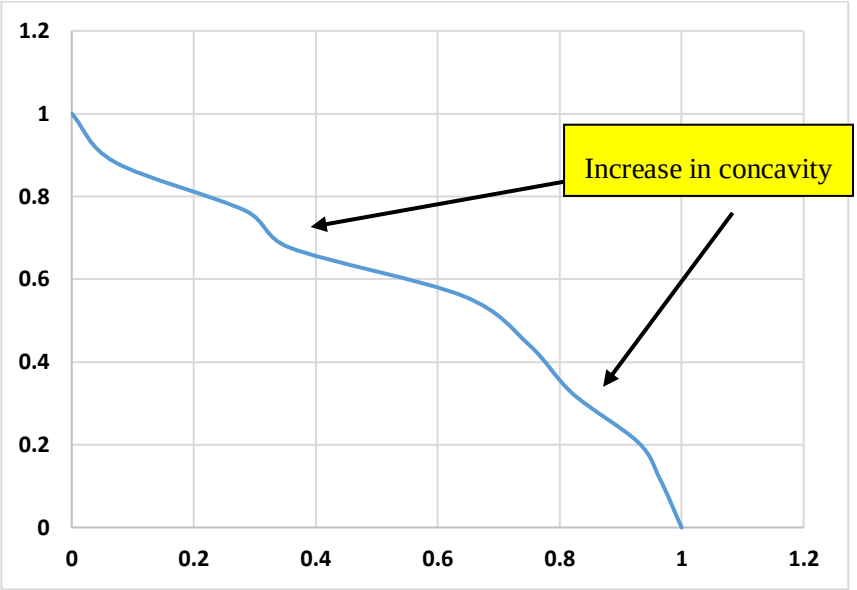

Figure A.49 increasing erosional process across this region.

Area B

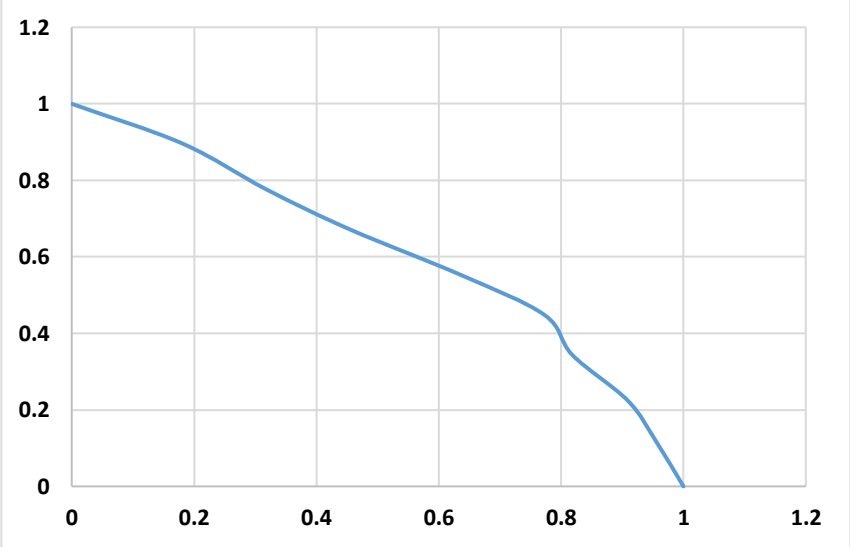

Figure A.50 youthful stage of a basin.

Area C

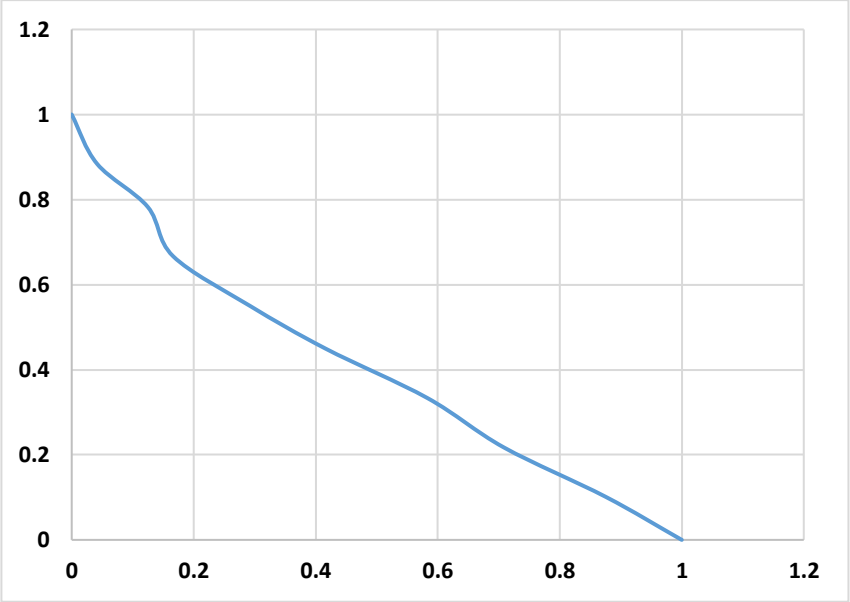

Figure A.51 increasing erosional process across this region.

Area D

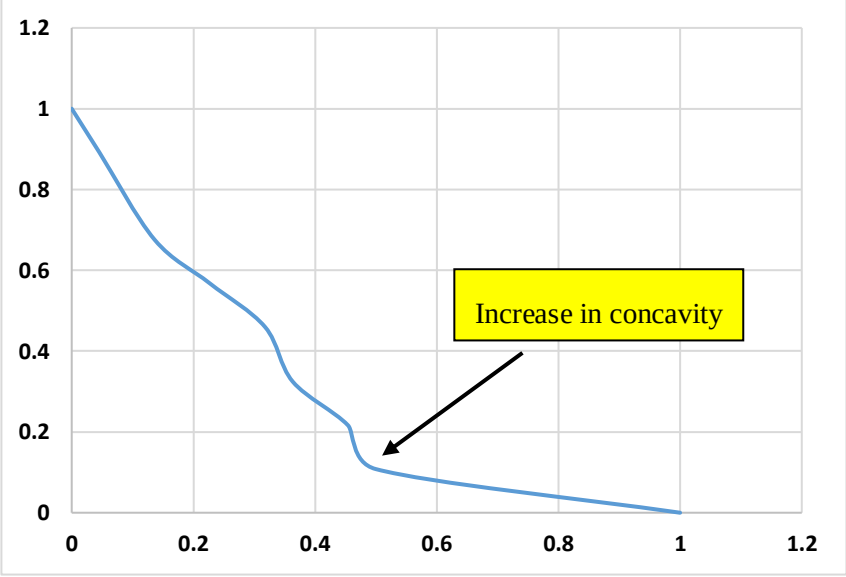

Figure A.52 increase in concavity as it moves downstream.

Area E

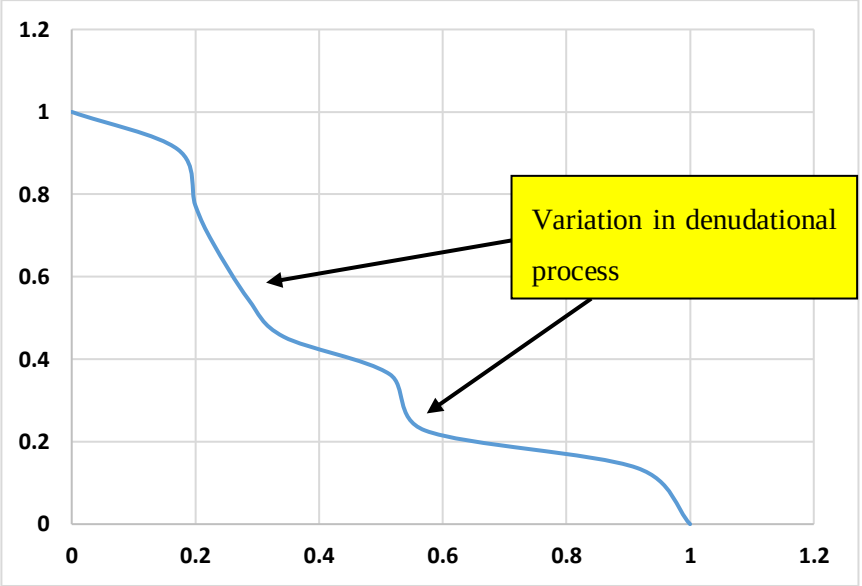

Figure A.53 increasing erosional process as it moves downstream.

Area F

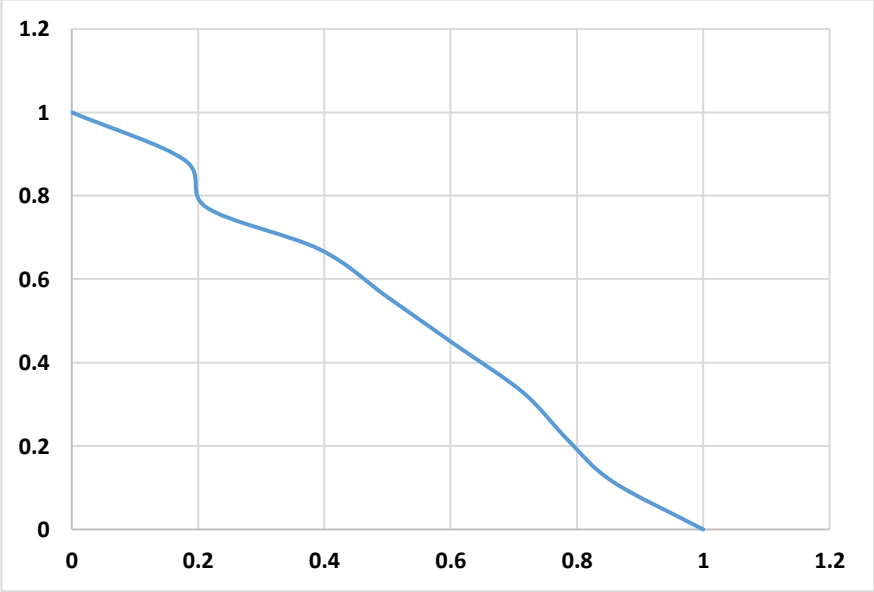

Figure A.54 youthful stage of a basin with slight concavity.

Area G

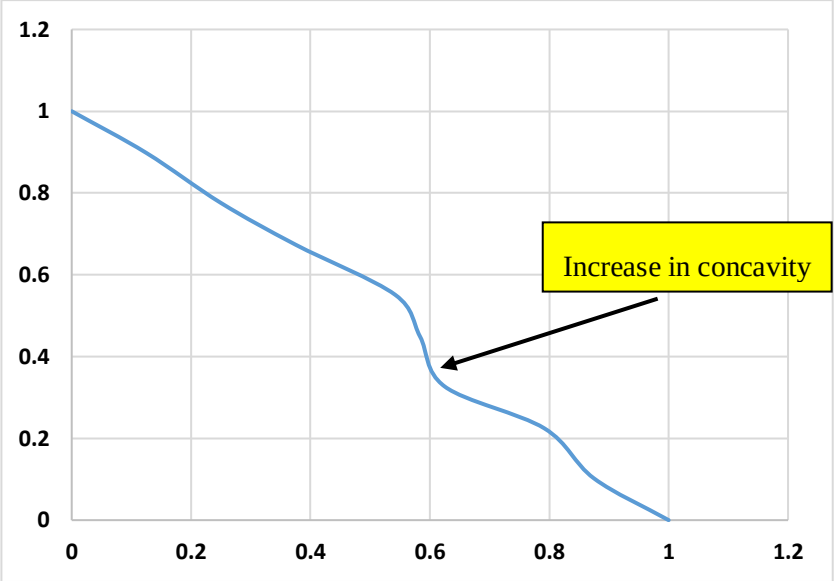

Figure A.55 young topography with slight denudational variation as it moves downstream.

Area H

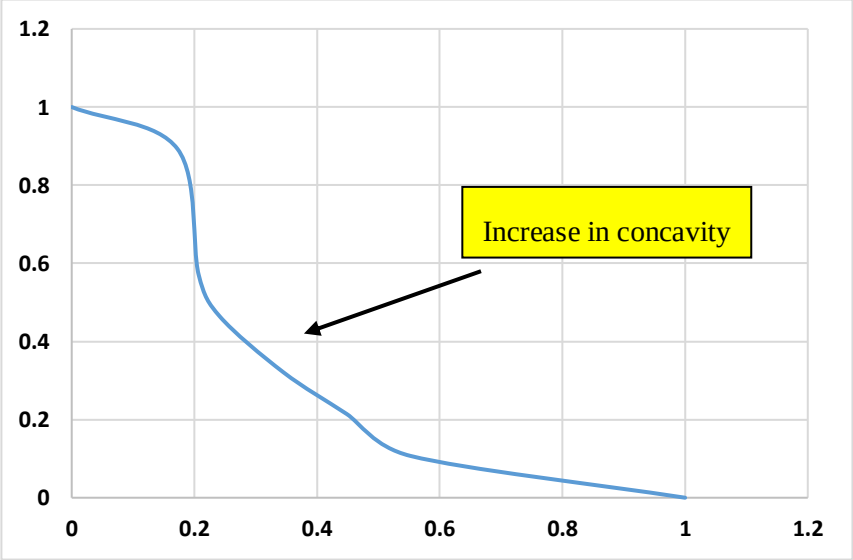

Figure A.56 young terrain in upstream area, but subdues as it progresses downstream.

Area I

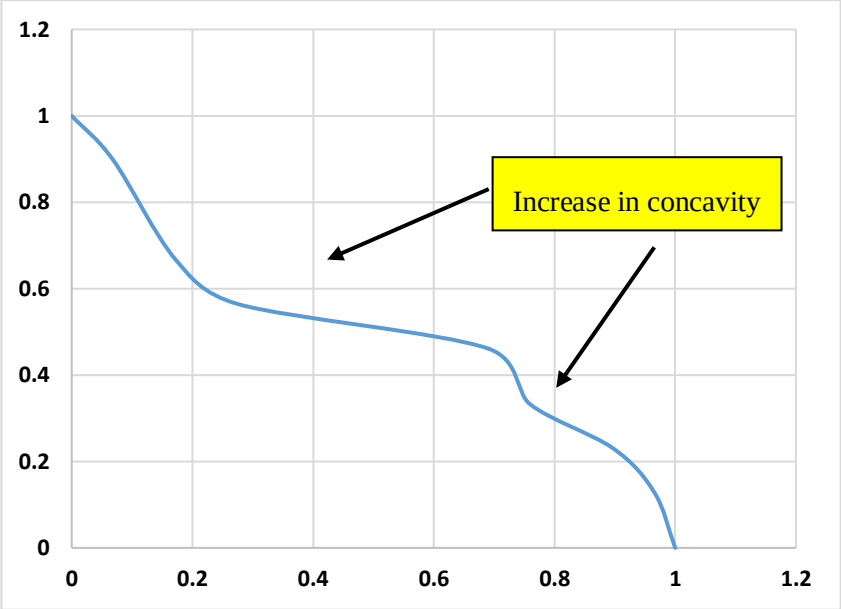

Figure A.57 variation in erosional processes with increase in concavity.

Area J

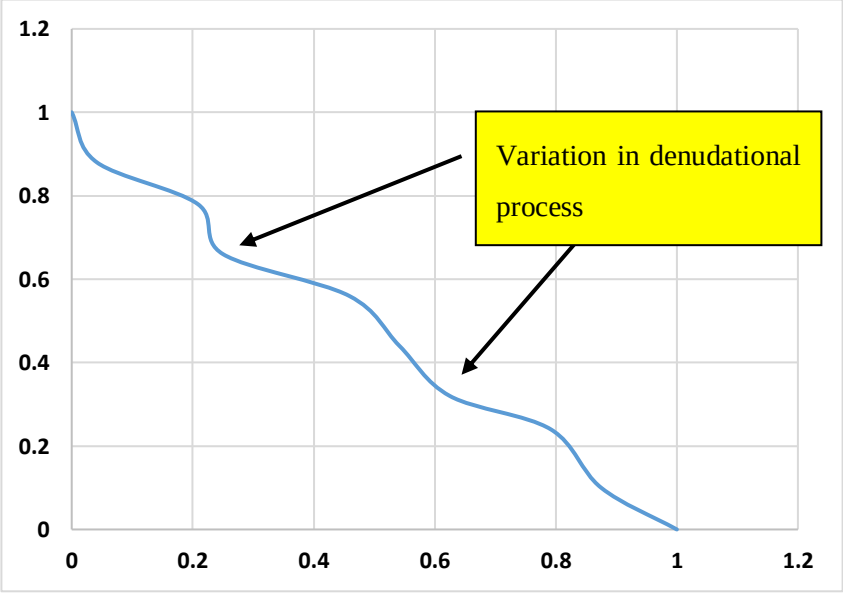

Figure A.58 complex features in sub – basin area.

Area K

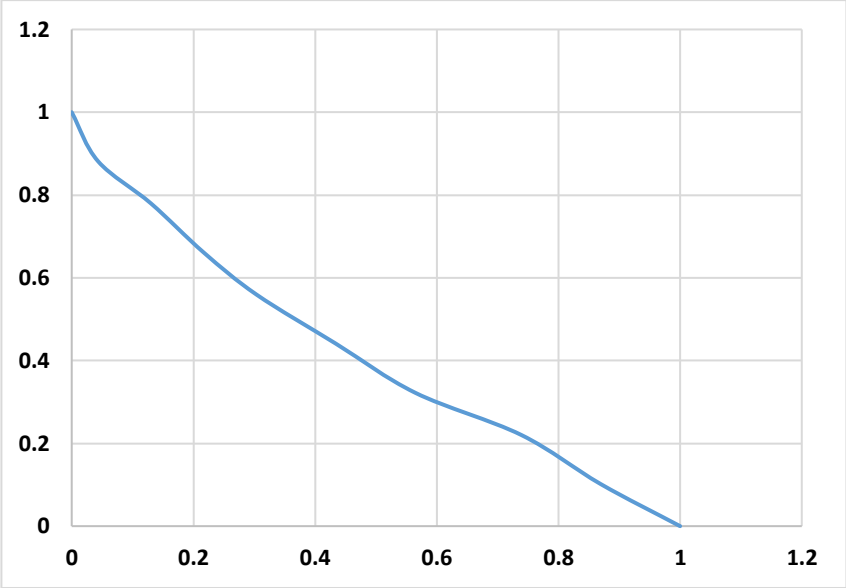

Figure A.59 increasing erosional process across this region.

Area L

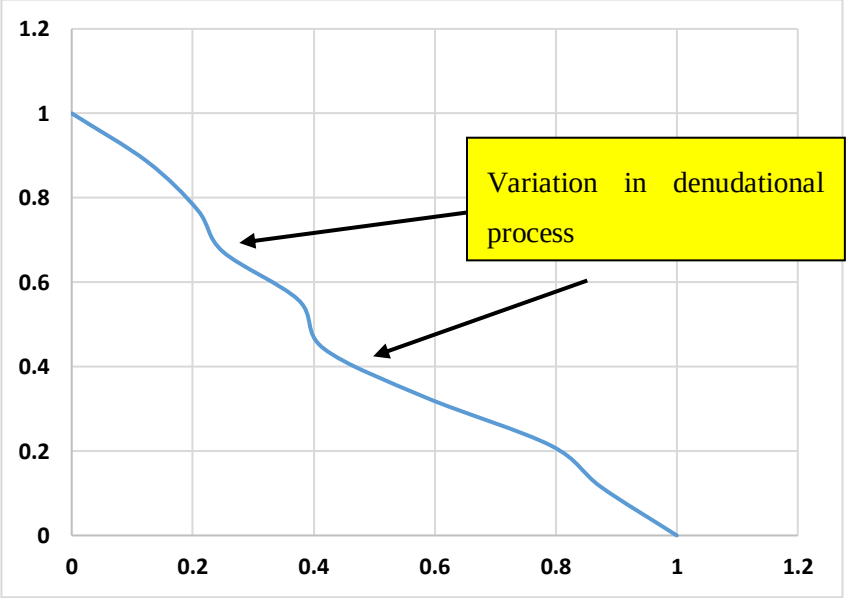

Figure A.60 complex features in sub – basin area.

Area M

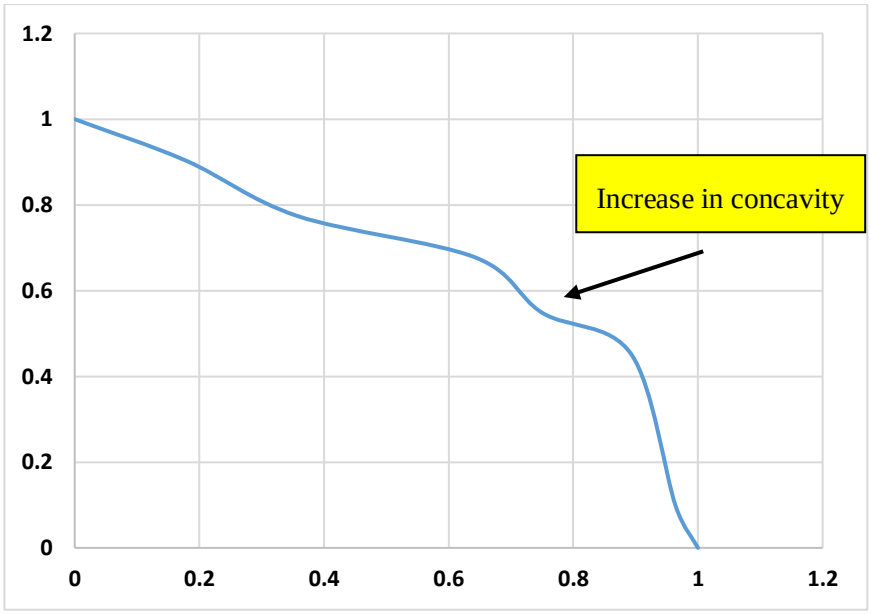

Figure A.61 youthful stage of a basin**.**

Area N

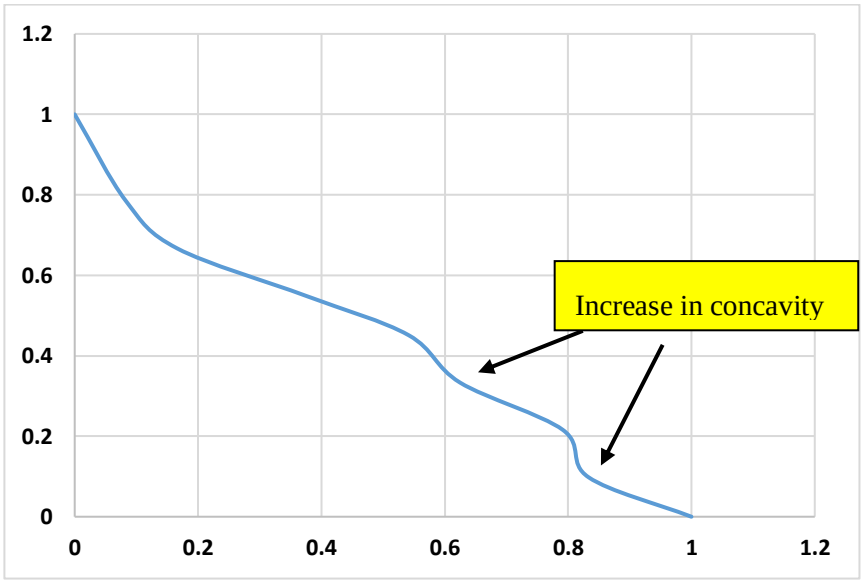

Figure A.62 increasing erosional process across this region.

Area O

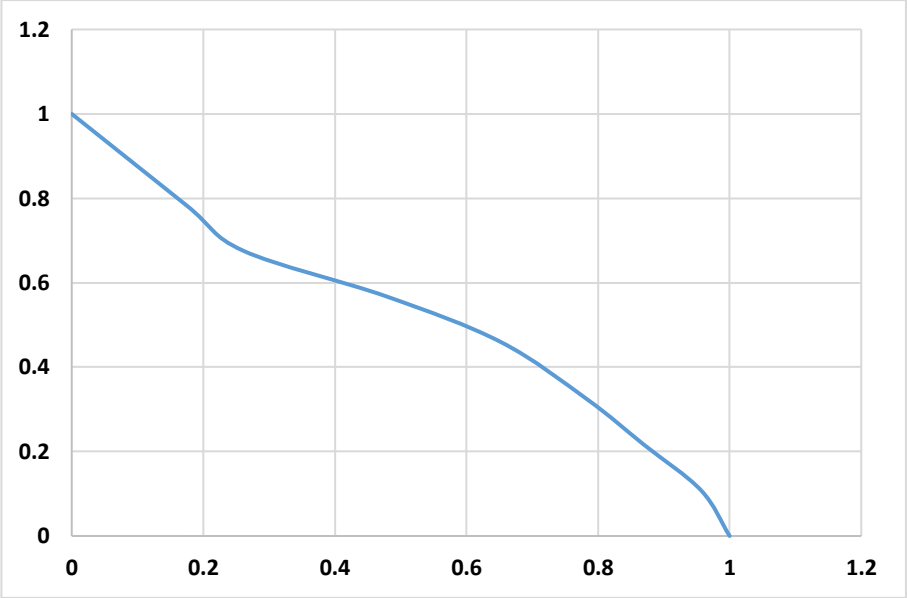

Figure A.63 mature stage of a sub – basin**.**

Area P

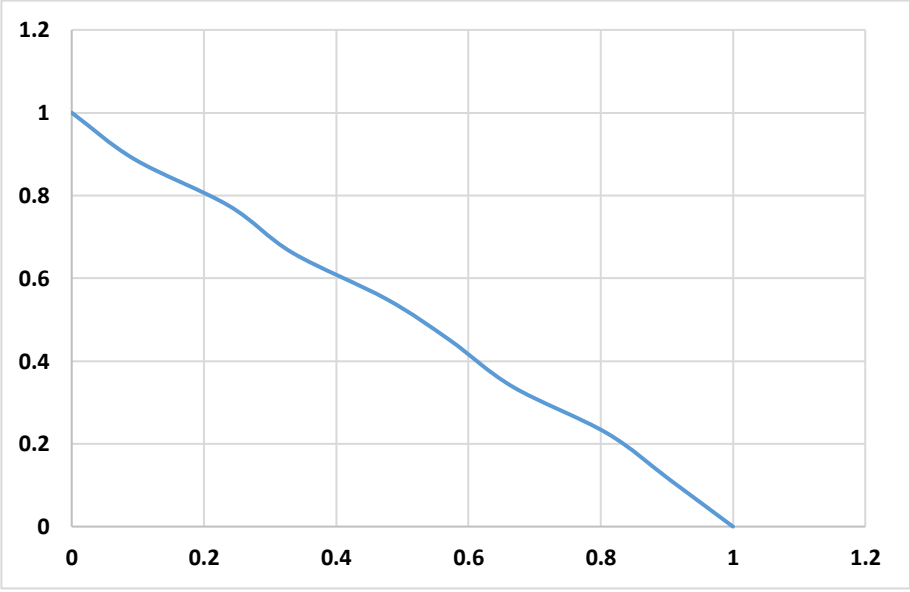

Figure A.64 steady erosional process.